Design and Optimization of a Mobile Hybrid Electric System to Reduce Fuel Consumption

Christopher Del Barga

Thesis submitted to the faculty of the Virginia Polytechnic Institute and State University in partial fulfillment of the requirements for the degree of

Master of Science

In

Mechanical Engineering

Alfred L. Wicks, Chair

John P. Bird

Pablo A. Tarazaga

May 29, 2015

Blacksburg, Virginia

Keywords: Off-grid power systems, hybrid energy, fuel efficiency

Design and Optimization of a Mobile Hybrid Electric System to Reduce Fuel Consumption

Christopher Del Barga

ABSTRACT

The high costs and high risks of transporting fuel to combat zones make fuel conservation a dire need for the US military. A towable hybrid electric system can help relieve these issues by replacing less fuel efficient standalone diesel generators to deliver power to company encampments. Currently, standalone generators are sized to meet peak demand, even though peak demand only occurs during short intervals each day. The average daily demand is much less, meaning generators will be running inefficiently most of the day.

In this thesis, a simulation is created to help determine an optimal system design given a load profile, size and weight constraints, and relocation schedule. This simulation is validated using test data from an existing system. After validation, many hybrid energy components are considered for use in the simulation. The combination of components that yields the lowest fuel consumption is used for the optimal design of the system. After determining the optimal design, a few design parameters are varied to analyze their effect on fuel consumption.

The model presented in this thesis agrees with the test data to 7% of the measured fuel consumption. Sixteen system configurations are run through the simulation and their results are compared. The most fuel efficient system is the system that uses a 3.8kW diesel engine generator with a 307.2V, maximum capacity $LiFeMgPO^4$ battery pack. This system is estimated to consume 21% less fuel than a stand-alone generator, and up to 28% less when solar power is available.

Acknowledgements

I would like to thank my Master's committee, comprised of Dr. Al Wicks, Dr. Pablo Tarazaga and Dr. John Bird, for their continued support and guidance. All of them have given me great advice at some point in my graduate career. I would like to especially thank my adviser Dr. Al Wicks for his encouragement, wise guidance, and friendship. He has been a great role model and a joy to work with. Under his supervision, I have matured as an engineer and person. I would like to also thank Dawn and Dave Dahn, Brent Azzarelli, Ben Baskett, and Ryan Blanding for their guidance.

Of course, most of this work would not be possible without a great team of graduate student engineers and friends to work with on my graduate research project. Special thanks to James Burns, Allan Kirchhoff, Matt Meeder, Ryan Munz, Tim Pierce, David Reeves, Christian Roa, and Marcus Thoreson. I am very grateful to have met and worked with all of them during my graduate career. I would also like to thank the other friends I have worked and lived with during my graduate career: Garret Burks, Carlos Caceres, Andrew Costain, Andrew Jung, Abhijit Khare, Matt Kvalo, Philip Jones, Eric Peterson, Phil Repisky, Ashley Taylor, and Andrew Zetts.

I would like to thank my family and childhood friends for their continued support and love. They mean the world to me. Finally, I would like to thank my beautiful girlfriend Lucy Fanelli for her infinite love, wisdom, tolerance, and strength. I am lucky to have her in my life.

Contents

List of Figures

List of Tables

List of Equations

List of Acronyms and Abbreviations

AC	Alternating Current
AoA	Analysis of Alternatives
ARMA	Autoregressive Moving Average
AWG	American Wire Gauge
BMS	Battery Management System
CMPA	Circular-Mils-Per-Amp
COC	Command Operations Center
DC	Direct Current
DoD	Department of Defense
DOD	Depth of Discharge
EPCC	Electronic Power Control and Conditioning
FPMRT	Full-Power Minimum-Run-Time
FY	Fiscal Year
HEIT	Hybrid Electric ITV Trailer
HFAC	High Frequency Alternating Current
HMMWV	High Mobility Multipurpose Wheeled Vehicle
HWFET	Highway Fuel Economy Test
IC	Internal Combustion
ITV	Internally Transportable Vehicle
JP-8	Jet Propellant 8
$LiFePO^4$	Lithium Iron Phosphate
$LiFeMgPO^4$	Lithium Iron Magnesium Phosphate
MEHPS	Mobile Electric Hybrid Power System
METSTAT	Meteorological-Statistical
MPPT	Maximum Power Point Tracking
NaS	Sodium Sulfur
NATO	North Atlantic Treaty Organization
NEC	National Electric Code

NEMA	National Electrical Manufacturers of America
Ni-MH	Nickel Metal Hydride
NOCT	Nominal Operating Cell Temperature
NSRDB	National Solar Radiation Database
O&M	Operation and Maintenance
PE	Power Electronic
PFAC	Power Frequency Alternating Current
PV	Photovoltaic
ROI	Return on Investment
SAE	Society of Automotive Engineers
SOC	State of Charge
STC	Standard Test Conditions
VT	Virginia Tech

1 Introduction

1.1 Problem Statement

The intent of this thesis is to determine a design for a mobile hybrid energy system that will minimize fuel consumption per electrical energy supplied to loads. The design will be developed through simulation given a certain set of design parameters. Minimizing fuel consumption by an energy system is important when the energy system is being used in off-grid, remote locations where it is difficult and expensive to resupply fuel. Such conditions exist in powering military operations on the battlefield and remote villages in developing countries. In an ideal world, a system relying solely on renewable energy sources for both mobilizing the system and supplying power to loads would not consume any fuel. Unfortunately, renewable energy sources cannot reliably provide necessary power 24 hours a day. Solar power is only available during daytime hours and the amount that can be harnessed heavily depends on weather conditions. Likewise, the amount of power that can be harnessed from wind energy is dependent on weather. A fuel-based power source like a generator or fuel cell is necessary for when renewable energy is not available and a critical electrical load requires more energy or power than the system's energy storage (batteries, fly wheel, ultra-capacitor, etc.) can deliver. A generator or fuel cell can provide power at any time of day, provided there is enough fuel on hand. Because petroleum-based vehicles are the primary means for transportation on land for now and the foreseeable future, accounting for the weight of the energy system will be important for reducing the fuel required to transport the system. To achieve minimal fuel consumption, there must be a balance between efficiency, weight, and energy storage capacity when selecting hybrid energy system components.

This thesis also analyzes how changing certain design parameters impacts the design and resulting fuel consumption. The design parameters that will be explored are:

- the frequency that the hybrid system is relocated;
- the travel distance during each relocation;
- cabling losses and weight;
- the proportion of DC and AC loads in the load profile;
- the effect of alternative load profiles;
- and the set points of the system's control strategy.

1.2 Motivation

As recently as 2011, the United States' Department of Defense (DoD) has begun prioritizing its energy management strategy, laying out a three part plan to ensure the energy needs of the present and future armed forces are met. The three principal parts of the DoD's energy strategy are: (1) reducing the demand for energy in military operations, (2) diversifying its energy sources to expand beyond petroleum-based fuel, and (3) integrating energy considerations into military strategy [1]. A mobile hybrid energy system directly helps the DoD's Operational Energy Strategy by meeting the first two principal parts. Firstly, A mobile hybrid energy system reduces the demand for energy by using that energy more efficiently. The mobile hybrid energy system proposed in this thesis will be replacing less fuel efficient standalone generators at the front lines. Secondly, a mobile hybrid energy system diversifies the armed forces' energy sources by harnessing energy from solar power and possibly other renewable energy types.

The DoD's Operational Energy Strategy outlines several positive outcomes to a more energy efficient armed forces. Among these positive outcomes are saving the lives of armed personnel responsible for moving and protecting fuel on the battlefield, reducing the logistical load of moving fuel around the battlefield, and "strengthening the DoD's resilience to energy price and supply volatility" [1].

The recent wars in Afghanistan and Iraq have seen increased threat to logistics forces. Between FY 2003 and FY 2007, the Army and associated defense contractors suffered over 3,000 casualties resulting from attacks on fuel and water resupply convoys [1]. For FY 2007, the Army estimates that one casualty occurred per twenty four fuel

resupply convoys in Afghanistan and one casualty occurred in thirty nine fuel resupply convoys in Iraq. These ratios gain some significance when considering over five thousand fuel resupply convoys were carried out in Iraq and over eight hundred fuel resupply convoys were carried out in Afghanistan in FY 2007 [2]. Figure 1 shows a US Army fuel convoy in Iraq, November 8, 2008 (Photo credit: US Marine Corps Lance Corporal Kelly R. Chase) [1].

Figure 1: US Army Fuel Convoy in Iraq [3]

Image from R. Rapier, "The U.S. Navy and Biofuels - Part III," EnergyTrends Insider, 30 October 2010. [Online]. Available: http://www.energytrendsinsider.com/2010/10/30/the-u-s-navy-and-biofuels-%E2%80%93-part-iii/. [Accessed 10 March 2015]. Used under fair use, 2015.

A more energy efficient armed forces not only will save lives, but reduce economic costs for the DoD. The United States DoD is one of the largest consumers of fuel in the world. The DoD consumed more than five billion gallons of fuel in 2010 for military operations, costing $13.2 billion. This is a 255 percent increase over 1997 costs [1]. Transporting the fuel to and around the battlefield increases related costs further. To bring fuel to its final destination on the battlefield in Iraq was $17.44 per gallon in 2011 [4]. The cost to bring fuel to the battlefield in Afghanistan could be even higher, up to an estimated $400 per gallon in extreme cases where the fuel is airlifted via helicopter [5]. In general, air delivery of fuel is ten times as expensive as ground delivery [1]. Figure 2 shows forty bundles of fuel being airdropped over Afghanistan from a US Air Force

Globemaster III aircraft, December 8, 2010 (Photo credit: US Air Force Staff Sergeant Andy Kin) [1].

Figure 2: Fuel Being Airdropped over Afghanistan [1]

Image from P. &. P. Assistant Secretary of Defense for Operational Energy, "Energy for the Warfighter: Operational Energy Strategy," United States Department of Defense, Washington, DC, 2011. Used under fair use, 2015.

Although the main focus of this thesis is to design a mobile hybrid electric system for military applications, there exist other applications for such a system. One possible application of a mobile hybrid electric system is for rural homes or communities in developing countries. As of 2011, 1.5 billion people in the world do not have access to electricity. Approximately 80% of these people live in rural areas [6]. These people living in rural areas are not likely to gain access to electricity in the near future [6]. Extending a national power grid to these locations is not likely for several reasons, the first of which is its extreme cost. The cost of extending a national power grid to these locations is driven high due to the great distance to these rural communities, difficult terrain, and small size of power demand [6]. A mobile hybrid power system could be used to provide power to individual houses in a rural area with a scattered population, where covering a large area would require high connection costs for a power grid. If a rural population is located in a more concentrated area, Rolland and Glania propose the use of a hybrid electric mini-grid that would be able to service a group of 15 or more households,

requiring up to about 100kW capacity [6]. Further analysis beyond the scope of this thesis can look at the feasibility of using one large capacity (up to 100kW) mobile hybrid electric system or multiple smaller capacity (1-10kW) mobile hybrid electric systems to supply power to a rural mini-grid. One presumed advantage of using mobile hybrid electric systems to supply a local mini-grid is the ability to deliver a working power system in one piece instead of constructing the system on site.

Another possible application of this technology is to provide power to disaster areas, like those ravaged by hurricanes or earthquakes. In these disasters, entire power grids can be brought down for long durations of time. When Hurricane Katrina struck the Gulf Coast in 2005, three million homes lost power in at least eight states [7]. Similarly, when Hurricane Sandy struck the United States' Atlantic Coast in 2012, 8.51 million homes lost power in sixteen states and Washington, D.C. [7]. A mobile hybrid energy system may be helpful in powering medical tents and individual residences after these disasters strike.

There are many goals that a hybrid system can be designed toward including maximizing reliability, minimizing economic cost, or minimizing carbon footprint. However, this thesis exclusively focuses on minimizing the fuel consumption of the hybrid power system. It can be pointed out that focusing on reducing fuel consumption ignores the possible additional economic costs from the inclusion of a battery pack or expensive power conversion equipment. However, it is important to remember that for military applications fuel consumption carries costs beyond just economic. The cost of a human life cannot be valuated with money. Nonetheless, reducing fuel consumption may also help reduce economic costs as batteries may eventually cost less, and the recent trend in rising fuel costs show that fuel will only become more expensive in the future.

1.3 Background of Hybrid Energy Systems

A hybrid energy system combines multiple power sources. Usually, a hybrid system combines a generator or fuel cell with a battery pack and possibly a renewable energy source. This combination of multiple power sources and energy storage is done

for many possible reasons, like reducing fuel consumption, decreasing carbon footprint, or decreasing maintenance costs. Figure 3 shows a general hybrid energy system. The four major components (primary power source, renewable energy source, energy storage, and loads) are marked with examples given in parentheses. Hybrid power systems are prevalent in off-grid applications where there isn't access to a large power grid.

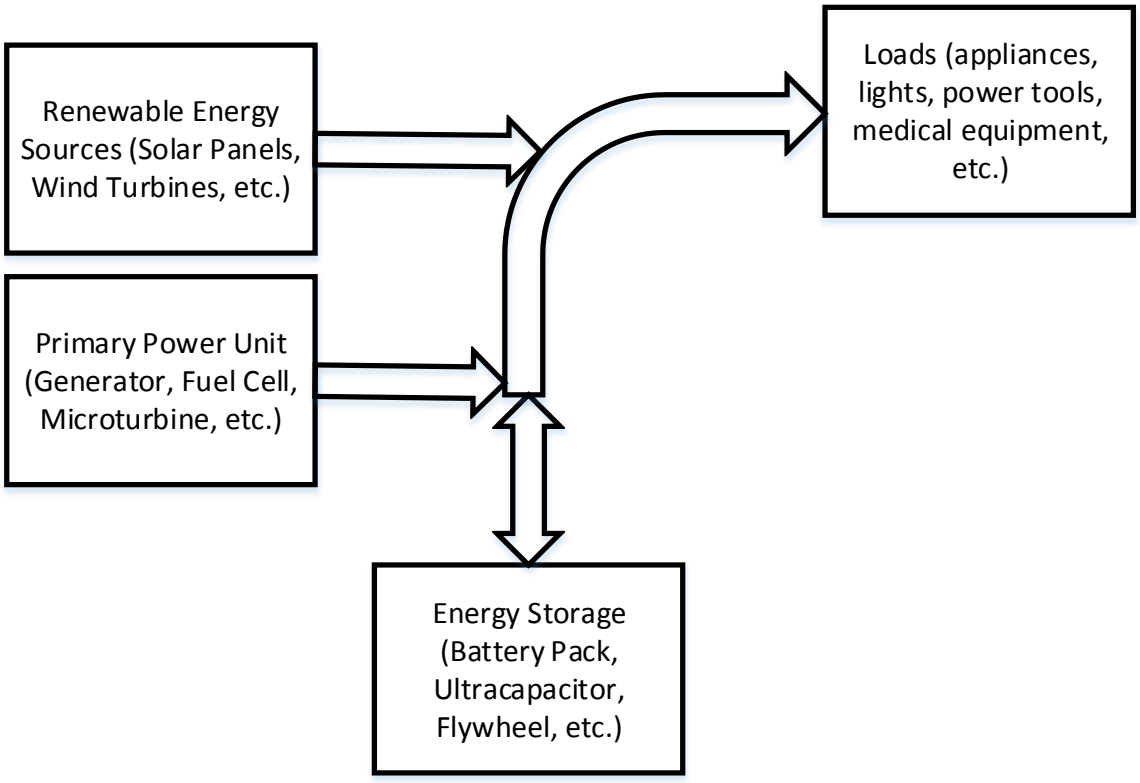

Figure 3: General Hybrid Power System

There are several examples of off-grid hybrid energy systems in use today. Many of these off-grid hybrid energy systems are stationary systems employed in rural parts of developing countries to power multiple households and buildings. A photovoltaic (PV)/diesel hybrid system was installed in rural China in 2006 to provide power to 55 households [8]. PV/diesel hybrid systems were also installed in rural parts of Tanzania, Algeria, and Ecuador in the 2000s [8]. Another system incorporating wind power with PV, diesel generation, and batteries was installed in China in 2002 to power three villages [8]. Even hydro power has been used in Laos in conjunction with PV and diesel power to power 98 households beginning in 2007 [8].

A few mobile hybrid systems have also been demonstrated. In 2010, Eroglu et al. demonstrated a mobile renewable house using a PV/wind/fuel cell hybrid system [9]. Yazici et al. demonstrated a similar system in 2013 [10]. Victron, a power component company based out of The Netherlands, manufactured the MultiPower system which combined a diesel generator with a battery pack to power residences [11]. A few mobile hybrid power systems have been created for military purposes, including the Electronic Power Control & Conditioning (EPCC) module developed by the U.S. Army CERDEC (Communications-Electronics Research, Development and Engineering Center). This system is housed in a shipping container and can incorporate renewable energy to reduce JP-8 fuel consumption [12].

The Hybrid Electric ITV (Internally Transportable Vehicle) Trailer, or HEIT is a system developed by Virginia Tech to provide power on the battlefield. This system is housed in the Expeditionary Fire Support System (EFSS) ammunition trailer from General Dynamics. The components and design of this system is explained in *4.1 Design of Existing System*. Test data for this prototype system is used to validate the model presented in this thesis.

1.4 Design Parameters

The work done in this thesis is divided into two parts. The first part is to validate the proposed model by comparing its results with data captured from a functioning hybrid electric prototype system. After validating the model, the second part is to use the model to determine a more fuel efficient hybrid electric system by comparing different combinations of components. These parts are called “validation” and “design” in this section. After the validation and design parts are finished, this thesis explores the effect of varying some of the design parameters. This section explains the design parameters used for the first and second parts of the work done in this thesis. These design parameters include the power characteristics of the system’s expected load profile; the system’s expected solar power profile; the system’s physical constraints; and the system’s expected relocation frequency and distance.

Power Characteristics and Load Profile

For validation, the design parameters used in the model are set to match those of the prototype system. The prototype system is tested using 1.3kW resistive load for 26.5 hours. This load profile is also applied to the model. Like the prototype, the modeled system is designed to supply a peak power of 3.5kW even though this load is not experienced during the load profile. The modeled system is expected to supply up to 2kW continuously. This 2kW continuous load is calculated by multiplying the average load of the validation load profile by 1.25. Since the prototype system is designed to output only 28V DC power, 100% of the modeled system's load profile is directed to powering DC loads; no AC loads are powered.

During the design portion of this thesis, the load profile is derived from literature. The Company Command Operations Center (COC) metered power profile from the Mobile Electric Hybrid Power System (MEHPS) Analysis of Alternatives (AoA) report is used for design. This 24 hour profile has a peak load of 4.8kW and an average load of about 2.3kW [13]. The peak power requirement for the designed system is 5kW, and the continuous load requirement is 2.9kW. As with validation, this continuous load requirement is calculated by multiplying the average load of the Company COC metered profile by 1.25. The load profile is divided so that 80% of the load goes to 120VAC, 60Hz loads, and the other 20% goes to 28V DC loads. The distribution of the load profile among AC and DC loads is determined somewhat arbitrarily. A distribution of 80% AC, 20% DC is selected because more AC loads are expected to be present than DC loads. Presently, more appliances and devices are powered on 120VAC, 60Hz power than on DC power because most national power grids are designed to supply AC power.

Both parts use three NATO slave receptacles for 28V DC loads. The design part of this thesis additionally includes three NEMA 5-20 connectors for 120VAC power. For both parts, cables are sized to meet NEC 310.16 cabling guidelines. A summary of the power design parameters is given in Table 1. These load profiles are further discussed in in *3.1 Load Profile Model*.

Table 1: Power Design Parameters

Design Parameter	Validation	Design
Load Profile	1.3kW Constant Load, 26.5 Hours	Company COC Metered Power Profile
AC/DC Load Distribution	0% AC, 100% DC	80% AC, 20% DC
Minimum Peak Power Output	3.5kW	5kW
Minimum Continuous Power Output	1.7kW	2.9kW
DC Output Receptacles	3 x 28V NATO receptacles rated to 500A each	3 x 28V NATO receptacles rated to 500A each
AC Output Receptacles	None	3 x 120V, 60Hz NEMA 5-20 receptacles rated to 20A each
Cable Standard	NEC 310.16	NEC 310.16

Solar Power Profile

For validation, the solar power profile recorded during prototype testing is used. This solar profile spans 26.5 hours from the afternoon of November 3, 2014 to the afternoon of November 4, 2014. Prototype testing took place in Blacksburg, Virginia under partly cloudy conditions.

For design, modeled global irradiance data from the National Solar Radiation Database (NSRDB) is used. This modeled solar irradiance data includes the presence of cloud cover. To build a 24 hour solar power profile, twenty years of irradiance data is averaged on a day-by-day basis. The solar power profiles are discussed further in *3.4 Solar Power Model*.

Physical Constraints

Both the validation and design parts of this thesis use the same physical constraints. These physical restraints are determined by the geometry and loading requirements of the trailer used to house the hybrid electric system. The ammunition trailer used for the prototype HEIT system is also used to house the systems being modeled in this thesis. The hybrid electric system needs to fit within the bounds of this

trailer, which has inside dimensions of 42” by 42” by 42”. The ammunition trailer can carry up to 1800lbs [14] while the trailer itself weighs 670lbs. Therefore, the weight limit of the entire system is 2470lbs. The physical requirements are summarized in Table 2.

Table 2: Physical Requirements for System

Physical Requirement	Value
System Weight	1800lbs + trailer weight of 670lbs
System Volume	74088 in^3
Longest Dimension Allowed	42 in

Relocation

This simulation estimates the fuel used to transport the system. To estimate the amount of fuel consumed during transportation, the relocation frequency and distance need to be defined. For the validation and design sections of this thesis, the system is assumed to be relocated once per week a distance of 40 miles. The author selected these parameters arbitrarily but attempted to choose values that would seem realistic.

1.5 Thesis Outline

In Chapter 1, the problem statement, motivation, and brief background of this work were presented. Then, the design parameters were explained. These design parameters are important for guiding the design of the most fuel efficient hybrid electric system.

This thesis continues by reviewing hybrid system technology in Chapter 2, including the major components, architectures, and control strategies. In Chapter 3, the hybrid system model is described in detail. The model for each individual component of the system is described and these individual models are combined into a large system model. At the end of this chapter, the derivation of the weight-based fuel penalty is explained. In Chapter 4, the design of the prototype system is described as well as the many components and configurations that are evaluated by the model to determine the most fuel efficient system. Chapter 5 begins by presenting the validation of the model using test data from the prototype HEIT system. It continues with the results of the design

phase where the multiple configuration and component options are evaluated by the model to determine the most fuel efficient system design. The most fuel efficient system design is then presented in this chapter. At the end of Chapter 5, some of the design parameters are further explored to determine their impact on a hybrid system's fuel consumption. Chapter 6 presents the conclusions drawn from the results and the future work that can be done to build on these results.

2 Review of Hybrid System Technology

Hybrid systems incorporate many different elements to provide electrical power. These elements include a fuel-based primary power source, renewable energy sources, energy storage systems, and the appropriate power conversion components. This section covers small off-grid hybrid design including the importance of the load profile, common hybrid system architectures, and specific components.

2.1 Load Profile Determination

The design of any power system begins with the determination of the expected power demand, or load profile. An example of a load profile is shown in Figure 4. The profile shown is an example daily profile for a household with each home appliance's contribution designated by its own color [15].

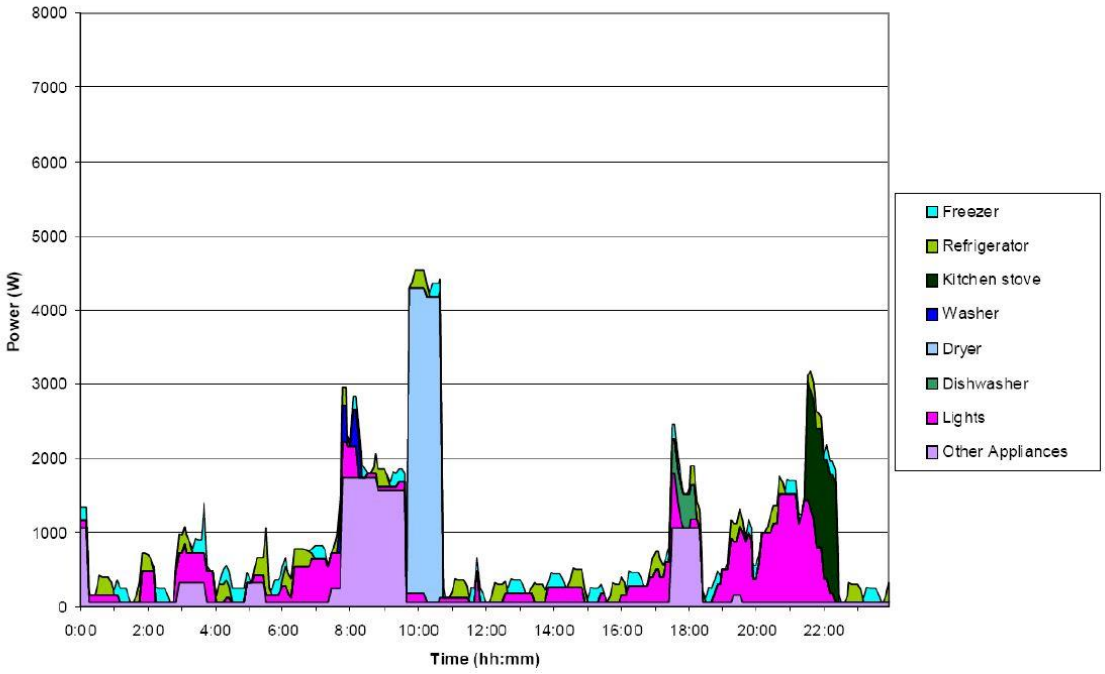

Figure 4: Example Load Profile for a Household [15]

Figure from Victron Energy, "Marine Generator Test," Victron Energy, 2007. Used under fair use, 2015.

A load profile is determined through research or measurement. For a large power grid, a load profile can be created by measuring the power demand for each distribution substation [16] or for each household [17]. A distribution substation is where power is converted from the transmission grid to the distribution grid to service local businesses and houses. For a person attempting to size a renewable energy system, like a solar panel system, for his or her household, a more specific load profile needs to be created that accounts for each home appliance and device [18]. The parameters that need to be determined for this more specific load profile are: input voltage specifications for each device, normal operating power for each device, surge power for each device, and expected duration of operation for each device during a cycle/day [18]. The appliance or device's demand under normal operation can be measured with a current sensor. Likewise, its surge power (inrush power after startup) can also be measured with a current sensor [18].

The development of a load profile for an off-grid system will be most similar to the development of a load profile for a household renewable energy system. For both cases, power demands are relatively small (~1 to 100kW) [15], [17], [19] and can be attributed to individual devices connected to the power system. For an off-grid system designed to power a rural household, the load profile will be similar to the load profile for a household that is connected to the power grid, in that the appliances, devices, and resident behavior will be mostly the same. As can be seen in Figure 4, for the majority of the day (about 15 hours), the power demand is low (<1kW). Power demand increases above 2kW for a few hours in the morning (between 7am to 11am) and again in the evening (between 5pm and 10 pm) [15]. Research performed by Ning and Kirschen following the power demand of 22 households in the United Kingdom agrees with the profile shown in Figure 4. In their report, they observe that individual domestic load profiles exhibit long durations of low loads with short durations of high loads. They also observe that household daily low load profiles usually have a morning peak or an evening peak or both [17].

A load profile is important for designing a power system because it helps answer the questions:

1. What is the maximum output expected from the system's power plant?
2. How much energy capacity or fuel capacity is required for the system?

A power system needs to have the capability to supply the maximum expected power demand. In the case of a power system consisting of only a standalone internal combustion (IC) engine generator, the generator needs to be rated to supply the maximum expected power in the load profile. For a load profile like the one shown in Figure 4 where the maximum load is only present for less than half the profile, a standalone IC engine generator will be oversized for the application through most of the day [15]. Most IC engine generators are designed to run at full load and can be damaged if running at a load much less than their rated power output [20]. Along with the increased risk of damage to the IC engine generator, there is a decrease in engine efficiency at lower loads [15]. A hybrid electric system, on the other hand, may not need the generator to be rated for the maximum possible load, since a battery pack can assist in meeting power demands. However, the combined rated output of the generator and battery pack needs to meet the maximum power demand.

2.2 Hybrid System Architectures

A hybrid electric power system can be arranged in a variety of different ways, each with its purpose, benefits, and drawbacks. This section will review three different hybrid electric system architectures: DC-coupled, AC-coupled, and hybrid-coupled.

2.2.1 DC-Coupled System

A DC-coupled hybrid system has a DC voltage internal bus. In this configuration the energy sources are connected to the DC voltage internal bus through appropriate power electronic (PE) circuitry [21]. Figure 5 shows a schematic diagram of a DC-coupled system. DC energy sources and DC loads can be directly connected to the internal DC bus, if appropriate, or can be connected through DC/DC converters. An inverter can convert DC bus power into AC power for AC loads and for connecting to a power grid. A DC-coupled system tends to be the simplest system architecture to design

for, since the different energy sources do not need to be synchronized. However, if the inverter fails, there is no redundant AC power supply to supply the power grid [21].

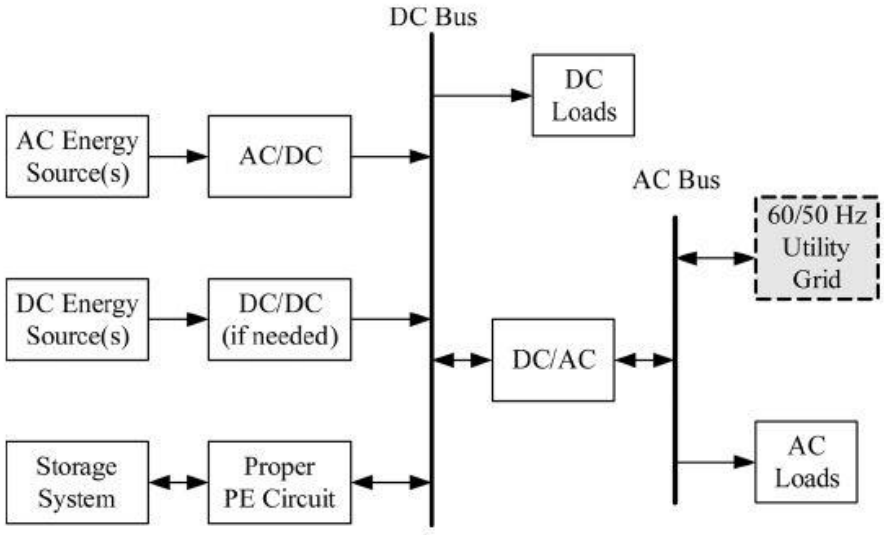

Figure 5: DC-Coupled Hybrid Energy System [21]

Image from M. H. Nehrir, C. Wang, K. Strunz, H. Aki, R. Ramakumar, J. Bing, Z. Miao and Z. Salameh, "A Review of Hybrid Renewable/Alternative Energy Systems for Electric Power Generation: Configurations, Control, and Applications," *IEEE Transactions on Sustainable Energy*, vol. 2, no. 4, pp. 392-403, 2011. Used under fair use, 2015.

There are two variants of the DC-coupled system architecture: one with a "floating" DC bus and one with a "fixed" DC bus. A "floating" DC bus architecture is where the battery pack is directly connected to the internal DC bus. In this configuration, the appropriate PE for charging the battery pack properly needs to be built into each energy source's converter. There is an added level of complexity in that all of the energy source converters need to be controlled and monitored for the correct battery charging scheme. A "fixed" DC bus is held at a constant voltage and a bi-directional DC/DC converter is used to charge and discharge the battery pack. This configuration is simpler in that the battery charging algorithm needs to be only programmed into the bi-directional DC/DC converter. However, the system may lose some efficiency due to the extra conversion process.

2.2.2 AC-Coupled System

An AC-coupled system configuration may be the most appropriate configuration for systems primarily receiving power from an AC energy source and/or primarily supplying AC loads. An AC-coupled system can directly supply AC loads from the internal bus without an extra conversion. Likewise, an AC-coupled system can directly receive power from AC energy sources without any extra conversion (unless AC/AC transformation is needed) [21]. The AC-coupled configuration can be divided into two subcategories: power frequency AC (PFAC) coupled and high frequency AC (HFAC) coupled configurations. A PFAC-coupled system has an internal AC bus that is low frequency (usually 50 Hz or 60 Hz). In contrast, an HFAC-coupled system has an internal AC bus that is high frequency AC (e.g. 400 Hz). An HFAC bus is usually needed in applications where there are high frequency AC energy sources and loads, such as in airplanes, ships, submarines, and space station applications [21]. Figure 6 shows a schematic diagram of a PFAC-coupled system, and Figure 7 shows a schematic diagram of an HFAC-coupled system.

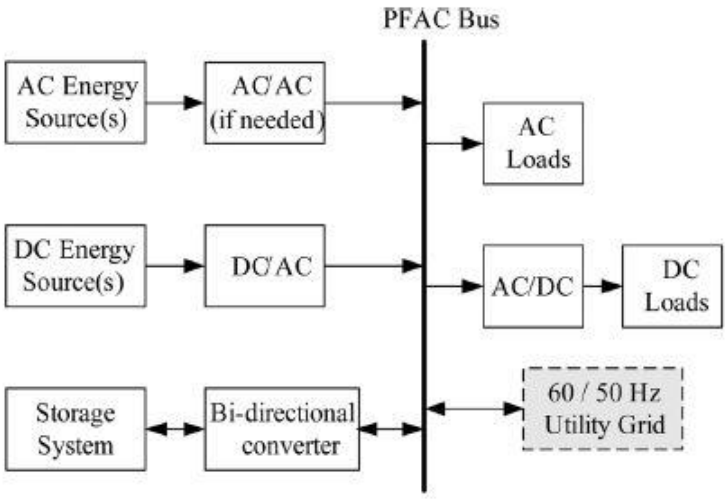

Figure 6: PFAC-Coupled Hybrid Energy System [21]

Image from M. H. Nehrir, C. Wang, K. Strunz, H. Aki, R. Ramakumar, J. Bing, Z. Miao and Z. Salameh, "A Review of Hybrid Renewable/Alternative Energy Systems for Electric Power Generation: Configurations, Control, and Applications," *IEEE Transactions on Sustainable Energy,* vol. 2, no. 4, pp. 392-403, 2011. Used under fair use, 2015.

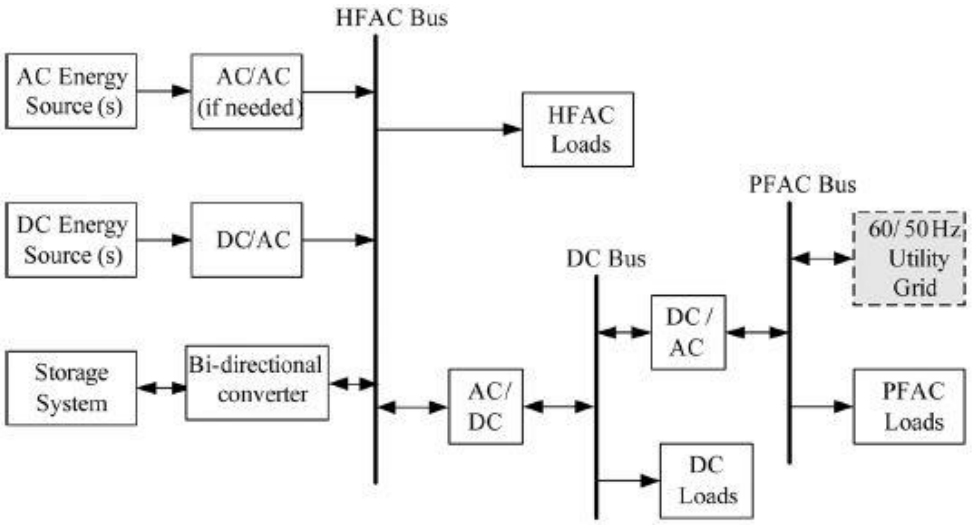

Figure 7: HFAC-Coupled Hybrid Energy System [21]

Image from M. H. Nehrir, C. Wang, K. Strunz, H. Aki, R. Ramakumar, J. Bing, Z. Miao and Z. Salameh, "A Review of Hybrid Renewable/Alternative Energy Systems for Electric Power Generation: Configurations, Control, and Applications," *IEEE Transactions on Sustainable Energy,* vol. 2, no. 4, pp. 392-403, 2011. Used under fair use, 2015.

2.2.3 Hybrid-Coupled System

A hybrid-coupled system includes both a DC bus and an AC bus. This configuration allows for both AC and DC energy sources and loads to be connected directly to its appropriate bus without extra interfacing circuits. This configuration can also limit conversion steps between energy sources and loads of the same electrical characteristics (e.g. an IC engine generator can supply its AC power to AC loads without a conversion step). Therefore, using this configuration can lead to higher system efficiency and lower cost than using one of the other configurations. The drawback of a hybrid-coupled system is that control and energy management may become more complicated [21]. Figure 8 shows a schematic diagram for a hybrid-coupled configuration.

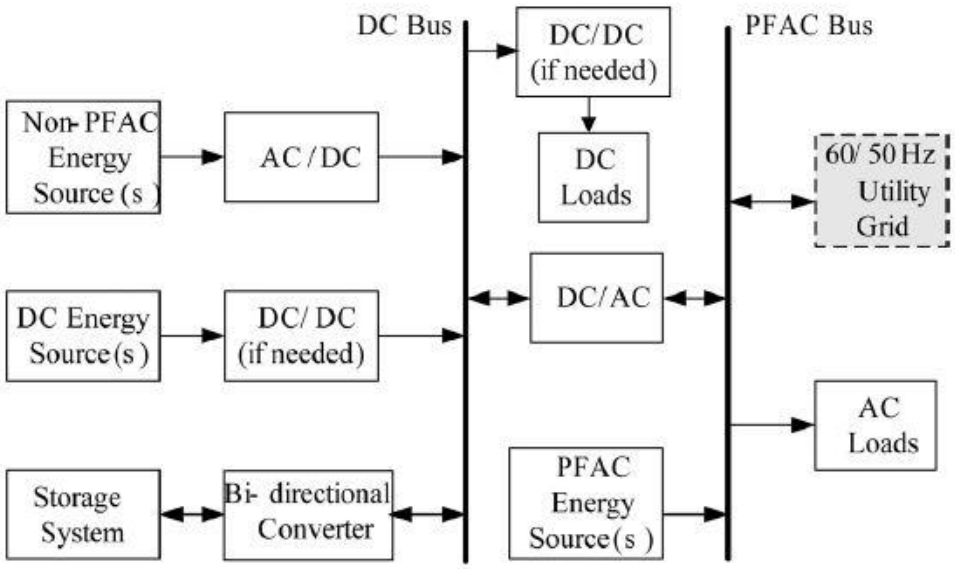

Figure 8: Hybrid-Coupled Hybrid Energy System [21]

Image from M. H. Nehrir, C. Wang, K. Strunz, H. Aki, R. Ramakumar, J. Bing, Z. Miao and Z. Salameh, "A Review of Hybrid Renewable/Alternative Energy Systems for Electric Power Generation: Configurations, Control, and Applications," *IEEE Transactions on Sustainable Energy*, vol. 2, no. 4, pp. 392-403, 2011. Used under fair use, 2015.

2.3 Energy Storage

Energy storage is a key component of the hybrid power system. This section focuses on battery pack selection and design as well as accompanying battery management circuitry. It also covers a few other energy storage types.

Power Dense and Energy Dense Storage Types

There are two major types of energy storage devices: power dense devices and energy dense devices. Power dense storage devices allow fast access to stored energy, i.e. they can deliver high levels of power. These devices have very high cycle life and have high round-trip efficiency of around 95%. Some examples of power dense devices are fly wheels, ultracapacitors, superconducting magnetic energy storage (SMES), and power dense batteries. Power dense storage devices are used more for performance applications where high levels of power are needed [21]. Energy dense storage devices, on the other hand are capacity-oriented. They can store more energy than power dense devices. These devices tend to be less expensive than power dense energy storage devices even though

their cycle life can be less. These energy dense storage devices include energy dense batteries and hydrogen fuel cells [21]. In some hybrid systems, power dense and energy dense storage devices have been used together to create multi-level storage. Although combining these devices increases the complexity of the system, having access to both high power and high energy can be an advantage [21].

Battery Chemistries

There are several battery chemistries available to use in hybrid power technology. Some of these chemistries have been used for many years while others are still developing. One of the most ubiquitous and well known battery chemistries is the lead acid battery. This battery chemistry is the least expensive to use for hybrid power applications and is also safe and easy to maintain. However, it does not have very high cycle life [21]. Another key disadvantage of this chemistry is its low energy density [22]. This low energy density may pose a problem for using this chemistry in a mobile hybrid power system that has strict space and weight restrictions.

There are many other battery chemistries that are improvements over the lead acid battery chemistry. These chemistries include nickel metal hydride (Ni-MH), sodium sulfur (NaS), and lithium ion. Ni-MH batteries are popular to use in hybrid electric vehicles and distributed renewable energy systems [21]. This battery chemistry has high energy density and has no toxic chemicals. However, this chemistry also has low cycle life, high self-discharge, high maintenance requirements, and high cost (compared to the cost of lead acid batteries) [23]. NaS batteries have been used in large scale wind energy applications. However, NaS batteries require an operating range of 300°C to 350°C, which is not suitable for mobile applications [21]. Lithium ion batteries are popular for hybrid vehicles despite their high cost [22]. These batteries offer high energy density and low maintenance [23]. The lithium ion chemistry is relatively new and is still being developed [23].

One lithium ion chemistry that has been attracting a lot of attention recently is the lithium iron phosphate ($LiFePO^4$) chemistry. The $LiFePO^4$ cathode material used in these batteries is naturally occurring and is very thermally stable. This stability makes it a safer

alternative than the other lithium ion chemistries. This chemistry has greater abuse tolerance because it is less prone to react under harsh conditions. This chemistry has long cycle life and very fast charge times. One of its drawbacks is its slightly lower energy density compared to other lithium ion chemistries though recent research has improved this deficiency [24]. A variation on this chemistry is used for the battery pack in the prototype HEIT system as well as for the design selection phase of this thesis.

Battery Charging Profiles

Many battery chemistries require a special charging profile. Lead acid batteries often have very long charge times compared to other battery chemistries. These batteries have three charge stages: a constant current stage, a constant voltage stage (or topping charge), and a float charge. During the constant current stage, the majority of the charging occurs. In this stage, the charge current into the battery pack is held constant while the battery voltage slowly increases. This stage occurs for approximately half of the lead acid battery's charge time. The topping charge holds the battery voltage constant while the charge current slowly decreases. This stage saturates the battery pack. This stage ends when the charge current drops below a pre-determined level. The float stage holds the battery at a slightly lower voltage to counteract the battery's self-discharge [25].

Lithium iron phosphate batteries are charged in a similar way. These batteries also have a constant current stage and constant voltage stage. However, these batteries do not need a float stage. The constant current stage for $LiFePO^4$ batteries lasts about an hour until the battery cell reaches 3.65V (about 60% SOC). The constant voltage stage holds the voltage at 3.65V for about another two hours until the current decreases below a pre-determined level. Unlike lead acid batteries, $LiFePO^4$ cells in series cannot balance each other. Therefore, a management system is needed [26]. The $LiFeMgPO^4$ battery pack used in the HEIT prototype system charges much in the same way. However the constant current stage lasts for almost two hours until the battery state of charge (SOC) is around 90%. Then, the constant voltage stage lasts for about forty minutes until the battery is fully charged [27].

Battery Management

It is recommended practice to use a battery management system to monitor and care for a hybrid power system's battery pack. A battery management system (BMS) reads battery parameters like cell voltage, current, and temperature to estimate the battery's state of charge (SOC) and monitor the health of the battery pack. A BMS is also used to control the battery's balancing.

State of charge (SOC) is the percentage of the battery's overall energy capacity that is currently storing energy. A battery's SOC can be difficult to determine and there are two primary methods used to estimate SOC. The SOC of the battery can be estimated using the open circuit voltage V_{OC} of the battery. The V_{OC} vs. SOC relationship is nonlinear with a large flat region in the middle range of SOC where V_{OC} does not increase much. Because of this flat region, a small error in the V_{OC} measurement can lead to a large error in the SOC estimation [28]. The second method, called "coulomb counting", works by integrating the current into and out of the battery pack to determine the state of charge of the battery. However, this method can carry a large integration error over a long period of time [28].

Health monitoring is performed to determine if one or multiple battery cells are damaged. If a battery cell is overcharged it may have a voltage higher than its specified charge voltage. Overcharging a battery cell can damage it. The ability to measure temperature of a battery can be helpful in determining if there is thermal runaway.

Balancing a battery is important to increase the battery's lifespan and working storage capacity. Not all battery cells in a battery pack may have the same electrical characteristics (internal resistance, capacity, and self-discharge rate) due to impurities. These differences in electrical characteristics can cause some cells to be less charged than others, causing an imbalance between the cells in the pack. This imbalance decreases the working capacity of the battery pack and can possibly lead to overcharging of the higher capacity cells [29]. Two battery balancing techniques exist: passive and active. Passive balancing uses resistors connected to each cell to remove extra capacity. The extra capacity is drained through the resistor. Though this method is simpler, energy is being

lost through the resistors leading to less system efficiency [29]. Active balancing uses capacitors or inductors that are shuttled between cells to move some of the capacity from higher charged cells to lower charged cells. This method is more complex but less energy is lost [29].

Other Energy Storage Methods

Although battery technology is the most popular energy storage technology, other energy storage technologies exist. Two other energy storage devices are ultracapacitors and flywheels.

Capacitors are used to store energy for short periods of time. However, they can provide and accept high levels of power. Ultracapacitors are double layer capacitors that have increased energy storage capacity resulting from the large increase in surface area gained from using a porous electrolyte. These devices are currently best used for high peak power, low energy applications. These devices are light and small. They can also hold full charge for up to ten years [22].

Flywheels are mechanical, rotational devices that can store energy for power systems when they are coupled to electric machines. The stored energy is dependent on the flywheel's moment of inertia and the square of the rotational velocity of the flywheel. When the machine acts as a motor, energy is transferred to the flywheel as the flywheel accelerates. The flywheel discharges energy when the electric machine slows the flywheel down and regenerates through its drive. Flywheels are considered for use with automobiles, buses, and locomotives [22].

2.4 Primary Power Units

Along with the energy storage system, the primary power unit is perhaps the most important component in a hybrid power system. The primary power unit is responsible for charging the battery and meeting load demand at any given time of operation. Proper supervisory control of the primary power unit is crucial in limiting its fuel consumption.

Three primary power unit options are introduced in this section: the internal combustion (IC) engine generator, the fuel cell, and the microturbine.

Internal Combustion Engine Generators

An internal combustion (IC) engine generator is the most common primary power unit used in hybrid power systems. The IC engine generator is composed of an IC engine coupled with an alternator (or electrical generator). This alternator converts the mechanical power created by the engine into electrical AC power.

While IC engine generators are common, well known, and not expensive, their major disadvantage is their poor fuel efficiency and performance at low load. An IC engine has an efficiency map similar to the one shown in Figure 9 [30]. The contours show levels of engine efficiency. In this representative figure, the island of peak efficiency exists around 2000 rpm and 50kW. In an IC engine generator, the engine is usually governed to run at a constant rotational speed, usually at 1800rpm for 60Hz power.

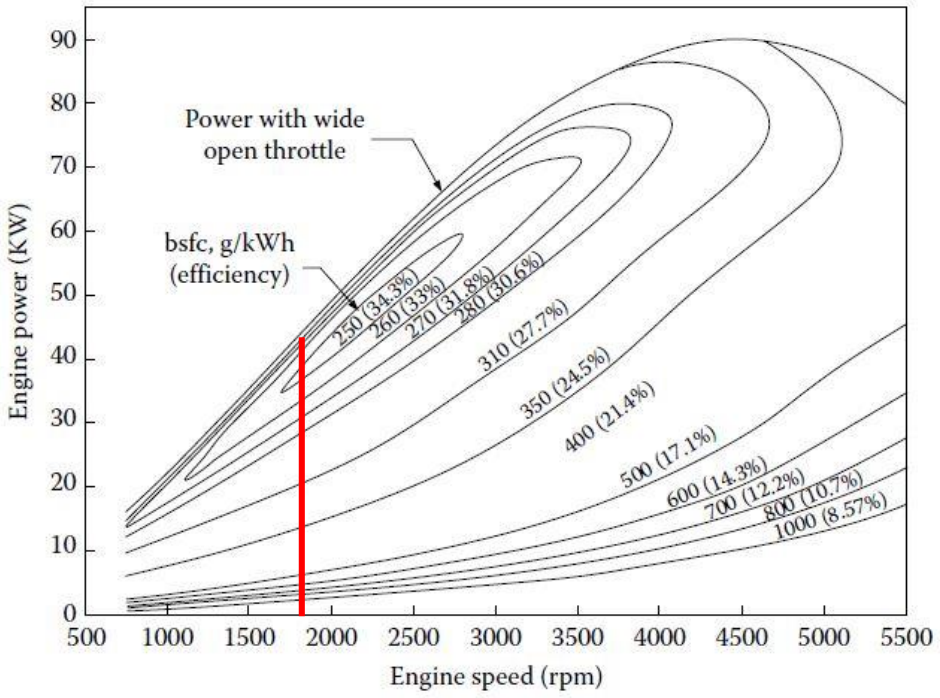

Figure 9: Efficiency Map for IC Engine [30]

Image from M. Ehsani, Y. Gao and A. Emadi, "Chapter 3: Internal Combustion Engines," in *Modern Electric, Hybrid Electric, and Fuel Cell Vehicles: Fundamentals, Theory, and Design - 2nd Edition*, Boca Raton, Florida, CRC Press, 2010, pp. 67-104. Used under fair use, 2015.

The red line on the plot corresponding to 1800rpm shows the cross-section of this engine efficiency map where the generator's engine operates. Figure 10 shows a representative engine efficiency curve at this operating point [31]. In this plot, the engine's output power has been normalized to 100%. An IC engine generator is not very efficient overall in converting the chemical energy of the fuel into electrical energy, with peak efficiency between 30 and 40%. At low loads, this efficiency dramatically decreases [31]. Along with this drop in efficiency, running an IC engine generator at low load can lead to engine damage and reduced reliability [20].

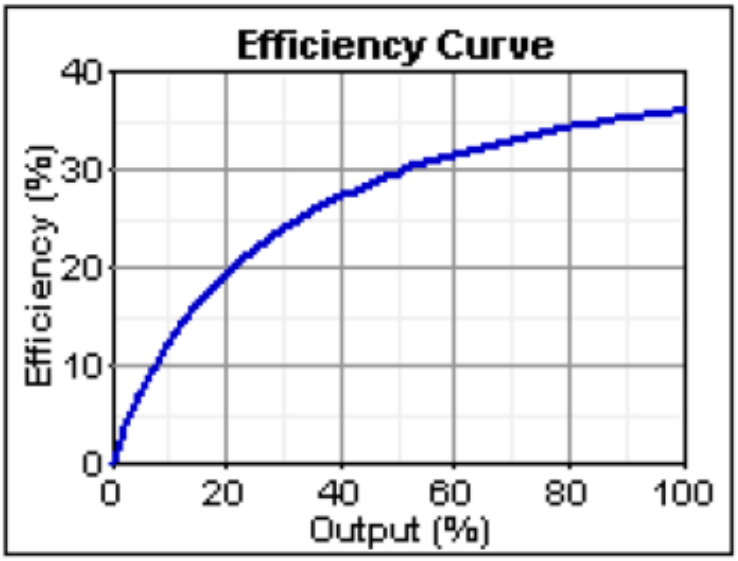

Figure 10: Representative Efficiency Curve of Generator's Engine [31]

Image from A. Stiel and M. Skyllas-Kazacos, "Feasibility Study of Energy Storage Systems in Wind/Diesel Applications Using the HOMER Model," *Applied Sciences*, vol. 2, no. 4, pp. 726-737, 2012. Used under fair use, 2015.

Fuel Cells

A fuel cell uses hydrogen as a fuel to produce electricity, heat, and water. Fuel cells are made of two electrodes (an anode and cathode) separated by an electrolyte. In

this way, they are similar to batteries. In fuel cells, hydrogen is supplied to the anode (negative terminal) and oxygen is supplied at the cathode (positive terminal). A chemical reaction splits the hydrogen into and electron and proton. Each of these particles moves toward the cathode. However, the electrons are directed into a load to produce electricity while the protons move through the electrolyte to the cathode. The two particles and oxygen combine at the cathode to form water [32].

The hydrogen fuel can be supplied from hydrocarbon fuel such as methanol or natural gas. Since electricity is created through a chemical reaction and the only byproduct is water, fuel cells have much cleaner emissions than an IC engine generator [32]. However, fuel cells are much heavier than IC engine generators for the same power output [33].

Microturbines

Microturbines use gas turbine technology to convert hydrocarbon fuel into electrical power. Originally, these devices were used to provide electricity for airplanes and buses. Recently, this technology has been used to provide power to the grid. These devices can provide power from around 15kW up to 1200kW. These devices are compact, lightweight, reliable, and require low maintenance. With recuperation of heat from exhaust gases, the thermal efficiency of these devices can reach 30%, which is similar to an IC engine's thermal efficiency. While these devices have many exciting advantages, low power versions (<15kW) of these devices are still being developed. Also, their high frequency power output (in the range of kHz), requires special AC/DC rectification to be used to charge batteries or power normal loads. On top of this drawback, microturbines produce high noise levels that require special acoustic systems to reduce [34]. Nonetheless, microturbine technology may become a realistic primary power unit alternative for future hybrid power systems.

2.5 Dispatch Strategies

This section will cover energy dispatch strategies that have been used for small-scale hybrid systems. The term "dispatch strategy" is used to describe how energy flow in

a hybrid energy system is managed and controlled [35]. Many of these dispatch strategies are based on optimization of one or several system parameters like efficiency, cost, or system reliability. This section will begin with describing possible dispatch strategy goals. It will then cover two of the major dispatch strategies: State of Charge (SOC) Set Point and Load Following. Other dispatch strategies will be summarized, including ones that use load and renewable energy prediction, as well as load shedding. The majority of the dispatch strategies described in this section use an IC engine generator as the secondary power source. A dispatch strategy using a fuel cell as the secondary power source is described briefly at the end of this section.

2.5.1 Dispatch Strategy Goals

The selection of a dispatch strategy is highly dependent on the hybrid energy system design goal. A hybrid energy system can be designed for one goal or a combination of several [36]. It should be noted that although a design goal may influence the selection of a particular dispatch strategy, the dispatch strategy that best fits an application is often determined through detailed analysis and modeling. A few of these possible design goals are covered in this section.

Best Economic Operation

For many hybrid energy system applications, the goal is to minimize the cost of operation and maintenance (O&M) of the system. This goal usually incorporates running the IC engine generator at its best efficiency levels to save fuel and to extend the life of the generator. Also, energy dumping is avoided. This goal does not necessarily extend to using the full amount of solar energy or minimizing the carbon footprint of the system [36]. This thesis's goal of limiting fuel consumption relates to the goal of best economic operation, but is not completely the same. This thesis does not take into account maintenance costs related to servicing the generator, battery pack, or power conversion components.

Highest Reliability

If highest reliability is the goal, scheduled maintenance of the system becomes a priority. Scheduled maintenance is done for the secondary power source, battery pack, and power conversion components. This continued maintenance of the system will usually increase maintenance costs. This goal may also impact service delivery, as a secondary power source may be periodically unavailable due to scheduled maintenance [36], [37].

Lowest Carbon Footprint

With the increased awareness of global warming and climate change, many hybrid energy systems have been designed with greenhouse gas emission and carbon footprint in mind. The goal of decreasing carbon emissions leads to the maximization of energy used from renewable energy sources to minimize petroleum-based secondary power source operation. Designing for this goal may lead to increased start-stop cycles for secondary power source equipment [36].

Service Delivery Optimization

Service delivery optimization is important when uninterrupted power is required for a critical load. Many power generation systems with multiple generators will size the generators to be slightly larger than the required power output. This practice is done so that if one generator fails, the other generators in the system have enough extra energy stored in their rotational inertia to continue meeting the power demand without a significant change in power flow or AC frequency. This extra energy stored in the generator's rotational inertia is called "spinning reserve" [38]. The practice of using spinning reserve in a generation system requires one or several generators to run at lower than optimal power output [37]. Running generators at lower than optimal power output requires higher O&M costs and reduced system lifetimes [36].

Battery Lifecycle Optimization

Battery lifecycle optimization focuses on maximizing the lifetime of the batteries. Designing for this goal leads to component sizing and generator control schemes that will optimize the battery cycling for extended battery life [36].

Load Optimization

Designing for load optimization requires that the power demand on the energy system can be controlled. Power demand is controlled by deferring loads to periods with plentiful solar or wind power input. By deferring these loads "energy storage demands can be minimized and generators are able to operate at better efficiencies" [36]. Optimizing the load through demand side management is often used when the system's energy storage capacity is limited [36]. Also, designing for this goal requires that the loads are not time critical.

Best Quality of Support

This goal of best quality of support focuses on maximizing the electricity quality. Maximizing electricity quality usually prioritizes variables like voltage range and harmonic distortion. Designing for this goal may require using generators as spinning reserve, which will decrease the efficiency of the system and increase costs [36].

2.5.2 State of Charge (SOC) Set Point Strategy

One of the most common dispatch strategies is the State of Charge (SOC) Set Point strategy [35]. This strategy is popular because it is simple to implement, reliable in meeting the load, and allows for the batteries to be cycled appropriately for increasing their lifetime [36]. The SOC Set Point strategy works by turning on the IC engine generator to charge the battery pack whenever the battery pack discharges to a predetermined low capacity set point, SOC_{low} (between 0 and 100% SOC). Usually, SOC_{low} is the lowest SOC the battery manufacturer determines is safe for the battery to discharge to. The IC engine generator will run at full power (maximum efficiency) to meet the system load and charge the battery pack with the excess power until the battery

pack SOC reaches the predetermined high set point, SOC_{high} [35]. The value of SOC_{high} can be changed to minimize the operating cost for the system under this dispatch strategy [35]. Barley and Winn advise that there is no advantage to charging a battery pack to completion, so SOC_{high} will usually be set a significant amount lower than 100% SOC [35]. Figure 11 shows the logic flow for this strategy.

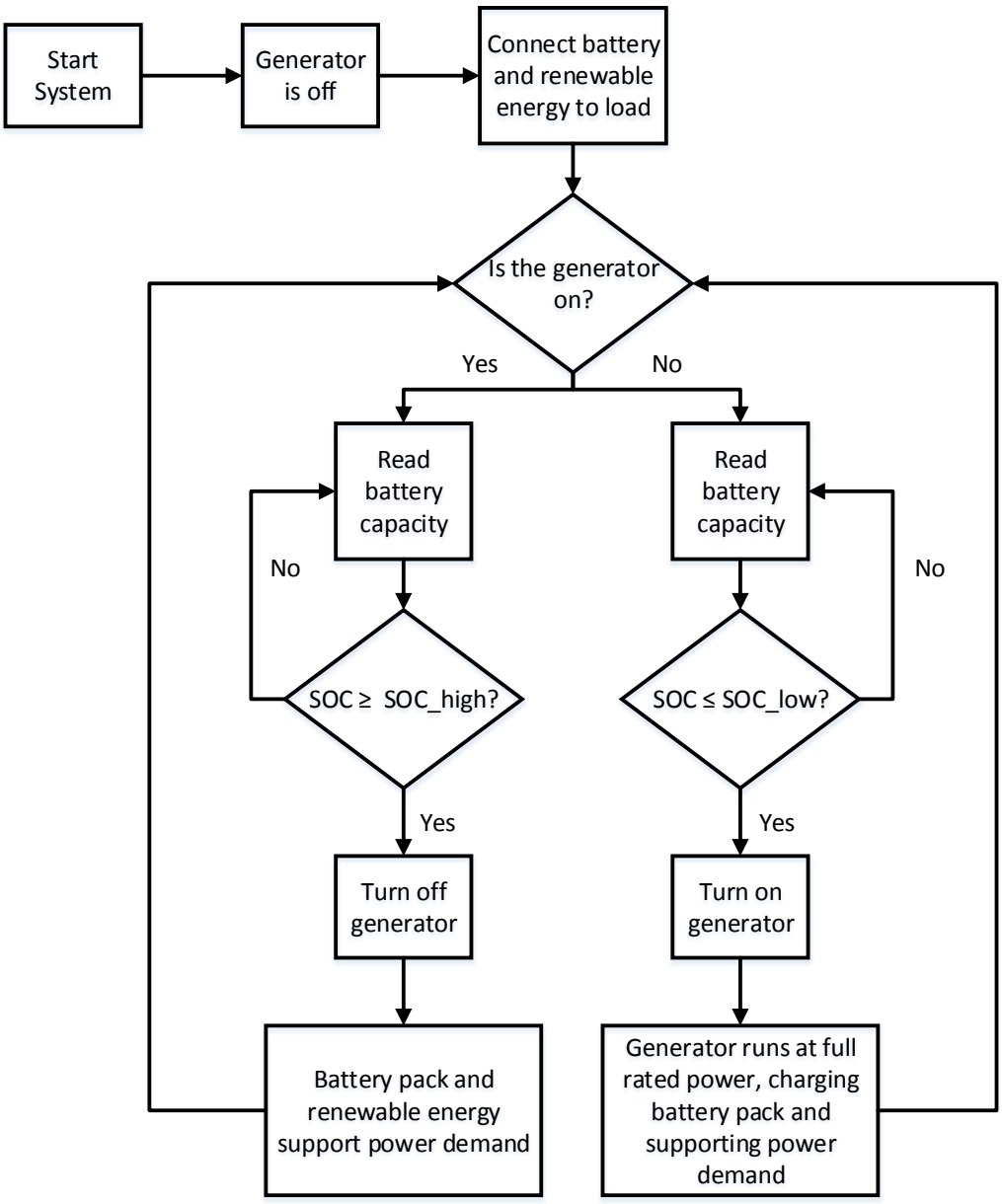

Figure 11: Logic Flow for State of Charge (SOC) Set Point Strategy

2.5.3 Load Following Strategy

Another common dispatch strategy is the Load Following strategy. Under this strategy, the IC engine generator does not charge the battery pack. All battery charging is supplied by renewable energy (i.e. solar or wind power) [36]. The IC engine generator will meet the system load whenever the load increases beyond a predetermined set point. The generator will continue to meet the load on the system while the load exceeds this set point. If the load is below the set point, the battery pack and renewable energy sources will meet the load; the generator will be off. Under this strategy, the generator would avoid running at low loads where it is less efficient and incurs more risk of damage. A higher load set point would lead to decreased usage of the IC engine generator [39]. An alternative to shutting the generator down at low system loads would be to have the generator charge the battery pack with the excess power whenever the system load decreases below the load set point [35]. A minimum run time for the diesel generator could also be applied to avoid excessive start/stop frequency [35]. Figure 12 shows the logic flow for this strategy.

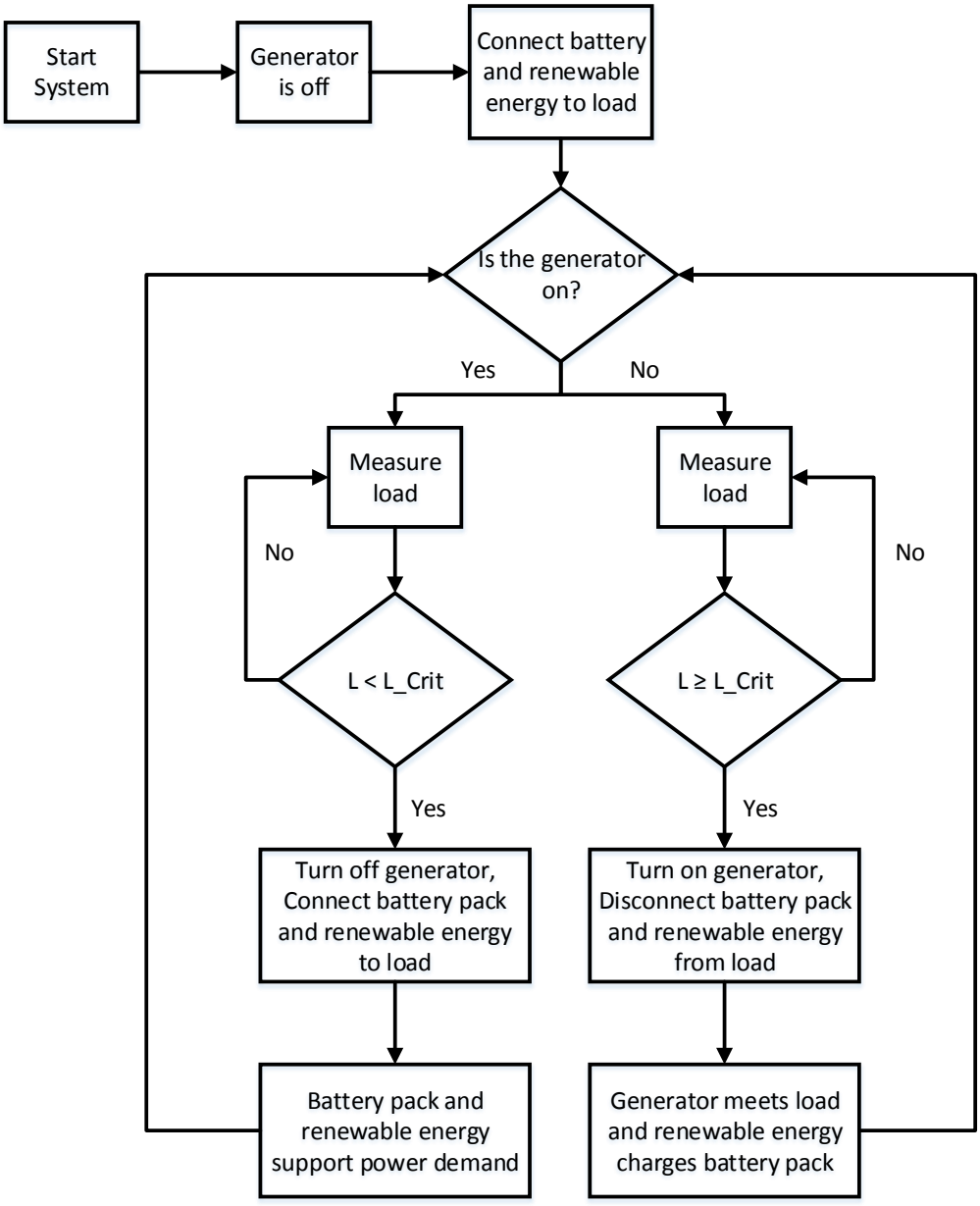

Figure 12: Logic Flow for Load Following Strategy

2.5.4 Other Dispatch Strategies

There are many other dispatch strategies used for hybrid energy systems, both in research and in practical application. Other dispatch strategies include: the Full-Power Minimum Run Time (FPMRT) strategy, the Frugal Discharge strategy, strategies including prediction and load shedding, and a strategy for systems with fuel cells.

Full-Power Minimum Run Time (FPMRT)

Another prevalent dispatch strategy is the Full-Power Minimum Run Time (FPMRT) strategy, where the IC engine generator will run at its full rated power for a minimum time span whenever it needs to turn on. While the generator is running, it is meeting the system load and charging the battery pack with the excess power [35]. In this strategy, the generator could either start at a predetermined low SOC set point [35] or at a scheduled time each day [36]. If the generator starts at a low battery SOC this dispatch strategy will yield similar results to the SOC Set Point strategy with a lower maximum SOC set point [35]. If the generator is scheduled to start a certain time each day, it could be difficult to optimize the battery charging according to fluctuations in the daily renewable energy input [36]. A common time for the generator to start is in the evening when there is no available solar energy to meet power demand. However, running the generator at this time may be wasteful if there is low night-time power demand [39].

Frugal Discharge Strategy

Overall, the Frugal Discharge strategy focuses on minimizing O&M costs. This strategy is similar in operation to the Load Following strategy, except the load set point is determined based on where the battery wear cost per kWh begins to exceed the IC engine generator's wear and fuel cost per kWh. If the system load exceeds this set point, the generator will meet the load. Once the load falls below this set point, the generator will shut off and the battery pack and renewable energy will meet the load [35]. This strategy runs under the premise that it is more expensive to replace batteries worn down from consistently running at high loads than it is to maintain, replace, and fuel a generator consistently running at high loads. This premise may remain true, but it should be noted that when Barley and Winn presented this strategy in 1996, the average fuel cost they used for set point calculation was $1.00/gallon [35]. Also, battery technology has evolved greatly since 1996. This strategy should be revisited taking into account fuel and battery costs that reflect the present day market.

Dispatch Strategies with Prediction and Load Shedding

Predicting future load and renewable energy input may help conserve IC engine generator usage and fuel consumption. By predicting future periods of high renewable energy supply and/or low power demand, the logic controller of a hybrid energy system can shut down the IC engine generator earlier. Shutting down the generator earlier will leave large enough capacity in the battery pack to accommodate the future renewable energy supply. Barley and Winn studied the possible impact of prediction as early as 1996. From that study, they determined that the possible cost savings gained from a prediction-based strategy are not significantly more than using a properly designed, less complex strategy like the SOC Set Point, Load Following, or Frugal Discharge strategy. They found that avoiding charging the battery pack to high states of charge can have the same effect on system performance as prediction, since this extra battery capacity could be charged by renewable energy available in the future [35].

Despite these findings, there have been many recent studies that have incorporated load and renewable energy prediction into an energy dispatch strategy. For example, Yamamoto et al. studied a strategy where a forecast of photovoltaic production and an hourly load profile were used to decide when the generator should be turned on and what level to set its output power. Under this dispatch strategy, the generator would only start whenever the battery SOC was between 50% and 70% and would always stop once 70% SOC was reached [40], [41].

Recently, prediction has been used in coincidence with load management, or load shedding. Load management is the structured disconnecting and reconnecting of system loads done to improve a power system's operation. Load management usually becomes an integral facet of an energy dispatch strategy when a system has limited or no energy storage capacity [36]. In these cases, the loads are deferred to times when greater renewable energy is available [36]. Deferring or shedding loads is only a viable option if the loads are non-critical, meaning no severe consequences will occur if these loads are shed.

One of the earliest load management strategies was employed by Groumpos et al. in 1984 for a standalone photovoltaic system in Arizona, where four loads were shed in order at four certain battery SOCs (50%, 40%, 30%, and 20%). The first load would be shed whenever the battery discharged below 50% SOC; the second load would be shed whenever the battery discharged below 40% SOC; and so on until the final load would be shed at 20% SOC. As the battery pack recharged, these loads would be reconnected in the reverse order at the same SOC set points [40], [42]. Classification of loads based on priority (convenient, essential, critical, and emergency) was included in load management strategies by Groumpos and Papegeorgiou and by Khouzam and Khouzam [40], [43], [44] .

Over time, load management strategies for hybrid and renewable energy systems evolved to incorporate some degree of forecasting. In Moreno et al., prediction of future loads was performed using fuzzy logic to determine when to shed lower priority loads [40], [45]. In Lujano-Rojas et al., an autoregressive moving average (ARMA) model was used to forecast wind power. In this work, the controllable loads were deferred to times of peak wind turbine power production, reducing the diesel generator operation time [40].

Dispatch Strategy for Fuel Cells

All of the dispatch strategies described in this section are primarily intended for systems using an IC engine generator as their primary power source. An IC engine generator is not used in every hybrid energy system. Instead, a few hybrid energy systems use a fuel cell as the primary power source. One dispatch strategy specific to fuel cells is summarized in this section for demonstration purposes only and is not all-inclusive.

Eroglu et al. present a dispatch strategy that is specific to a fuel cell in their mobile house project. In their hybrid energy system, renewable energy and a battery pack are used primarily to meet power demand until the state of charge of the battery pack discharges below 50% SOC and the power demand exceeds the power production of the renewable energy sources. Once this occurs and if enough hydrogen fuel is available, the fuel cell is started and meets the load directly while the renewable energy sources and battery pack are disconnected from the load. The renewable energy sources will charge

the battery pack while the fuel cell is meeting the power demand. This configuration will continue until the battery state of charge increases above 50% SOC or the power production from the renewable resources begins to exceed the power demand. When this occurs, the fuel cell will shut off and the renewable energy sources and battery pack will meet the load again [9].

2.6 Power Conversion

While IC engine generators and renewable energy sources provide power, and a battery pack provides energy storage for the hybrid power system, power conversion equipment is required to properly deliver the power to the energy storage and loads. This section explains the power conversion equipment necessary in a hybrid system. A discussion on converter efficiency is also included.

2.6.1 Necessary Hybrid System Conversion Equipment

There are three pieces of conversion equipment commonly used in hybrid power systems: rectifiers, DC-DC converters, and inverters. A fourth piece of conversion equipment is also covered, the solar charge controller, though it is a special DC-DC converter used for harnessing power from solar panels.

AC-DC Rectifiers

Rectifiers are used to convert AC power to DC power (e.g. converting an IC engine generator's AC power to DC power for charging a battery pack). These components achieve this conversion using a configuration of diodes and filter circuits that help transform the cyclical AC voltage into an almost steady DC voltage. Common rectifier circuits are the half wave rectifier, full wave rectifier, and bridge rectifier. The bridge rectifier is preferred because it has high efficiency while not reducing the voltage [46]. This thesis does not get into the details of how these rectifiers function.

Rectifiers are crucial components in power supplies and battery chargers. This thesis sometimes refers to power supplies and battery chargers as "rectifiers" though, in

reality, these devices include other power conditioning circuitry and are not merely rectifiers.

In some hybrid power systems multiple rectifiers are required to share and convert AC power beyond the power requirements of a single rectifier. In these situations, the rectifier outputs need to be paralleled to charge the battery pack. Special care is needed to parallel these rectifier outputs correctly to avoid damaging them.

DC-DC Converters

DC-DC converters are used to convert DC power at one voltage to DC power at a different voltage (e.g. converting battery power to 24VDC power for DC loads). Several different types of DC-DC converters exist: series converters, shunt converters, charge pump converters, series-parallel step-up converters, series-parallel step-down converters, and inductive type converters [47]. More detail on how these converter types work can be found in Chapter 2 of *Design and Implementation of Fully-Integrated Inductive DC-DC Converters in Standard CMOS* by Wens and Steyaert. When multiple DC-DC converters are used in parallel, special care should be used when paralleling the outputs to avoid damaging the converters.

DC-AC Inverters

Inverters are used to convert DC power to AC power (e.g. converting battery power to 120VAC power for loads). Information on how inverters work can be found in "An Introduction to Inverters and Applications" by Reitsma [48]. To tie an inverter's power output to an AC power grid, the inverter needs to have phase matching capability.

Solar Charge Controllers

Solar charge controllers are important in converting solar power into power that can be used to charge a battery pack. Many solar charge controllers use Maximum Power Point Tracking (MPPT) to draw the maximum power from solar panels. In many ways, solar charge controllers are elaborate DC-DC converters that are able to vary their input voltage to find the solar panels' maximum power point.

2.6.2 Converter Efficiency

The efficiency of power conversion equipment is not usually a constant parameter. Efficiency can depend on load and temperature. Figure 13 shows an efficiency vs. load plot for one of the converters used in the HEIT prototype system [49]. As can be seen in the figure, efficiency is not constant for all load currents. In fact, at very low load currents conversion efficiency can decrease dramatically.

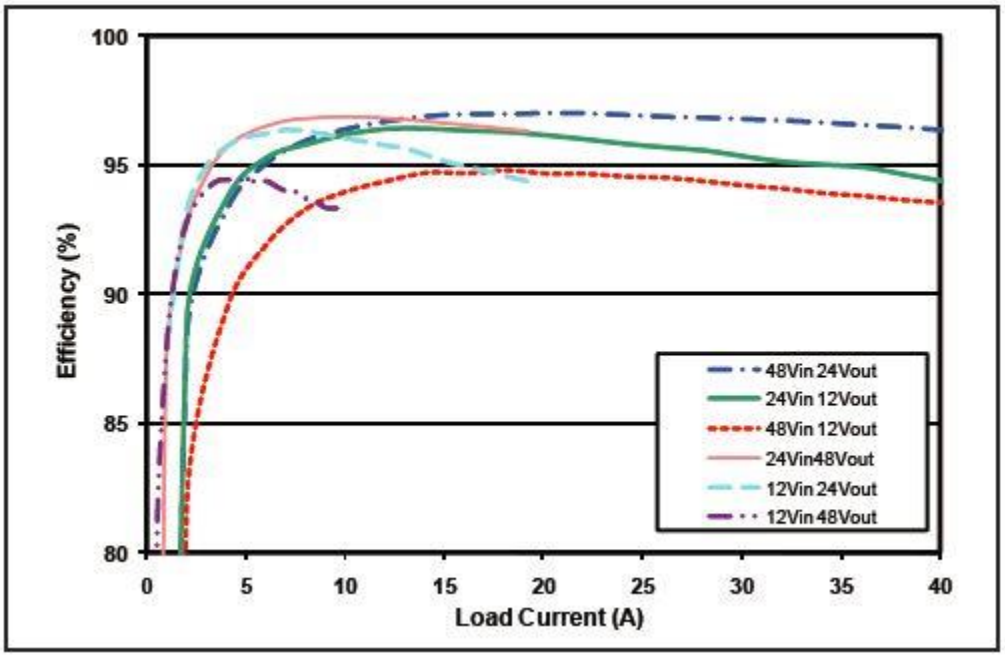

Figure 13: Efficiency versus Load Current for Converters used in Prototype System [49]

Image from SynQor, Inc., *Technical Specification: NQ60W60HGx40,* Boxborough, Massachusetts: SynQor, Inc., 2013. Used under fair use, 2015.

3 Description of Model

An accurate and well thought-out model needs to be used to evaluate the many hybrid system design options. This section covers how this system model is created. Each major component's modeling strategy is described. The strategies for modeling the load profile, generator, battery pack, solar panels, conversion equipment, and cabling are discussed in order. Then the models for each individual component are combined into one large system model. Finally, the process of determining the weight-based fuel penalty is described.

3.1 Load Profile Model

In the simulation process, first a load profile is chosen and then it is distributed among DC and AC loads. The mobile hybrid system used in this analysis has three receptacles for 120VAC loads and three receptacles for 24VDC loads. This section will also explain how load is divided amongst these receptacles during simulation.

A different load profile is used for validation of the simulation than is used for determining the most fuel efficient system design. The validation load profile (shown in Figure 14) is from data measured during a 26.7 hour test of the HEIT prototype system. During prototype testing a ~1300W resistive load bank was connected to the prototype system. The voltage and current of the prototype system's DC output were sampled at 1Hz with transducers while the system was delivering power to the load bank. The resulting load profile is mostly constant around 1280W with a standard deviation of 60W. There are four sudden drops of load during the load profile. The first three (at 0.5 hours, at 9.1 hours, and at 18 hours) correspond to when the generator starts. During the starting of the generator, the prototype system disconnects from the load. The fourth and last drop of load (at 25.8 hours) occurs because the prototype system was restarted to correct a communication loss. The system computer lost communication with the battery management system and stopped updating the battery data. A quick restart of the system

(the system was down for 2 minutes) fixed this communication issue. Although these drops of load are problems that will need to be fixed in future revisions of the prototype, they are still included in the load profile used by the simulation for validation.

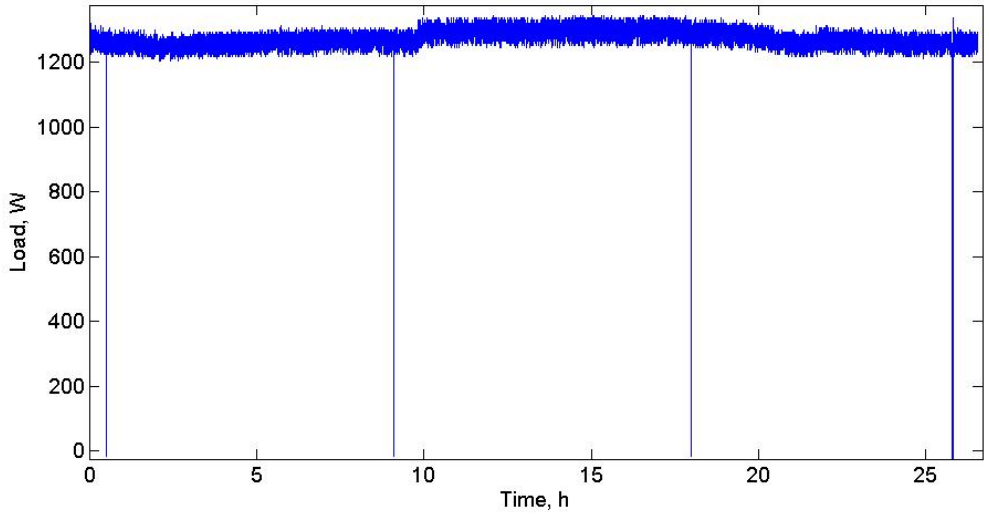

Figure 14: Validation Case Load Profile

The target load profile for which the most fuel efficient system design is determined is shown in Figure 15. This load profile is the company Command Operations Center (COC) metered profile from the Mobile Electric Hybrid Power System (MEHPS) Analysis of Alternatives (AoA) report [13]. This load profile is reproduced for use in the simulation using the open source Plot Digitizer 2.6.6 software. The digitized profile is resampled to match the 1 sample per minute sampling rate shown in the AoA report [13]. The peak load experienced in this load profile is 4.8kW, but the average load is approximately 2.3kW.

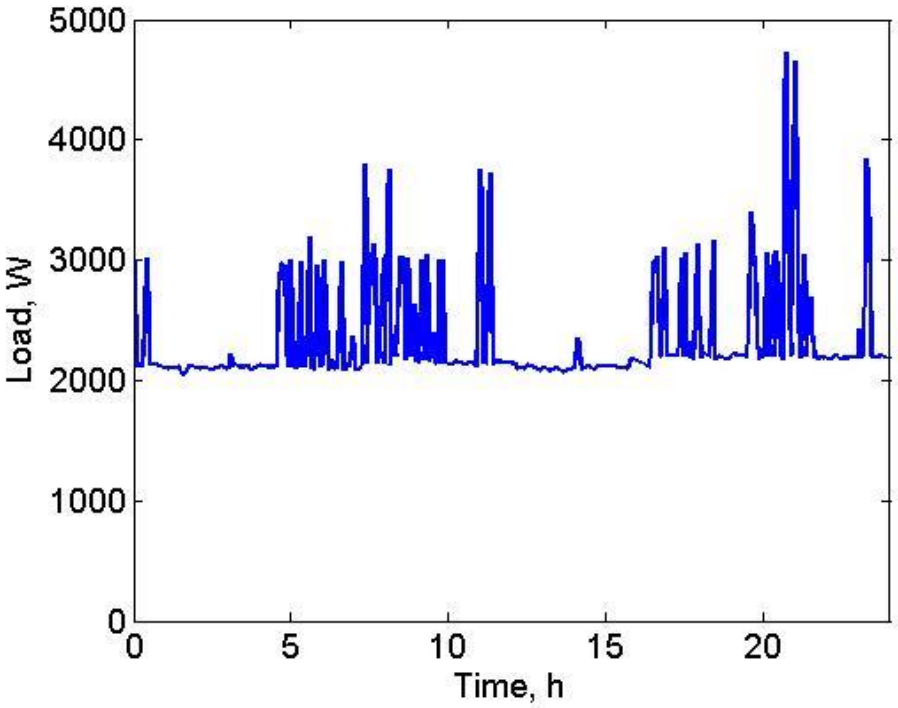

Figure 15: Company COC Metered Load Profile from MEHPS AoA Report

Although the focus of this thesis is to design a mobile hybrid electric system that minimizes fuel consumption given the company COC metered profile in Figure 15, the simulation is run again to analyze the impact of two alternative profiles shown in Figure 16 and Figure 17. The first alternative profile includes extended time spans of high load. This alternative profile is different from the company COC profile where high loads are only experienced for a few minutes at a time. This more aggressive alternative load profile was manufactured by the author to see how a load profile with longer duration of high load impacts system design and fuel consumption. Like the company COC profile, this alternative profile is implemented at a rate of once per minute. The time intervals between 0 and 5 hours and between 11 and 17 hours have constant load equal to 2.2kW. Between 5 and 11 hours the load is a constant 3.5kW and between 17 and 24 hours the load is a constant 4kW. These periods of high load correlate with the same periods of high load seen in the company COC profile.

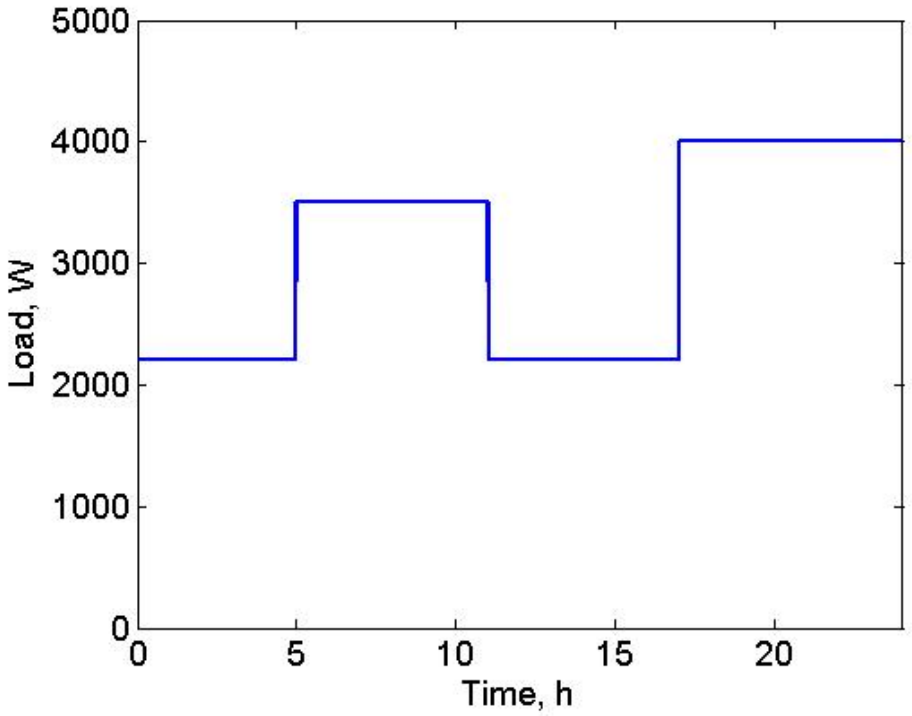

Figure 16: Aggressive Load Profile

The second alternative load profile is the residential load profile that was shown in Figure 4 (and again in Figure 17). This load profile was selected from an industry study on generators and should be representative of the power demand for a single household. It has peak load of 4550W and an average load of 960W. This profile has many long periods of low load (below 1000W) which is a very inefficient operating point for a stand-alone generator, but may be much more efficient for a hybrid system.

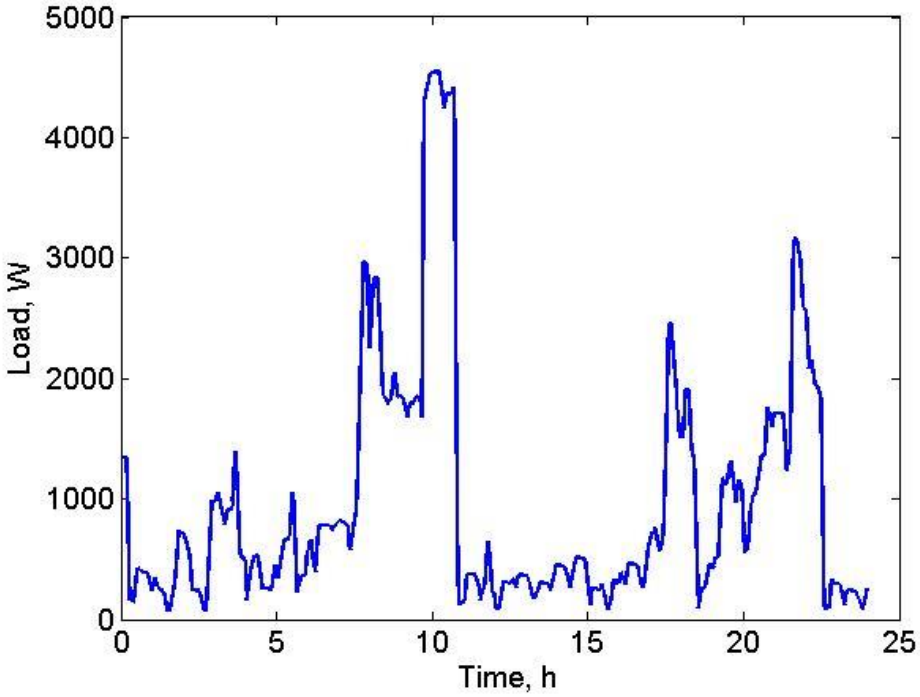

Figure 17: Residential Load Profile from Victron Report

After determining the load profile to be used in the simulation, the load is distributed between AC and DC loads. The fraction of the load devoted to DC loads is set prior to running the simulation. The fraction of the load directed to AC loads is equal to $1 - \mathrm{DC}_{\mathrm{fraction}}$. The load is divided amongst AC and DC loads simply by dividing power at each time step according to these load fractions. For example, if the DC load fraction is 0.3 and the load at one time step is 1000W, the DC load will be 300W and the AC load will be 700W at this time step. By dividing the power at each time step, the DC and AC load profiles retain the same shape as the original load profile but are scaled in magnitude according to their load fraction. In reality, the distribution of the load profile between DC and AC loads would not be the same for each time step. The fraction of the load at each time step devoted to AC or DC loads is dependent on the hardware being powered by the system and on the timing this hardware is being connected to the system. A more detailed load profile analysis would need to be done to get a more accurate distribution between AC and DC loads. A more detailed load profile analysis is outside the scope of this thesis.

After the load is distributed between AC and DC loads, the load is distributed amongst each load receptacle. In this simulation, there are three NEMA 5-20 receptacles devoted to AC loads and three NATO slave receptacles devoted to DC loads. The NEMA 5-20 receptacles are rated up to 20A at 120VAC [50] and the NATO slave receptacles are rated up to 500A at 28VDC [51]. The AC load is applied to only one receptacle up to 20A. When the AC load exceeds 20A, a second receptacle is used to carry the excess current while the first receptacle carries 20A. When the AC load exceeds 40A, a third receptacle is used to carry the excess current while the first two receptacles carry 20A each. Because the peak power of the system is held to 5kW for this thesis, there is never a time when a fourth NEMA 5-20 receptacle is needed to carry AC load. For DC loads, only one receptacle is needed to carry load because the NATO receptacle can accommodate well beyond the 5kW peak load used in this thesis. The other two receptacles are only included to count as extra cable weight for the system. In reality, these receptacles will be connected as the system user dictates. Probably a better model of the load on the system would incorporate distinct load profiles for each individual load receptacle. The overall system load would be the aggregate of the individual receptacle load profiles. However, since only the overall load profile is known for this thesis, the distribution amongst receptacles is left to the author's best judgment.

3.2 Generator Model

The simulation first will check if the selected IC engine generator meets the physical and electrical requirements described in *1.4 Design Parameters*. The generator's longest dimension must not exceed the trailer envelope dimensions. Also, the generator needs to be able to meet the average system load demand (after conversion efficiencies have been taken into account). This average system load demand is the sum of the average AC load and average DC load on the system with conversion efficiencies taken into account. A safety factor of 1.25 is used to determine that the generator's rated power meets the average load demand (i.e. the rated generator power needs to be at least 1.25 times larger than the average load demand, including conversion efficiency losses).

After it is determined that the generator meets the physical and electrical requirements for the application, the IC engine generator's specific fuel consumption curve is used to determine fuel consumption over the simulation. For the validation case, the specific fuel consumption curve was measured for the Northern Lights NL673L4.2 generator used in the prototype hybrid energy system. The test procedure for this measurement is given in *Appendix A: Test Procedure for Measuring Specific Fuel Consumption of Northern Lights 5kW Generator*. The relation of specific fuel consumption to apparent output power measured for this IC engine generator is shown in Figure 18. At higher apparent output power, the generator consumes less fuel.

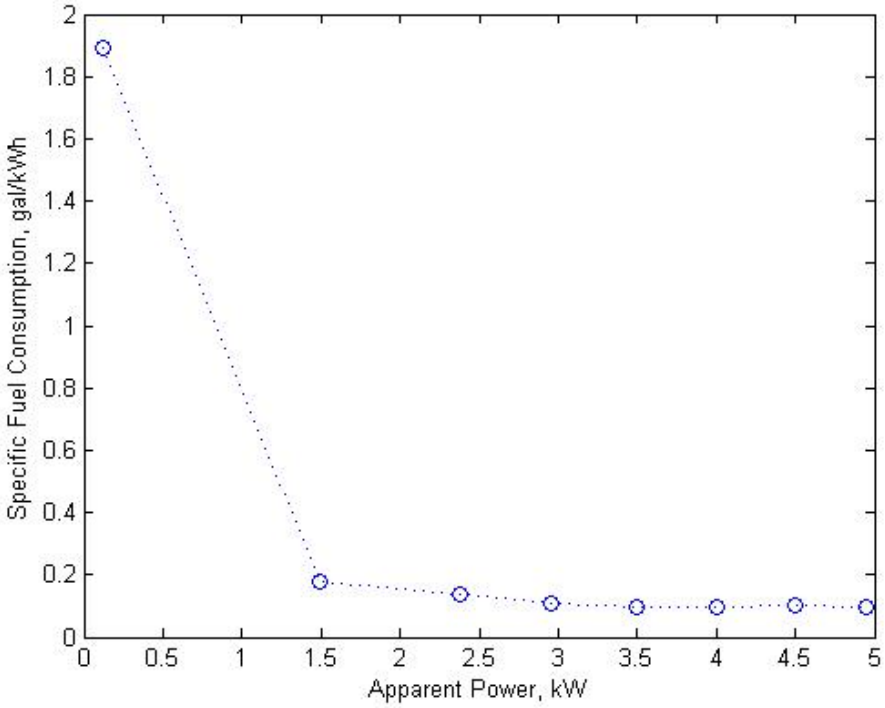

Figure 18: Measured Specific Fuel Consumption of Northern Lights NL673L4.2 Generator

The volume of fuel V_{fuel} consumed over the simulation is found using Equation 1, where $P_{Gen,i}$ is the generator's average output power at the i^{th} time step, $SFC(P_{Gen,i})$ is the specific fuel consumption evaluated at the interval's average output power, Δt is the time interval of one iteration, and N is the number of time steps in the simulation.

Equation 1: Fuel Consumption over Simulation

$$V_{fuel} = \sum_{i=1}^{N} SFC(P_{Gen,i}) P_{Gen,i} \Delta t$$

In the prototype system, the Northern Lights generator is set to run at an approximately constant 4.5kW apparent power whenever it is running. The prototype system uses the SOC Set Point dispatch strategy, where the generator will turn on whenever one of the batteries in the battery pack discharges to 20% SOC. The generator, running at the constant 4.5kW power output, will meet the system load and charge the battery pack with the excess power until one of the batteries in the battery pack charges to 99% SOC. Therefore, $P_{Gen,i}$ is set to 4.5kW whenever the generator is running in the validation case of the model. The specific fuel consumption SFC also remains constant whenever the generator is running. This specific fuel consumption value is derived from the measured specific fuel consumption curve for the Northern Lights generator. The time interval Δt is also constant throughout the simulation. Because the values of the parameters in Equation 1 are constant, the validation case fuel consumption is proportional to the amount of time the generator is running.

For the validation case, the generator's fuel consumption is proportional to generator run time because the system is employing the SOC Set Point dispatch strategy. In fact, any hybrid electric system using an SOC Set Point dispatch strategy will consume fuel in proportion to the generator run time. For simulations beyond the validation case, the selected generator's iterative power output $P_{Gen,i}$ is equal to the rated full power output for that generator. The iterative specific fuel consumption $SFC(P_{Gen,i})$ is equal to the specific fuel consumption given in the selected generator's specifications for that rated full power output.

3.3 Battery Model

The performance of the battery is modeled in the simulation in two different ways to analyze the impact of using a more complex model. Both methods use a simple

voltage-resistor model. The first method uses constant values extracted from the battery's specifications for the open circuit voltage and internal resistance. The second method uses test data to determine the open circuit voltage and internal resistance as a function of battery state of charge. The two methods are used during validation to analyze how each model impacts the accuracy of the overall system model. However, only the second method is used during the design phase. In this section, the voltage-resistor model and the two different methods will be explained in more detail. This section will also describe SOC correction method used to increase the accuracy of the fuel consumption estimate.

3.3.1 Voltage-Resistor Model

One of the simplest battery models to use is the voltage-resistor model. In this model the battery is modeled as a voltage source in series with a resistor [52]. Figure 19 shows the modeled circuit. The voltage source has voltage V_{OC} which is the open-circuit voltage of the battery pack. The resistor has resistance R_{int} which is the internal resistance of the battery pack. The other resistor shown has resistance R_{load} and this is the load on the battery. The current I_{batt} being discharged from the battery is also pictured. This current is positive when the battery is discharging and negative when the battery is charging.

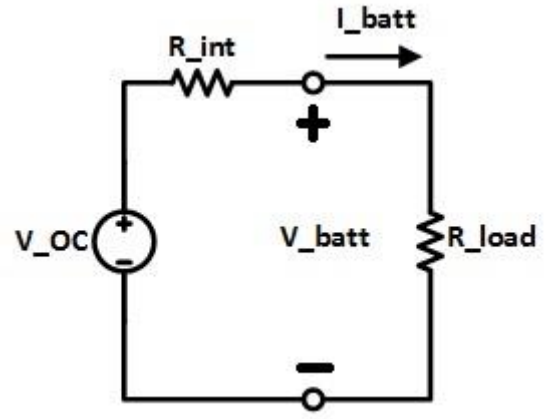

Figure 19: Voltage-Resistor Battery Model

The voltage V_{batt} is the voltage read at the battery terminals and is described in Equation 2 for the i^{th} iteration of the simulation [52]. The open circuit voltage and internal

resistance of the battery need to be determined. These terms are dependent on many factors including the battery's state of charge and temperature [52], [53]. One estimation method for the open circuit voltage is the Shepherd model which factors in the battery capacity along with an exponential component [52]. However, the parameters described in the Shepherd model are not easily obtained from a battery's specifications. Therefore, the open circuit voltage $V_{OC,i}$ and internal resistance $R_{int,i}$ have to be estimated in other ways. Two estimation methods are used in this work. The first method simply used the battery pack's listed nominal voltage and maximum internal resistance described in the battery's specifications for $V_{OC,i}$ and $R_{int,i}$, respectively. The second method uses test data for the battery pack to estimate $V_{OC,i}$ and $R_{int,i}$ as a function of battery SOC. These methods are described further in the next two subsections.

Equation 2: Voltage-Resistor Battery Model

$$V_{batt,i} = V_{OC,i} - I_{batt,i}R_{int,i}$$

The current $I_{batt,i}$ needs to be determined using Equation 3, where $P_{batt,i}$ is the power being delivered to and from the battery pack's terminals at the i^{th} iteration. This term $P_{batt,i}$ is calculated using the known load profile, generator power, and solar power profile along with the known converter efficiencies and cable resistances. More detail on calculating the battery terminal power $P_{batt,i}$ can be found in *3.7 Overall System Model*.

Equation 3: Battery Current

$$I_{batt,i} = \frac{P_{batt,i}}{V_{batt,i}}$$

Because the battery terminal voltage $V_{batt,i}$ is found using the battery current $I_{batt,i}$, Equation 2 needs to be substituted into Equation 3 and rearranged to solve for $I_{batt,i}$. When this substitution and rearrangement is carried out, the result is the quadratic equation shown in Equation 4. This equation is solved for $I_{batt,i}$ using the quadratic formula. The resulting solution is shown in Equation 5. This equation yields two solutions. However, the larger of the two solutions (the one using the "+" term) is ignored

because it is a value that gives unrealistic results. Using this value would lead to battery current orders of magnitude higher than the real current and battery voltage orders of magnitude less than the real battery voltage.

Equation 4: Battery Current Quadratic Equation

$$0 = R_{int,i}{I_{batt,i}}^2 - V_{OC,i}I_{batt,i} + P_{batt,i}$$

Equation 5: Solution to Battery Current Quadratic Equation

$$I_{batt,i} = \frac{V_{OC,i} \pm \sqrt{{V_{OC,i}}^2 - 4R_{int,i}P_{batt,i}}}{2R_{int,i}}$$

After the battery current is determined, the power loss from the battery $P_{loss,batt,i}$ can be determined for each i^{th} iteration. This power loss is found using Equation 6. This power loss is expelled in the form of heat due to the battery's internal resistance. The amount of energy lost through the battery can be found by integrating the battery power loss term. The total internal battery power $P_{batt,internal,i}$ is then found using Equation 7 for each i^{th} iteration.

Equation 6: Battery Power Loss

$$P_{loss,batt,i} = {I_{batt,i}}^2 R_{int,i}$$

Equation 7: Internal Battery Power

$$P_{batt,internal,i} = P_{batt,i} + P_{loss,batt,i}$$

The battery pack capacity is tracked by integrating the internal battery power over the simulation. Equation 8 performs this integration at each iteration. For the validation of the model, the battery capacity is initialized at 38% of the battery's total capacity. The capacity is initialized to this value to match the prototype test's initial battery pack capacity. For the design phase of this thesis, the initial battery capacity is adjusted for state of charge correction. The subsection *3.3.4 State of Charge (SOC) Correction* covers how the initial battery capacity is changed in more detail. The simulation times t_i and

t_{i-1} in Equation 8 are in terms of hours. The battery pack SOC at the i^{th} iteration can be found by dividing the battery pack's capacity at the i^{th} iteration by the battery's total battery capacity (in Wh) and multiplying by 100%. Because the battery pack's internal power can be both positive (discharging) and negative (charging), the battery capacity and SOC will fluctuate throughout the simulation.

Equation 8: Battery Capacity

$$E_{batt,internal,i} = E_{batt,internal,i-1} - P_{batt,internal,i}(t_i - t_{i-1})$$

The voltage-resistor battery model ignores transient effects that would be better modeled with a model including capacitance [52]. However, this simpler model is still used in this thesis because it is assumed that transient current changes are few and minimal. Transient currents would only last a few milliseconds while the overall simulation time length can be 24 hours or longer. Also, the simulation uses a time step of 1 second for validation and 1 minute for the design phase. These time intervals are too large to monitor transient effects that may only last a few milliseconds.

3.3.2 Simple Model with Constant V_{OC} and R_{int}

The voltage-resistor model described in the previous subsection requires that the battery pack's open circuit voltage V_{OC} and internal resistance R_{int} are known through the entire simulation. The first method for determining these terms uses information available in the battery pack's specifications. The open circuit voltage $V_{OC,i}$ is set to the battery pack's nominal voltage for every iteration of the simulation. Likewise, the battery pack's internal resistance is set to the maximum internal resistance listed in the battery's specifications for every iteration of the simulation.

For validation, two 12.8V Valence U24-12XP LiFeMgPO^4 battery modules are used in series for a pack voltage of 25.6V [27]. This nominal voltage of 25.6V is used for $V_{OC,i}$ throughout the simulation. Four of these Valence U24-12XP LiFeMgPO^4 battery modules are used in parallel. Since the maximum internal resistance of one battery module is 6 mΩ [27], the internal resistance $R_{int,i}$ of the entire battery pack is calculated

to be 3 mΩ for the entire simulation. This internal resistance is calculated by determining the equivalent resistance of four parallel legs of two 6 mΩ resistors in series.

After determining these terms, the rest of the battery model can be carried out from Equation 2 onward.

3.3.3 Simple Model with SOC-dependent V_{OC} and R_{int}

The second method for determining V_{OC} and R_{int} uses test data for the same Valence U24-12XP modules used in the prototype system. Data for the prototype system was collected over the entire lifespan of the system (over 100 hours of operation). This data was collected at one sample per second. Among the parameters recorded were the voltage, current, and state of charge of each individual battery module in the system's battery pack. These parameters are used to determine V_{OC} and R_{int} as functions of battery pack state of charge.

The open circuit voltage of each battery module is found by collecting all the data points where the current to or from a module is close to zero. To find these points of zero current, a threshold of 1 amp magnitude is used. All module data points are isolated where the module current is less than this 1 amp threshold. These voltage data points are plotted versus SOC in Figure 20. A linear regression is fit to these voltage data points to determine a relation between V_{OC} and SOC for one battery module. This linear regression equation is shown in Equation 9. This linear regression fit has an R^2 value of 0.6675.

Equation 9: Open Circuit Voltage vs. SOC for One Battery Module

$$V_{OC} = 0.0036 \times \mathrm{SOC} + 13.045$$

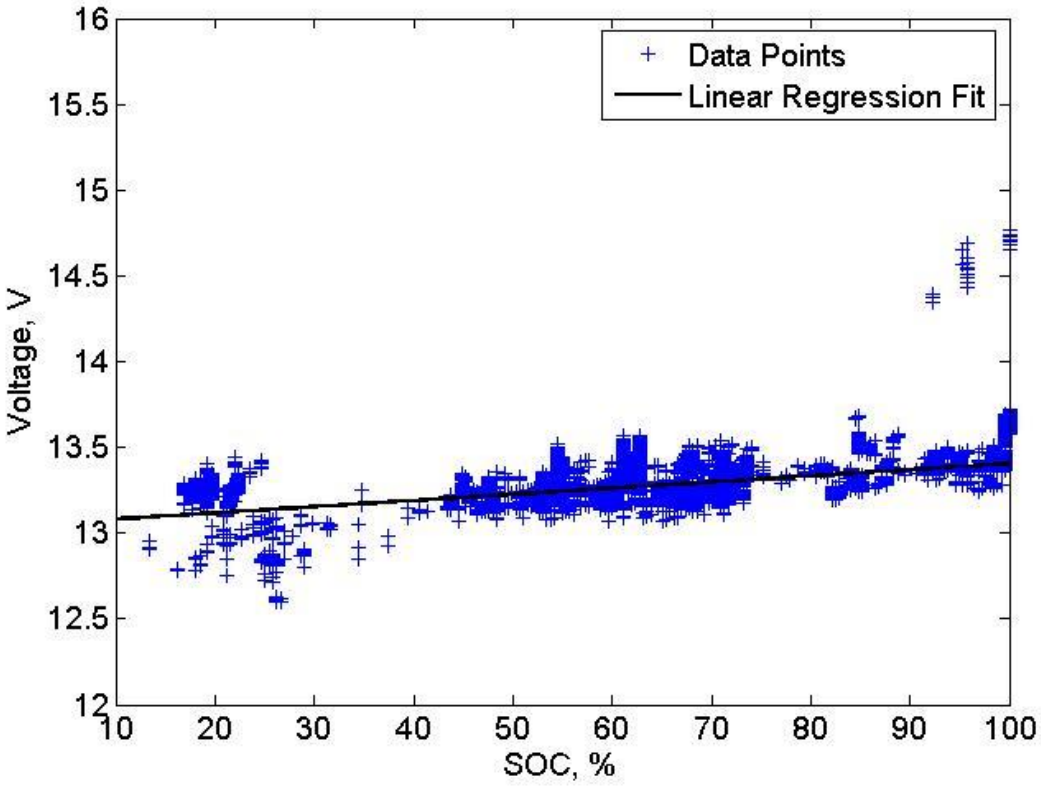

Figure 20: Module Open Circuit Voltage versus SOC

The linear regression described in Equation 9 for one module's open circuit voltage is scaled up to be used for the entire battery pack during validation. Since the prototype system has a 25.6V battery pack, Equation 9 is multiplied by two before being used in the battery model described in Equation 2 onward. For the design phase of this thesis, the simulated battery packs are sized based on individual cells instead of 12.8V battery modules. These individual cells are the Valence 18650 cells that make up the larger U24-12XP modules. These cells have nominal voltage of 3.2V and capacity of 1.35 Ah [54]. In the design phase, battery packs are built out of individual cells to gain more flexibility in the battery pack designs. For the design phase, Equation 9 is divided by four (the number of 18650 cells in series within the U24-12XP module) and then multiplied by the number of cells in series within each battery pack used in the design phase. This scaled relation is then used in the battery model from Equation 2 onward.

A different internal resistance is used during battery discharging than for battery charging. This strategy is used because lithium ion battery packs can have different

internal resistance while discharging than while charging [55]. Therefore, the system data points are divided into two groups: one group with positive battery module current and a second group with negative battery module current. After the data points are separated into two groups, the internal resistance at each data point is determined using Equation 10 for charging and discharging. These internal resistance values are plotted in Figure 21. A 7th-order polynomial is fit to each internal resistance group.

Equation 10: Internal Resistance Calculation for Discharging and Charging Modules

$$R_{int,discharge} = \frac{V_{OC}(\mathrm{SOC}) - V_{module,discharge}}{I_{module,discharge}}$$

$$R_{int,charge} = \frac{V_{OC}(\mathrm{SOC}) - V_{module,charge}}{I_{module,charge}}$$

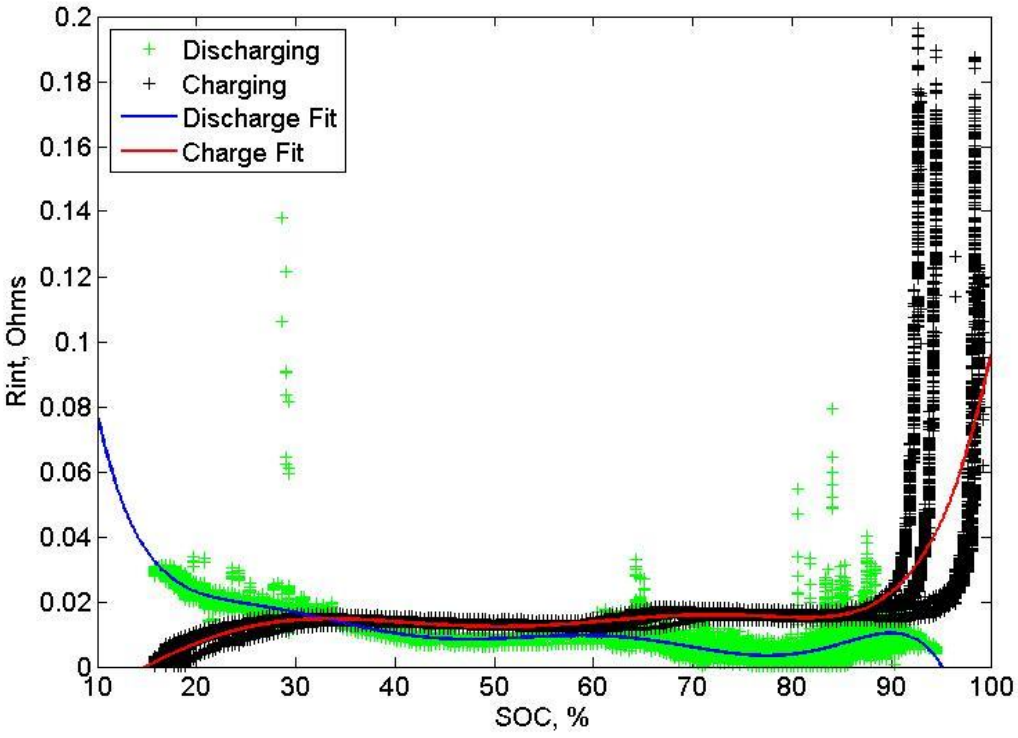

Figure 21: Module Internal Resistance versus SOC for Discharging and Charging

These 7th-order polynomials are used within the larger simulation to determine the internal resistance $R_{int,i}$ at each i^{th} iteration. However, the internal resistance values are first scaled to correspond with the battery pack size. For validation, the internal resistance

values from the polynomial equations are divided by two to find the equivalent internal resistance of the entire battery pack. This division by two was determined by calculating the equivalent resistance of four parallel legs of two equal resistors in series. For the design phase, the internal resistance of an individual 18650 battery cell is determined to be 81/4 of the resistance found using the polynomial equations. Within each U24-12XP module there are 4 cells in series and 81 in parallel. After multiplying the resistance from the polynomial equation by 81/4, the resistance is multiplied by the number of cells in series and divided by the number of cells in parallel to find the internal resistance of the entire battery pack. This internal resistance is then used as $R_{int,i}$ in Equation 2 onward.

3.3.4 State of Charge (SOC) Correction

For an accurate estimation of a hybrid electric system's fuel consumption, the simulation needs to account for the energy stored in the battery pack. This energy stored in the battery pack can skew the fuel consumption results for the system [56]. If more energy is stored in the battery at the end of the simulation cycle than at the beginning, the fuel consumption results for the system will be artificially higher than the actual fuel consumption of the system over the cycle. In other words, more fuel is consumed than necessary to meet the load, and this extra fuel is only being consumed to add energy to the battery pack. On the other hand, if less energy is stored in the battery at the end of the simulation than at the beginning, the fuel consumption results will be artificially lower. The battery pack is supplying energy to the load in a way that could deceive a person into thinking the overall fuel consumption of the system is lower than it actually is. In order to estimate the system's operational fuel consumption correctly, the change in the battery pack's energy from the beginning to the end of the simulation needs to be zero, or at least less than some small predetermined tolerance [56]. The ratio of the change in battery pack energy to the total battery pack energy capacity can be denoted by $\Delta\mathrm{SOC}$, where SOC is the state of charge of the battery pack and is expressed as a percentage. SOC correction is the practice used in simulation and testing to ensure there is zero net energy change in a battery over a cycle.

There are a few SOC correction methods used in testing and in simulation. Many of the methods used in testing are for hybrid electric vehicles, where the system's load profile is derived from the vehicle's drive cycle. SOC correction methods for testing will be discussed briefly. There are three main correction methods used in testing: a continuous repeating method, a linear interpolation method, and the method described in the SAE J1711 test standard [56], [57]. The continuous repeating method is the running of a system through a test cycle multiple times in succession. The fuel consumption values for each individual cycle are then averaged [56], [57]. This average is assumed to be close to the actual fuel consumption of the system according to the law of large numbers, where the average of the results of multiple trials should converge to the expected value for the system as more trials are carried out [58]. The linear interpolation method is the running of a system through a test profile at low initial battery SOC and again at high initial battery SOC to find the fuel consumption at zero ΔSOC. The fuel consumption at zero ΔSOC is estimated through linear interpolation between the two fuel consumption results with respect to the change in SOC [56], [57], [59]. This method assumes that the relation of ΔSOC to the change in fuel consumption is linear [59]. The method described in SAE J1711 iterates the initial state of charge of the system until the change in battery energy over the cycle is less than 1% of the fuel energy consumed by the system [56], [57], [59].

The SOC correction methods used for simulations are similar to those used for testing. The linear interpolation method and a variant on the method described in SAE J1711 have been used in hybrid electric simulations [60]. The variant on the method described in SAE J1711 iterates the initial state of charge using Equation 11 [59] until the change in state of charge ΔSOC is less than a predetermined threshold (Wipke et al. use 0.5% for their threshold [60]). In Equation 11, $\mathrm{SOC}_{initial}^{n}$ is the initial SOC for the n^{th} iteration of the simulation, $\mathrm{SOC}_{initial}^{n+1}$ is the initial SOC chosen for the next iteration ($n+1$), and a is a convergence factor (between 0 and 1). Increasing the magnitude of the convergence factor a increases convergence speed [59].

Equation 11: Iteration of Initial State of Charge for State of Charge Correction

$$\mathrm{SOC}_{initial}^{n+1} = \mathrm{SOC}_{initial}^{n} + a\Delta\mathrm{SOC}$$

The simulation done in this thesis uses the second correction method described in the previous paragraph. The initial state of charge is changed according to Equation 11 until $\Delta\mathrm{SOC}$ is less than 0.5% for the simulation cycle. The correction factor a is chosen to be 0.1.

It should be noted that state of charge correction is not used for validation. It is the intention that the initial SOC for the test and simulation be the same for comparison purposes.

3.4 Solar Power Model

Solar power is used as the renewable energy source for this simulation. For the validation case, test data for the prototype system is used as the solar power input in the simulation. This data comes from current and voltage transducer readings of the solar charge controller output during the test of the prototype and is shown in Figure 22. The solar charge controller's output voltage and current are recorded once per second and are multiplied together to produce the validation case solar profile. The solar profile data contains noise that has amplitude of about 100W. This solar profile was collected during partly cloudy conditions spanning 26 hours in the month of November.

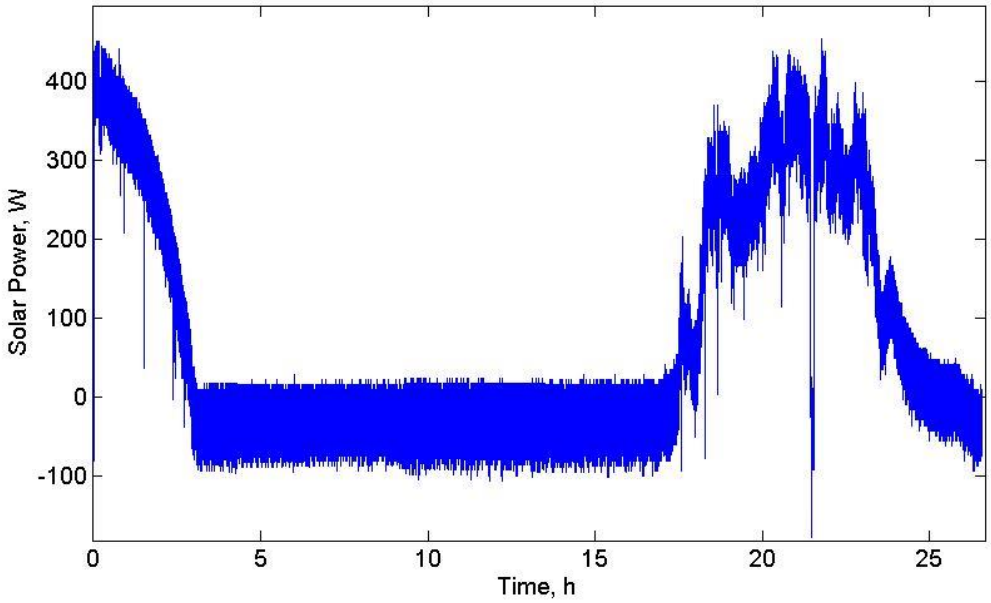

Figure 22: Validation Case Solar Profile

For the simulation done to find the optimal system components, the solar power input is estimated using available solar radiation data with a solar cell model employed by Rouhani et al. The solar radiation data used in this model comes from the Meteorological-Statistical (METSTAT) solar model for the Virginia Tech (VT) Airport from the years 1991 to 2010. METSTAT data is furnished by the National Solar Radiation Database (NSRDB). The hourly METSTAT global irradiance data for the years of 1991 through 2010 is averaged on a daily basis. The final outcome is an average daily global irradiance profile for the VT Airport, as seen in Figure 23. Global irradiance is defined as the total amount of direct and diffuse solar radiation received on a horizontal surface [61]. This global irradiance data also includes effects from cloud cover.

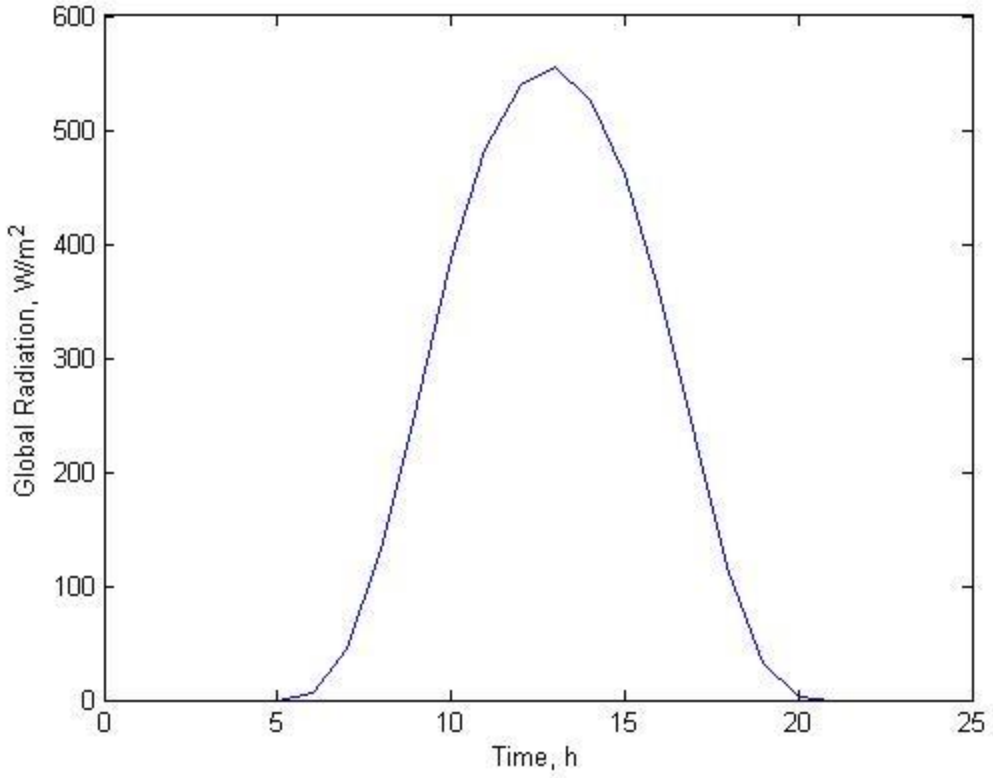

Figure 23: Average Daily Global Irradiance Profile for Virginia Tech Airport

This global radiation data is used as the input into the photovoltaic (PV) model described by Rouhani et al. to determine the power output from the solar array. Rouhani et al. use Equation 12 to estimate power output P_{PV} from a solar array, where η_g is the instantaneous PV array efficiency, A_m is the area of a single module (m^2), N is the number of modules used in the system, and G_t is the global irradiance incident on the titled plane (W/m^2) [62].

Equation 12: Photovoltaic Power Output

$$P_{PV} = \eta_g N A_m G_t$$

The global irradiance profile is obtained from METSTAT data provided by the NSRDB, as mentioned earlier. The number of modules N and module area A_m are determined during the solar cell selection. The instantaneous PV array efficiency is represented by Equation 13, where η_r is the solar cell reference efficiency; η_{pt} is the efficiency of the power tracking equipment (solar charge controller); β_t is the

temperature coefficient of efficiency, ranging from 0.004 to 0.006 (per °C); T_c is the temperature of the PV cell (°C), and T_r is the PV cell reference temperature (°C) [62].

Equation 13: Instantaneous Photovoltaic Efficiency

$$\eta_g = \eta_r \eta_{pt}[1 - \beta_t(T_c - T_r)]$$

The solar cell reference efficiency η_r, temperature coefficient of efficiency β_t, and PV cell reference temperature T_r are dependent on the solar cell selected for the simulation. These values can usually be found in a solar cell's specification sheet. The efficiency of the power tracking equipment η_{pt} is dependent on the solar charge controller selected for the simulation. This efficiency can be found in the solar charge controller's specification sheet. The cell temperature T_c is estimated using Equation 14, where T_a is the ambient temperature (25°C is used in this thesis), U_L is the overall heat loss coefficient (W/m^2 per °C), τ is the transmittance coefficient of the PV cell, and α is the absorptance coefficient of the PV cell [62].

Equation 14: Photovoltaic Cell Temperature

$$T_c = T_a + G_t\left(\frac{\tau\alpha}{U_L}\right)$$

The term $(\tau\alpha/U_L)$ can be estimated using Equation 15, where the nominal operating cell temperature (NOCT) is given in the PV cell's specifications and ranges from 40 to 70°C [62].

Equation 15: Estimation of Overall Heat Loss Coefficient Term

$$\left(\frac{\tau\alpha}{U_L}\right) = \frac{NOCT - 20[°\mathrm{C}]}{800[\mathrm{W/m^2}]}$$

These equations, with the inclusion of appropriate PV cell characteristic parameters, are applied to the global irradiance data from the NSRDB to develop a daily PV array output profile. This output profile is then used as an input for the larger system model.

3.5 Model of Power Conversion Components

Before the simulation is initiated, the program checks that the selected power conversion components match the voltage, frequency, and power requirements of the generator, battery pack, solar panels, and load profile. The program also checks that the longest dimension of the conversion equipment fits within the dimensions of the trailer. The weight and volume of each conversion component is also recorded to be used in the program's procedure to determine whether the combined weight and volume of all system components do not exceed the physical requirements of the trailer described in *1.4 Design Parameters*.

While the efficiency of power conversion components η_{conv} usually depends on temperature and load conditions, as described in *2.6.2 Converter Efficiency* , the model used in this thesis ignores these conditions for the sake of simplicity. The efficiencies used for power conversion components in this model are static and are derived from the efficiencies given in the power conversion components' specifications at their rated operation load under ambient temperature conditions. Equation 16 shows how a power converter's output power is determined, in general. For rectifiers, the efficiency and power factor listed in the rectifier's specifications are multiplied together to determine η_{conv}. This practice is only done for the sake of simplicity in this model.

Equation 16: General Power Conversion Efficiency Equation

$$P_{out} = \eta_{conv} P_{in}$$

3.6 Cabling Model

In the MATLAB program used in this thesis, first the gauge of the cabling between components is selected using appropriate guidelines found in literature. Then, the weight and resistance of the cabling is calculated. The weight of the cabling is added to the weight of all the system components. The program checks that the weight of the

cabling and system components does not exceed the physical requirements of the trailer. The resistance is used in the simulation to estimate cabling power losses.

The National Electric Code (NEC) describes guidelines for sizing electrical cable in its table 310.16 [63]. This table gives the allowable ampacity (the amount of current a cable is rated to carry) for insulated conductors at a voltage below 2 kV. Ampacities are given for cables with American Wire Gauge (AWG) from 18 AWG to 4/0 AWG and temperature ratings of 60 °C, 75 °C, and 90 °C [63]. The cables used in the prototype system and in this model are rated to 90 °C. MIL-STD-810G, the military standard for testing technologies to be used in the field, describes the maximum operational temperature for a product in a "hot dry" climate to be 49 °C [64]. Therefore, this work will size cables to function in temperatures up to 49 °C. NEC Table 310.16 advocates multiplying the ampacities listed in the table for each AWG cable by 0.82 for ambient temperatures between 46 °C and 50 °C. The correct gauge cable is then selected by comparing its expected maximum current to the temperature-corrected ampacity listed in Table 310.16 [63]. For example, a 2 AWG, 90 °C cable should be selected for an application where it is expected to carry 100 A in 49 °C ambient temperature because its temperature-corrected ampacity of 106.6 A is larger than the expected current of 100 A.

A reasonable approximation of the ampacities given in NEC 310.16 can be made using the conservative 700-circular-mils-per-amp (700-CMPA) rule of thumb. The unit "circular mil" is used to describe the cross-sectional area of a wire, where a "mil" is 1/1000th of an inch. A circular mil is the square of the diameter of the wire (d^2), where the diameter of the wire is measured in mils [65]. Therefore, the 700 CMPA rule states that a cable should be sized so that it has at least 700 circular mils of cross-sectional area to every amp of current it is expected to carry [66]. This rule of thumb is a good approximation of the 49 °C temperature-corrected NEC 310.16 at larger gauges (4 to 4/0 AWG 90 °C cable) and is more conservative than the 49 °C temperature-corrected NEC 310.16 at smaller gauges (6 AWG and smaller 90 °C cable). Because of its reasonable approximation of NEC 310.16, the 700-CMPA rule is used in the MATLAB program to determine the cable sizes between components.

To implement the 700-CMPA rule, the expected current running through each cable in the system and the diameter for each cable gauge need to be known. The expected current running through each cable can be estimated easily because the system's load profile, solar power profile, generator's rated output, and efficiencies of the power conversion equipment are all known. The calculation of the expected current in each individual cable is not covered in this thesis. However, a couple example calculations are covered in *Appendix B: Example Calculations for Expected Cable Currents*. The diameter, in mils, of each cable gauge is determined using Equation 17, where n is the gauge of the cable ($n = 0$ for 1/0 AWG cable, $n = -1$ for 2/0 AWG cable, $n = -2$ for 3/0 AWG cable, and $n = -3$ for 4/0 AWG cable) [67]. The circular mil area of each cable gauge is then found by squaring the diameter term. This circular mil area is then divided by the expected current in the cable to find the CMPA of each cable gauge for the expected current. Equation 18 shows how the CMPA is calculated, where $I_{expected}$ is the expected current through the cable, in amperes.

Equation 17: Cable Diameter

$$d_n(\text{mil}) = (5\ \text{mil}) \times 92^{(36-n)/39}$$

Equation 18: Cable Circular Mils per Amp

$$\text{CMPA} = \frac{d_n(\text{mil})^2}{I_{expected}}$$

The smallest cable gauge with CMPA more than 700 and expected voltage drop less than 3% of the cable voltage is then selected for that cable route. Voltage drop is the amount the voltage decreases at the load side of a cable from the voltage at the source side of the cable. This decrease in voltage is due to the resistance of the cable and increases with the current running through the cable. A cable's voltage drop V_{drop} can be calculated using Ohm's Law, given in Equation 19, where I is the current through the cable (set to the maximum expected current for cable sizing) and R_{cable} is the resistance of the cable, in ohms. Equation 20 shows how the cable resistance R_{cable} is calculated, where L is the roundtrip length of the cable from the power source to load, in feet, and

ρ_{cable} is the cable's resistivity, in ohm-meters [67]. The units for the cable diameter d_n are in mils when used in Equation 20. The work in this thesis assumes a roundtrip cable length L of 10 feet since it assumes that system components will be at most 5 feet from each other. The work in this thesis uses a cable resistivity of $1.72 \times 10^{-8}\ \Omega \cdot \mathrm{m}$ for annealed copper [68]. Although the NEC does not list any requirements for maximum allowable voltage drop in a cable, it does recommend sizing cables so that voltage drop doesn't exceed 3% [69]. This recommendation is for performance purposes, not for safety purposes [69].

Equation 19: Voltage Drop According to Ohm's Law

$$V_{drop} = IR_{cable}$$

Equation 20: Cable Resistance

$$R_{cable} = \frac{(3.048 \times 10^{11})\rho_{cable}L}{(25.4^2)(\pi/4){d_n}^2}$$

After the cables between system components are selected, the weight of the cabling is determined by summing the weight of each individual cable. The weight of each individual cable W_{cable} is found through Equation 21, where d_n is the cable diameter in mils, L is the length of cable in feet, and δ_{cable} is the density of the cable in lb/ft^3. The density of copper (558 lb/ft^3) is used for this work. This cabling weight is then added to the weight of all other system components to be used to determine the weight-based fuel penalty FP_w for the proposed system. The process of calculating the weight-based fuel penalty is described in *3.8 Weight-based Fuel Penalty*.

Equation 21: Weight of Individual Cable

$$W_{cable} = \frac{(\pi/4){d_n}^2 L\delta_{cable}}{1.2 \times 10^7}$$

The cabling power losses during operation are calculated using Equation 22, where $I_{k,i}$ is the current flowing through cable k at the i^{th} time step, $R_{cable,k}$ is the resistance of cable k, and M is the total number of cables in the system. The total energy

loss through cabling $E_{loss,cabling}$ would then be the summation of all $P_{cable\ loss,i}$ over the entire simulation period.

Equation 22: Cabling Power Losses

$$P_{cable\ loss,i} = \sum_{k=1}^{M} {I_{k,i}}^2 R_{cable,k}$$

3.7 Overall System Model

The models implemented for the load profile, generator, battery pack, solar panels, conversion equipment, and cabling are combined into a large system model. This section describes how these models are combined in more detail by describing how the floating DC bus is modeled, how the operational specific fuel consumption is determined, and how the SOC Set Point dispatch strategy is implemented.

Floating DC Bus

A DC-coupled system architecture with a floating DC bus is used for both the model validation and design phase. Figure 24 shows how the power flows in this DC-coupled system. The variables P_1, P_2, and P_3 are place holders for the equations shown in the dashed-line box. Cable losses in each line are captured in the variables $P_{cable,loss,1}$ through $P_{cable,loss,7}$ and are determined using the modeling techniques described in *3.6 Cabling Model.* All variables that are known prior to running the simulation are listed in their component boxes. The simulation starts out at the edges of this power flow diagram and works its way toward the battery pack at the center because the solar profile, DC load profile, and AC load profile are known before the simulation is run. The generator power is either the full rated power of the generator or zero according to the SOC Set Point dispatch strategy. At the beginning of the simulation, the generator is off and the battery pack is discharging.

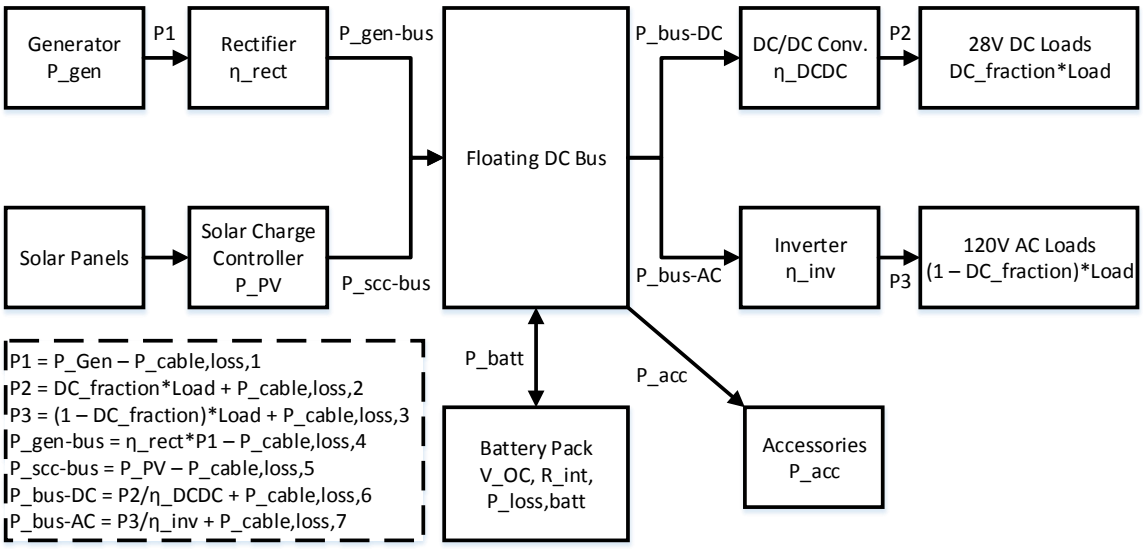

Figure 24: DC-Coupled System Power Flow

The power going into or out of the battery pack $P_{batt,i}$ is the sum of all power streams into and out of the DC bus. Equation 23 shows how $P_{batt,i}$ is calculated for each i^{th} iteration. The accessory power $P_{acc,i}$ is taken to be a constant 150W for all system simulations. This accessory load includes the power that goes to the computer, microcontrollers, and cooling equipment and is estimated using the prototype system's approximate accessory load. The battery power is positive when the battery is discharging and negative when it is charging. This battery power is then used in the battery model described in *3.3 Battery Model* to calculate the battery pack's internal losses and update the battery's state of charge.

Equation 23: Battery Power

$$P_{batt,i} = P_{bus-AC,i} + P_{bus-DC,i} - P_{SCC-bus,i} - P_{gen-bus,i} + P_{acc,i}$$

Operational Specific Fuel Consumption

The fuel consumption V_{fuel} is tracked whenever the generator is running and is calculated using Equation 1 in *3.2 Generator Model*. After the simulation is completed, the operational specific fuel consumption FC_o is calculated using Equation 24, where E_{load} is the total energy consumed by the AC and DC loads on the system.

Equation 24: Operational Specific Fuel Consumption

$$FC_o = \frac{V_{fuel}}{E_{load}}$$

Implementation of SOC Set Point Dispatch Strategy

The SOC Set Point dispatch strategy uses the battery's SOC to determine when the generator is supplying full rated power P_{gen} and when the generator is supplying no power. When the battery pack's SOC decreases to the low set point, the simulation sets the generator's output to full rated power in order to charge the battery. Once the battery pack's SOC increases to the high set point, the simulation sets the generator's output to zero.

3.8 Weight-based Fuel Penalty Calculation

Not only is the operational fuel consumption being analyzed in this work, but so is the fuel consumption required for system transport. The fuel required to transport the system is adjusted into a fuel penalty that is added to the operational fuel consumption to determine the overall fuel consumption of the hybrid system. This weight-based fuel penalty FP_w is calculated through a dynamic model. A few elements are needed before the model can be performed: an appropriate drive cycle for the system's tow vehicle during transport and the characteristics of the tow vehicle. After these elements are determined, the model is carried out to determine the tow vehicle's fuel consumption over the drive cycle. This fuel consumption is adjusted for the expected relocation frequency and travel distance the system will undergo during application in the field.

The drive cycle used for this model is the "Convoy Drive Cycle" described by Frame et al. in their report *M1078 Hybrid Hydraulic Vehicle Fuel Economy Evaluation*, and can be seen in Figure 25 and Figure 26 [70]. This profile was selected because it attempts to represent the expected drive cycle of a military convoy. The hybrid electric system that is proposed in this work would most likely be transported as part of a ground convoy when it is being transported over land. Figure 25 shows the speed profile of the

drive cycle while Figure 26 shows the grade profile. The convoy drive cycle is similar to a highway drive cycle in that it does not include any vehicle stops (other than at the end of the cycle), has a high average speed (between 40 and 50mph), and has a top speed of over 70mph. Only the speed profile is used in the simulation because the grade of the cycle mostly oscillates about 0% grade with peaks reaching no more than 7.5% for short periods of time. Therefore, it is assumed that the fuel consumption due to changes in grade is negligible.

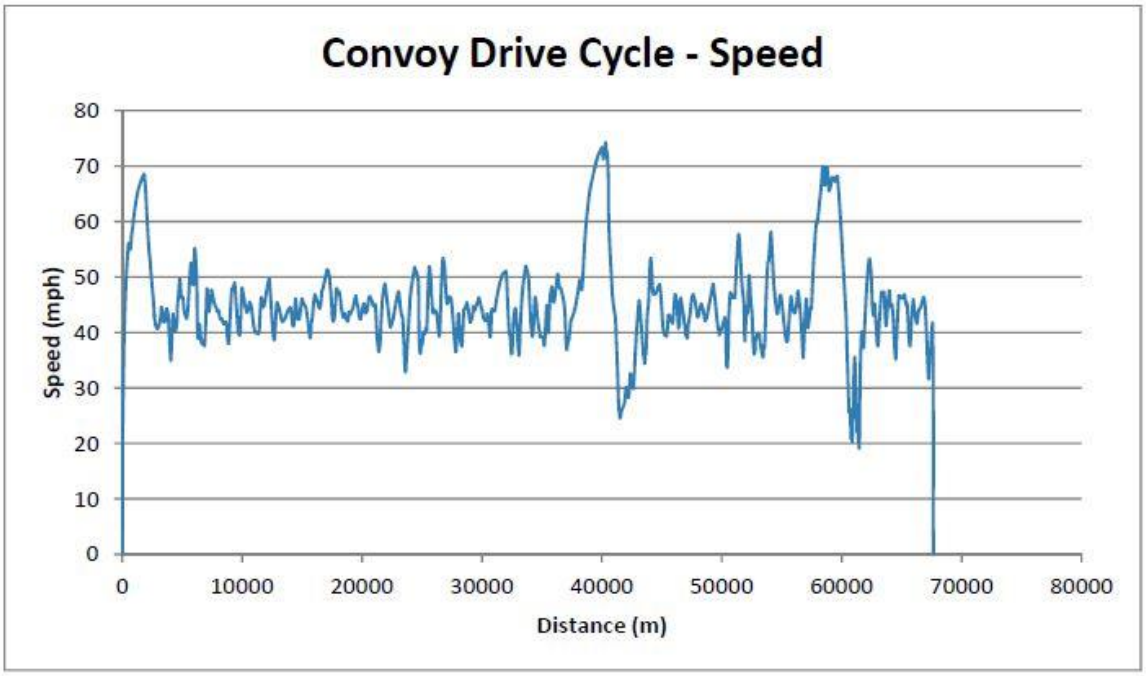

Figure 25: Convoy Drive Cycle - Speed [70]

Image from E. A. Frame, J. Redfield, G. Wendel, V. Iyengar, J. Harris and W. Olson, "M1078 Hybrid Hydraulic Vehicle Fuel Economy Evaluation," US Army TARDEC Fuels and Lubricants Research Facility, Southwest Research Institute (SwRI), San Antonio, Texas, 2012. Used under fair use, 2015.

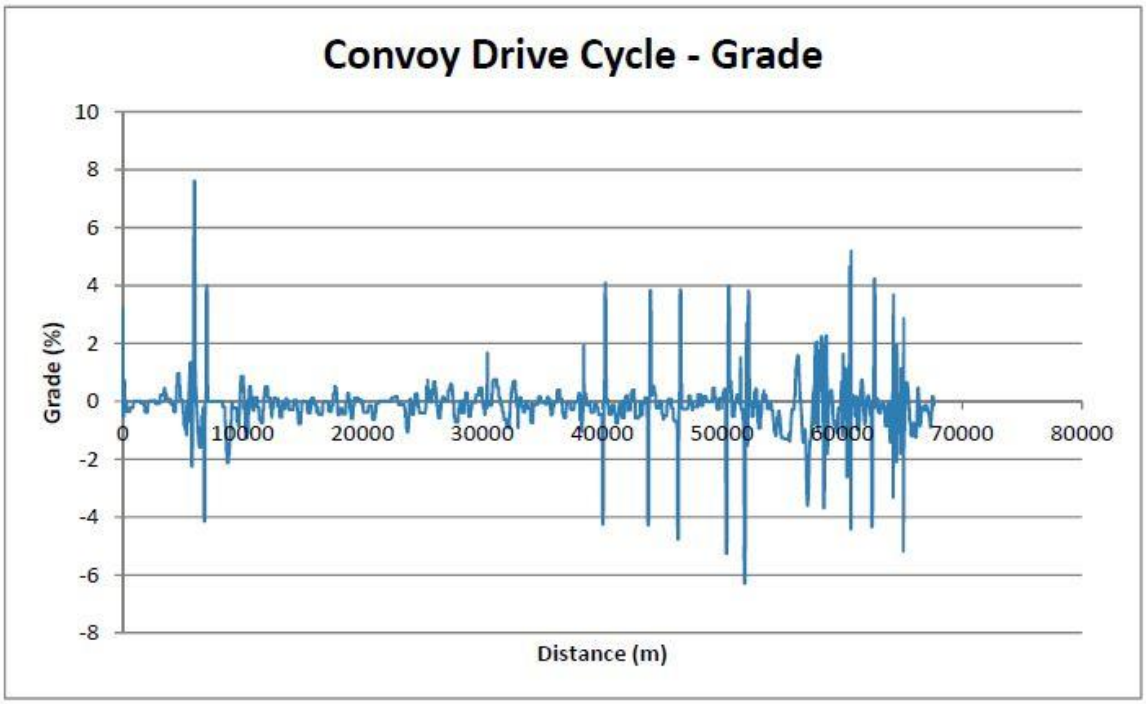

Figure 26: Convoy Drive Cycle - Grade [70]

Image from E. A. Frame, J. Redfield, G. Wendel, V. Iyengar, J. Harris and W. Olson, "M1078 Hybrid Hydraulic Vehicle Fuel Economy Evaluation," US Army TARDEC Fuels and Lubricants Research Facility, Southwest Research Institute (SwRI), San Antonio, Texas, 2012. Used under fair use, 2015.

After selecting a drive cycle, the characteristics of the tow vehicle need to be known. For this simulation, a High Mobility Multipurpose Wheeled Vehicle (HMMWV), commonly known as Humvee, was used as the tow vehicle of the hybrid energy system. This vehicle was chosen for the model because it is a common military vehicle and its characteristics (e.g. weight, fuel efficiency, drag coefficient, and frontal area) are readily available. The characteristics of the HMMWV M097 A2 vehicle are shown in Table 3 [71]. The characteristics used in the model are the empty vehicle weight, frontal area, coefficient of drag, coefficient of rolling resistance, highway fuel economy, and approximate powertrain efficiency. This powertrain efficiency encompasses the engine efficiency as well as the efficiency of the transmission and drive train. In reality, the engine efficiency varies with its torque and angular speed (revolutions per minute, rpm). However, this powertrain efficiency is more of an average efficiency over the entire drive cycle, and is dependent on the dynamics of the drive cycle.

Table 3: HMMWV M1097 A2 Vehicle Characteristics [71]

Characteristic	Value
Engine Fuel Type	Diesel
Aspiration	Natural
Engine Displacement (L)	6.5
Engine Peak Power (kW)	119 @ 3,400 rpm
Transmission	Automatic
Empty Vehicle Weight (kg)	2,676
Gross Vehicle Weight (kg)	4,672
Frontal Area (m^2), A_f	3.58
Coefficient of Drag, C_D	0.5
Wheel Base (m)	3.3
Coefficient of Rolling Resistance, C_{rr}	0.013 paved/0.045 off road
Acceleration 0-30 mph (seconds)	10
Acceleration 0-50 mph (seconds)	29
Highway (HWFET) Fuel Economy (mpg)	13.4
City (UDDS) Fuel Economy (mpg)	9.2
Approx. Powertrain Efficiency (%), η_{pt}	15.7

In reality, General Dynamics Ordnance and Tactical Systems' Prime Mover is designed to tow the ammunition trailer housing this hybrid electric system [14], but its fuel economy and aerodynamic characteristics could not be obtained. Although a HMMWV is heavier than the Prime Mover (5900lbs versus 3900lbs), has a larger engine than the Prime Mover (6.5 L versus 2.8 L), and has different dimensions than the Prime Mover, it is being used in this model due to the availability of its fuel economy characteristics. Figure 27 shows the HMMWV M1097 A2 and General Dynamics Ordnance and Tactical Systems' Prime Mover. The point of this model is not to necessarily be the most representative of reality, but to investigate the impact of system weight on the fuel consumption required to move the system to forward encampments. Since the HMMWV is heavier and more powerful than the Prime Mover, using it in the model leads to larger fuel penalties than if the Prime Mover is used. If it turns out that the fuel penalty for transporting the hybrid energy system around a combat zone is negligible using this more conservative tow vehicle, the weight of the hybrid energy system can be ignored in future design cycles. However, if the fuel penalty for transporting the system turns out to be significant, further analysis can be done that includes characteristics of the Prime Mover in the model.

Figure 27: HMMWV M1097 A2 Vehicle (left) [72] and General Dynamics Prime Mover (right) [14]

Image (left) from AM General, "M1097A2 HMMWV Specifications," [Online]. Available: http://www.amgeneral.com/files/specs-sheet-m1097a2.pdf. [Accessed 1 April 2015]. Used under fair use, 2015.

Image (right) from General Dynamics Ordnance and Tactical Systems, *EFSS: Expeditionary Fire Support System*, St. Petersburg, Florida: General Dynamics Ordnance and Tactical Systems, 2008. Used under fair use, 2015. Used under fair use, 2015

The powertrain efficiency is determined by first simulating the Humvee's required propulsion energy to perform the Highway Fuel Economy Test (HWFET) drive profile. Second, the Humvee's HWFET fuel economy of 13.4 mpg is converted to a Wh/mi energy consumption value by taking its inverse and multiplying it by the lower heating value of diesel fuel, 37,645 Wh/gal [73]. Finally, the Humvee's required propulsion energy is divided by this HWFET energy consumption value and the distance covered during the HWFET cycle to obtain the powertrain efficiency of the Humvee during the HWFET cycle. Because the HWFET and convoy drive cycles are similar, it is assumed that the powertrain efficiency for the HWFET cycle can be applied to the model for the convoy drive cycle.

Once the drive cycle and tow vehicle characteristics are selected, a model of the tow vehicle and trailer performing the drive cycle can be carried out. To build the model, first a free body diagram needs to be made showing the active forces on the vehicle, as seen in Figure 28. This work adopts the conventions used by Ehsani et al. in their book *Modern Electric, Hybrid Electric, and Fuel Cell Vehicles: Fundamentals, Theory, and*

Design, 2nd Edition to describe the forces on the vehicle and trailer. The forces working on the vehicle and trailer are weight $(M+m)\boldsymbol{g}$, aerodynamic force $\boldsymbol{F_{aero}}$, the rolling resistance force $\boldsymbol{F_{rr}}$, the grade force $\boldsymbol{F_{grade}}$, the inertial force $\boldsymbol{F_i}$ (net force), and the tractive force $\boldsymbol{F_{tr}}$.

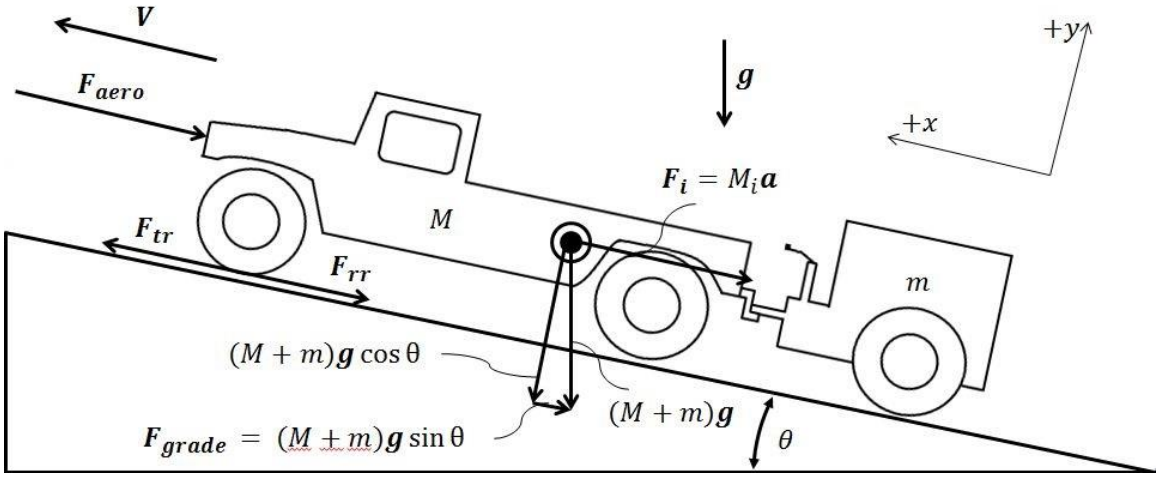

Figure 28: Free Body Diagram of Forces on Tow Vehicle and Trailer

The vehicle and trailer weights are combined into one force vector, as shown in Figure 28. This force vector is applied to the center of mass of the entire system (vehicle and trailer). The weight of the system is $(M+m)g$, where M is the mass of the Humvee, m is the mass of the trailer, and g is the acceleration of gravity on Earth (9.81 m/s^2). The counteracting normal force $(M+m)g\cos\theta$ (not pictured) acts upon the contact area between the wheels and the road, and is distributed among the six tires in the system. The angle θ is the grade of the road. Because the grade portion of the convoy drive cycle is being ignored, this angle θ is equal to zero, and the normal force is the same magnitude as the weight of the system.

The mass term m is the one term that is dependent on the selection of system components as it includes the mass of the generator, battery pack, solar panels, a 12 gallon fuel tank (always assumed to be full during transport), power conversion components, and cabling. The procedure to find the mass of the cabling is described in *3.6 Cabling Model*.

The aerodynamic force $\boldsymbol{F_{aero}}$ is found using Equation 25, where ρ is the density of air (1.2 kg/m^3 at 20°C [74]), C_D is the drag coefficient of the vehicle (as shown in Table 3), A_f is the frontal area of the vehicle (also listed in Table 3), and V is the speed of the vehicle (determined from the driving profile) [75]. The aerodynamic force always opposes the motion of the vehicle. There are a few assumptions being used when determining the aerodynamic force active on the vehicle. The first assumption is that the movement of the system will take place in environmental conditions between 10°C and 30°C and 1 atm of pressure, where the air density of 1.2 kg/m^3 is applicable. The second assumption is that the presence of the trailer will not significantly affect the drag coefficient and frontal area of the vehicle. In reality, the drag coefficient would most likely increase with the presence of the trailer. Determining the effect of the trailer on the drag coefficient is beyond the scope of this thesis, as drag coefficient is highly dependent on the geometry of the vehicle and trailer. The point of this model is to estimate the effect of system weight on transportation fuel consumption. The weight of the system plays no direct role in the aerodynamic drag force on the vehicle. Therefore, accuracy in the aerodynamic model is not a focus.

Equation 25: Aerodynamic Drag Force

$$F_{aero} = \frac{1}{2}\rho C_D A_f V^2$$

The rolling resistance force $\boldsymbol{F_{rr}}$ is found using Equation 26, where C_{rr} is the rolling resistance coefficient (listed in Table 3), and always opposes the motion of the vehicle [75]. The rolling resistance coefficient for the Humvee on paved road ($C_{rr} = 0.013$) is being used for this model. Due to the higher speeds seen in the convoy drive cycle, it seems safe to assume the convoys are driving on roads that are maintained reasonably well. Of course, some amount of off-road driving may be seen during fuel transport, but this work is under the assumption that off-road driving does not occur frequently. Because grade is being ignored in this work, Equation 26 can be reduced to $F_{rr} = C_{rr}(M + m)g$. Also, in Figure 28, the rolling resistance force is only applied at the first wheel of the Humvee. This depiction is for the sake of simplicity. In reality, the

rolling resistance force would be distributed among all the wheels of the vehicle and trailer.

Equation 26: Rolling Resistance Force

$$F_{rr} = C_{rr}(M + m)g\cos\theta$$

The grade force $\boldsymbol{F_{grade}}$ will be zero for this model, since the road grade is assumed to always be zero degrees. The inertial force $\boldsymbol{F_i}$ is found using Equation 27, where M_i is the inertial mass, and a is the acceleration of the vehicle and trailer [75]. The inertial force is applied to the system at the center of mass of the vehicle and trailer and opposes the direction of positive acceleration. The inertial mass is the mass of the system that includes the rotational inertias of the wheels and can be determined through Equation 28, where I_w is the moment of inertia for a wheel and r_w is the wheel radius [76]. The inertial mass can also be estimated to be 1.04 times larger than the mass of the vehicle. Therefore, this work uses an inertial mass M_i that is the mass of the vehicle and trailer multiplied by 1.04. It should be mentioned that the inertial force is technically not an actual force applied to the vehicle, but is the net force on the vehicle resulting from the other forces being applied to the vehicle. In many dynamic models, all the applied forces on an object are known, and the object's acceleration is being solved for. However, in the case of this model, the acceleration of the object is known by taking the derivative of the drive profile's velocity, and the required traction force $\boldsymbol{F_{tr}}$ at the wheels is being solved for. Because this traction force is being solved for, it is easier to group the effects of the vehicle's inertia into a force of its own $\boldsymbol{F_i}$.

Equation 27: Inertial Force

$$F_i = M_i a$$

Equation 28: Inertial Mass

$$M_i = M + m + \frac{I_w}{r_w^2}$$

As just mentioned, the traction force $\boldsymbol{F_{tr}}$ is being solved for in this model. This traction force is the force required at the wheels for the vehicle to evaluate the convoy drive profile. This is the force being provided by the vehicle's engine through its transmission and drive system to the wheels. The traction force is found through the force balance equation shown in Equation 29 [75]. The directions of the force vectors shown in Figure 28 correspond with the positive directions of each force (i.e. positive traction force is in the opposite direction from the other four forces shown in the free body diagram).

Equation 29: Traction Force

$$F_{tr} = F_{aero} + F_i + F_{rr} + F_{grade}$$

Once the traction force is solved for, the traction power P_{tr} is determined by multiplying the traction force by the average system velocity at each time step, as shown in Equation 30, where j denotes the j^{th} time step. The average velocity at the j^{th} time step is determined by averaging the j^{th} and $(j-1)^{th}$ velocities in the drive profile. This traction power is then split into positive traction power $P_{tr,pos}$ and negative traction power $P_{tr,neg}$. For positive traction power, $P_{tr,pos,j}$ is equal to $P_{tr,j}$ when the traction power is positive and equal to zero when the traction power is negative. Likewise, for negative traction power, $P_{tr,neg,j}$ is equal to $P_{tr,j}$ when the traction power is negative and equal to zero when the traction power is positive. Positive traction power means the engine is providing positive power to the wheels in attempt to propel the vehicle. Negative traction power means the vehicle is braking in attempt to slow down. Because there is no regenerative braking on the Humvee, no energy returns to the vehicle when traction power is negative; energy from braking is released in the form of heat through the brake pads.

Equation 30: Traction Power at the j^{th} Time Step

$$P_{tr,j} = F_{tr,j} V_{avg,j}$$

The positive and negative traction powers are then integrated (summed) over the entire time span of the convoy drive cycle to determine the positive and negative traction

energies applied over the cycle, $E_{tr,pos}$ and $E_{tr,neg}$, respectively. Equation 31 shows how this summation is carried out for the positive traction energy, but the process can also be applied to the negative traction energy.

Equation 31: Positive Traction Energy

$$E_{tr,pos} = \sum_{j=1}^{N} P_{tr,pos,j}[t(j) - t(j-1)]$$

Sovran et al. calculate fuel consumption as a sum of the engine's fuel consumption during periods of positive traction power (propelling), negative traction power (braking), and zero traction power (coasting) [76]. However, since the fuel consumption rate of the Humvee engine during periods of coasting and braking aren't known, these contributions are ignored in this model. Therefore, the fuel consumption of the Humvee over the convoy drive cycle $V_{fuel,convoy}$ (on a gallon per mile basis) is found through Equation 32, where x_{tot} is the total distance covered during the convoy drive cycle, LHV_{diesel} is the lower heating value of diesel fuel (37,645 Wh/gal), and η_{pt} is the powertrain efficiency given in Table 3.

Equation 32: Fuel Consumption for Convoy Drive Cycle

$$V_{fuel,convoy} = \frac{E_{tr,pos}}{x_{tot} LHV_{diesel} \eta_{pt}}$$

From this fuel consumption value, the weight-based fuel penalty FP_w can be determined. The expected frequency to relocate the system f_r (in relocations per day) and the expected distance per relocation x_r (in miles per relocation) are needed as inputs into the model. For example, if it is expected that the system will be relocated once a week a distance of 40 miles, the expected frequency will be $f_r = 1/7$ and the relocation distance will be $x_r = 40$. The weight-based fuel penalty FP_w (in gallons of diesel per day) is found using Equation 33.

Equation 33: Weight-Based Fuel Penalty

$$FP_w = V_{fuel,convoy} x_r f_r$$

This fuel penalty FP_w is combined with the operational fuel consumption of the system FC_o (in gal/kWh) through Equation 34 to get the weight-adjusted, total fuel consumption for the system FC_{tot} (in gal/kWh), where $E_{load,tot}$ is the total energy (kWh/day) required in the daily electrical load profile chosen for the simulation. The process of determining the operational fuel consumption of the system is described in *3.7 Overall System Model.*

Equation 34: Total Fuel Consumption of System

$$FC_{tot} = FC_o + \frac{FP_w}{E_{load,tot}}$$

4 Design

When designing a hybrid electric system, multiple components and configurations should be analyzed to determine the most fuel efficient design. This section starts with the design of the existing prototype system used for validation and then covers the configurations and components considered for determining the most fuel efficient system.

4.1 Design of Existing System

The prototype HEIT system uses off-the-shelf components for its battery pack, generator, solar panels, and conversion equipment. Figure 29 shows a power flow diagram of the prototype HEIT system with components identified. This section will briefly describe each component with a summary of information in Table 5.

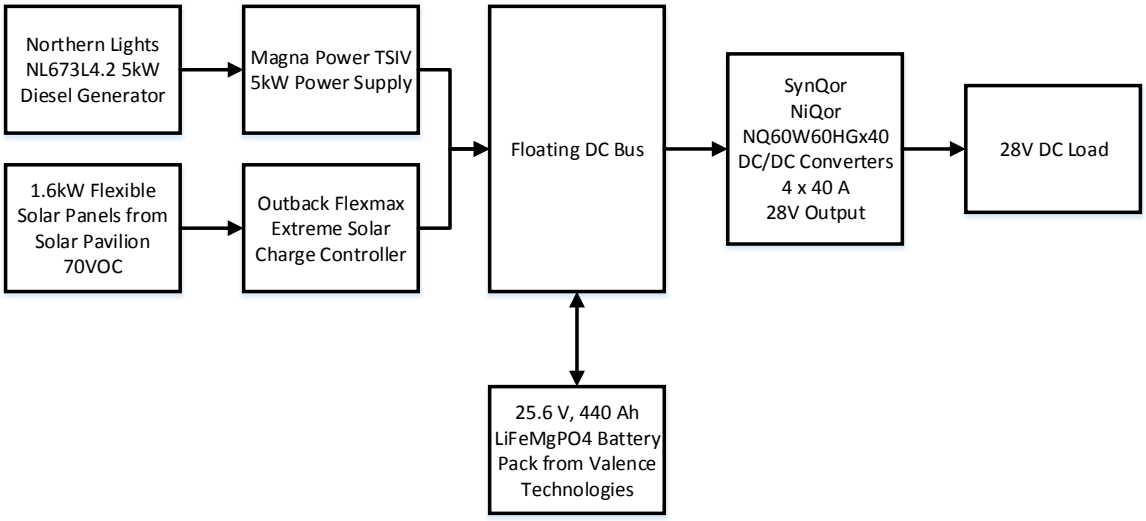

Figure 29: Design of Prototype HEIT System

Generator

The generator used in the prototype system is a Northern Lights NL673L4.2 diesel engine generator. This generator weighs 390lbs without fuel and has dimensions of 32.8” long by 17.1” wide by 26.8” tall [77].

The generator can be configured for two different power levels, 4.5kW and 5kW, by configuring its rotational speed. In the 4.5kW configuration, the generator runs at 1500 rpm and delivers power at 220VAC, 50Hz. In the 5kW configuration, the generator runs at 1800 rpm and delivers power at 120/240VAC, 60Hz [77]. The generator on the prototype system is configured for 5kW, and power is drawn only from the 240VAC circuit by the power supply.

The generator's fuel consumption rate, as listed in its specification sheet for the 5kW configuration, is 0.59 gal/hr at full load and 0.32 gal/hr at half load [77]. These fuel consumption rates correspond to specific fuel consumptions of 0.118 gal/kWh at full load and 0.128 gal/kWh at half load. These specifications state these fuel consumption values can vary depending on operating conditions [77]. The specific fuel consumption of the generator at other load points was measured in order to give an accurate estimation of the generator's fuel consumption over a variety of loads. These measurements were taken at 2,080 feet elevation at an ambient temperature of 23°C. The details and procedure of this testing are described in *Appendix A: Test Procedure for Measuring Specific Fuel Consumption of Northern Lights 5kW Generator*. The results of these measurements are shown in Figure 18 in section *3.2 Generator Model*. The simulation uses the measured fuel consumption data instead of the fuel consumption data available in the specification sheet. It is assumed that this data will be more viable for use in the validation because it is representative of the generator running at the same altitude as it was run during the system test.

Battery Pack

The prototype system uses a 25.6V, 440Ah $LiFeMgPO^4$ battery pack from Valence Technology, Inc. This battery pack consists of eight 12.8V, 110Ah U24-12XP modules. These modules are situated four in parallel, two in series as seen in Figure 30 with one module labeled. The recommended charge profile of these U24-12XP batteries is a constant current bulk charge of at most 55A until the battery module reaches 14.6V at about 90% SOC and then a constant voltage trickle charge at 14.6V until the battery reaches 100% SOC [27]. The maximum internal resistance listed for these batteries is

6mΩ [27]. These batteries weigh 34.8 lbs each and have dimensions 10.2” by 6.77” by 8.86” [27].

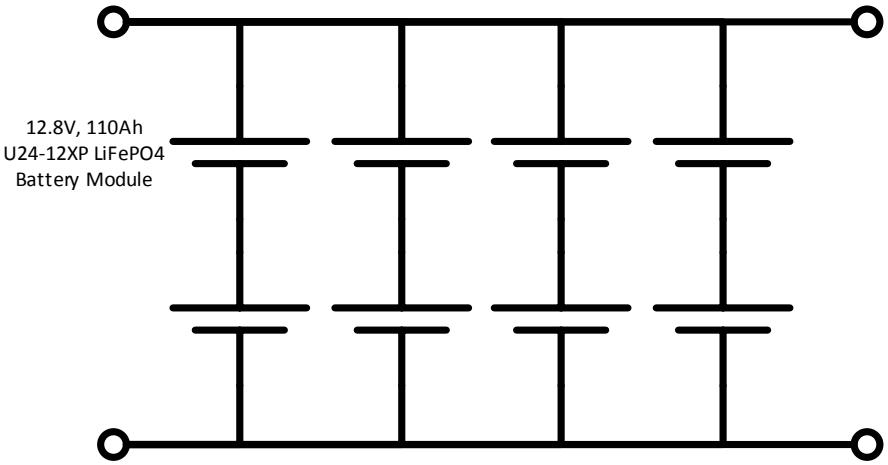

Figure 30: Prototype System Battery Configuration

Solar Panels

The prototype system uses flexible solar panels from Pvilion Solar. The entire solar array is rated to 1600W maximum power output. This solar array consists of two foldable arrays of 800W each. Each array weighs 40 lbs and has dimensions of 72” x 72” when unfolded. When folded, the longest dimension of the panels is 36”. The panels are approximately ¼” thick.

Bus Structure

The prototype system is DC-coupled with a 25.6V-nominal internal bus. The voltage of this internal bus floats with the battery pack voltage.

Conversion Equipment

The prototype system includes a solar charge controller, DC power supply, and DC-DC converters. Since the prototype system does not supply AC power, no inverter is included in the system.

The solar charge controller used in the system is an Outback FLEXmax Extreme. This solar charge controller can supply up to 80A to battery packs with nominal voltages of 12V, 24V, 36V, 48V, and 60V [78]. The FLEXmax Extreme charge controller on the prototype system is configured to charge a 24V nominal battery pack. This charge controller can accept solar arrays with up to 150V open circuit voltage [78]. The efficiency of this charge controller is approximately 96% at full rated power [79]. This charge controller weighs 26.0 lbs and has dimensions 18.56" by 8.8" by 6.0" [78].

The DC power supply used in the prototype system is a 5kW Magna-Power TSIV. This power supply is used to convert the generator's AC power to DC power for charging the battery pack. This power supply can accept either 208VAC single phase power or 240VAC single phase power [80]. The power supply in the prototype system is configured to accept 240VAC single phase power. The power supply can accept input power frequencies between 50Hz and 400Hz [80]. The power from the prototype system's generator is 60Hz and fits within this range. This power supply can output power from 0V to 32V with a maximum current limit of 150A [80]. This power supply has a power factor of at least 0.70 and efficiency of at least 86% at full rated power. The efficiency listed in the power supply's specifications does not include power loss from the 0.70 power factor [80]. The power supply is water-cooled, weighs 74 lbs, and has dimensions of 5.25" by 19" by 24" [80]. Because the power supply is not environmentally rated for rain, dust, and vibration; it needed to be housed in a waterproof, vibration-rated enclosure. This enclosure is a 3U Zarges Rackmount Case 45803 and adds 38.2 lbs to the weight of the power supply. The overall dimensions of this case are 8.44" by 21.02" by 27.32" [81].

During operation of the prototype system, the current limit of the power supply is configured to be 120A. This current limit is set so the power supply acts like a current source during the bulk charging stage of the batteries and the generator runs close to its rated output power during bulk charging. The maximum voltage limit is set to be 29.2V for the battery pack's constant voltage charge stage. As the batteries charge during the constant current stage, the battery pack voltage will increase until it reaches 29.2V. Once

the battery pack voltage reaches 29.2V, the power supply will decrease the current to the battery pack to maintain 29.2V.

The DC-DC conversion from the battery pack to the 28V load is done through paralleling four SynQor NiQor NQ60x60HGx40 non-isolated converters. Although the battery pack voltage (ranging from 24V to 29.2V) is close to the 28V required by the loads, it was decided that converters were necessary to guarantee a constant 28V for loads that have more delicate voltage requirements. Each converter can accept between 9V and 60V input and can output from 0V to 60V [49]. Since each converter is limited to a maximum output current of 40A [76], the maximum current that can be supplied to DC loads is 160A. These converters are 95% efficient at full load and are cooled through natural convection [49]. These converters weigh 5.5 ounces each and have dimensions 2.49" by 2.39" by 0.512" [49]. The weight and dimensions of the converters' heat sinks are ignored in this work.

Cabling

The cabling between components was selected according to NEC 310.16 guidelines. Table 4 shows the cable gauges selected for each cable route. Each run of cable is assumed to be 10 feet long roundtrip. The quantity of components in the table can be used to determine the number of runs that are needed between each component. For example, four runs of 8 AWG cable are required between the internal DC bus and the output converters since there are four output converters. The outputs of these DC/DC converters are tied together at a nearby bus bar. The run of cable from the output of each DC/DC converter to this bus bar is not long enough to be considered in analysis. The runs of cable from this bus bar to the DC loads are considered as three runs of 2/0 AWG cable. There are two more assumptions being used for the prototype system cabling (as well as for the cabling of other possible configurations moving forward in the simulation). The first assumption is the cabling from the solar panels to the solar charge controller can be ignored since this cabling length is determined by the end user and can change day-to-day. The second assumption is the length of cabling runs from the internal bus to each battery in the battery pack is insignificant. In the prototype system the internal DC bus is

placed close to the battery pack so the cable runs are short. It is assumed that the battery pack will also be close to the internal DC bus in the simulated systems.

Table 4: Gauges of Cable in Prototype System

Component 1	Quantity of Component 1	Component 2	Quantity of Component 2	Gauge Cable
Generator	1	DC Power Supply	1	10 AWG
DC Power Supply	1	Internal DC Bus	1	2/0 AWG
Solar Charge Controller	1	Internal DC Bus	1	4 AWG
Internal DC Bus	1	DC/DC Converters	4	8 AWG
DC DC/ Converter Output	1	DC Loads	3	2/0 AWG

Dispatch Strategy

The SOC Set Point energy dispatch strategy is used in the prototype system with SOC set points at 20% and 99%. The system starts the generator to charge the batteries as soon as one battery module's SOC decreases below 20%. The generator runs to charge the batteries until one battery module's SOC increases above 99%. If there are large differences between module SOCs, the charge range of the battery pack can actually be less than 20% to 99%. For example, if one module tends to have 10% less SOC than the other modules, the system will start charging the batteries once the one battery discharges below 20% even if the other seven batteries are still at 30%. Likewise, if one battery has 10% higher SOC then the other seven, the battery pack will stop charging once this one battery exceeds 99% SOC even if the other seven are at 89% SOC. Thus, the actual depth of discharge of the battery pack will be less than the intended depth of discharge.

This decreased depth of discharge was seen during testing of the prototype system. The states of charge of all eight battery modules were averaged over the test. It was shown that, on average, the generator started charging the battery pack when the average battery state of charge decreased below 33.2% SOC and stopped charging the battery pack when the average battery state of charge increased above 94.5% SOC. Even

though the set points used in the prototype system's programming were 20% and 99%, the set points used for validation reflect the average battery SOC set points of 33.2% and 94.5% seen during the prototype system test. These set points are used to increase the simulation's accuracy of representing the prototype system.

Table 5: Description of Prototype HEIT System Components

Component	Generator	Batteries	Solar Panels	DC Power Supply	Solar Charge Controller	DC-DC Output Converters
Manufacturer	Northern Lights	Valence Technology	Pvilion Solar	Magna-Power	OutBack Power	SynQor
Part Number	NL673L4.2	U24-12XP	N/A	TSIV	FLEXmax Extreme	NiQor NQ60
Quantity	1	8	1	1	1	4
Weight (lbs)	390 (w/o fuel)	34.8	80	112	26	0.34
Volume (in^3)	15,032	614	1,296	4,847	980	3
Longest Dimension (in)	32.8	10.2	36	27.3	18.6	2.5
Rated Power (kW)	5	N/A	1.6	5	2	1.1
Input Voltage	N/A	N/A	N/A	240VAC	0V to 150V	9V to 60V
Output Voltage	120/240VAC at 60 Hz	11V to 14.6V	70V Open Circuit	0V to 32V	0 to 30V	28V
Specific Fuel Consumption (gal/kWh)	See Figure 18	N/A	N/A	N/A	N/A	N/A
Efficiency (%)	N/A	N/A	N/A	86 with 0.70 PF	96	95
Internal Resistance (mΩ)	N/A	< 6	N/A	N/A	N/A	N/A

4.2 Component Options for Design Phase

During the design phase of this work, multiple components are considered to be used in the hybrid system. These components are selected around three design focuses. These design focuses are the battery pack voltage, battery pack capacity, and generator power. Three different battery voltages are analyzed: 25.6V, 51.2V, and 307.2V. Battery packs with the minimum required capacity and maximum allowed capacity are also considered. Three levels of generator power are also considered: a 3.8kW generator, a 5kW generator, and a 8kW generator. The same solar panels are used for every design configuration. Power conversion equipment is selected to work with these battery pack voltages, capacities, and generator power levels. Cabling is selected that meets NEC 310.16 standards for each considered configuration. All configurations considered in this design phase use a DC-coupled architecture with a floating DC bus. All configurations also use an SOC Set Point dispatch strategy with battery SOC set points of 20% and 90%. This section describes the generators, battery packs, solar panels, and conversion equipment considered in the design phase. It finishes with summarizing the configurations that are eventually used to determine the most fuel efficient system design.

Generator Options Considered for Design Phase

Three diesel engine generators are considered during the design phase of this thesis: a 3.8kW generator, 5kW generator, and 8kW generator. Generators with different power levels are used to see if selecting a higher or lower power generator has any noticeable effect on the system's fuel consumption. All three generators meet the continuous load requirement set forth in the design parameters. However, the 3.8kW generator would not be able to meet the 5kW peak load requirement alone. This deficiency is acceptable since the battery pack can assist the generator for higher loads, as long as these high loads are not sustained for long durations of time. Table 6 lists the properties of these three generators.

Table 6: Generator Options Considered for Design Phase

Generator	3.8kW	5kW	8kW
Model	Volpi Tecno Move 4000	Northern Lights NL673L4	Isuzu 8kW Turbo
Weight (lbs)	271 [82]	390 [77]	665 [83]
Volume (in^3)	11,106 [82]	15,032 [77]	20,160 [83]
Longest Dimension (in)	26.0 [82]	32.8 [77]	36 [83]
Output Power Characteristics	115 VAC, 60 Hz, 1ϕ [82]	240 VAC, 60 Hz, 1ϕ [77]	240 VAC, 60 Hz, 1ϕ [83]
Specific Fuel Consumption at Full Power (gal/kWh)	0.0925 [82]	0.098	0.1025 [83]

Battery Pack Options Considered for Design Phase

The only battery chemistry considered for the design phase is the $LiFeMgPO^4$ chemistry used by the same Valence U24-12XP modules in the prototype system. This chemistry is not just chosen due to its safe characteristics and good energy density, but also because the author is familiar with this chemistry and is able to obtain its parameters easily. Instead of constructing the battery packs out of the U24-12XP modules, as was done for the prototype system, the battery packs are constructed from many individual 18650 cells. These cells are the building blocks of the Valence modules. These cells have the characteristics shown in Table 7. The cell weight and volume are determined by dividing the weight and volume of the U24-12XP modules by the number of cells they contain.

Table 7: $LiFeMgPO^4$ 18650 Cell Characteristics

Parameter	Value
Cell Weight (lbs)	0.107
Cell Volume (in^3)	1.90
Cell Nominal Voltage (V)	3.2 [54]
Cell Capacity (Ah)	1.35 [54]

Three battery pack voltages are considered for the design phase: 25.6V, 51.2V, and 307.2V. A lower voltage battery pack is safer to handle and maintain but may be less efficient than a high voltage pack. Also, a lower voltage battery pack requires larger cabling than a higher voltage battery pack does. This larger cabling increases the system weight and is hard to design for in tight confines. The low voltage battery packs used in

this design phase have 25.6V pack voltage. Battery packs with slightly higher voltage of 51.2V are also analyzed. Battery packs with this voltage may be considered safe enough to handle and maintain, but will still decrease the required cabling size. The 307.2V battery packs are considered because this voltage is within the range of the battery packs used in the hybrid vehicle industry [55]. Therefore, power conversion equipment in this voltage range may be more available.

Battery packs with different capacities are also considered. For each pack voltage and generator power, one battery pack is designed with the minimum required capacity and another battery pack is designed with the maximum allowable capacity. Therefore, for each combination of pack voltage and generator power, there are two battery packs considered: a small capacity pack and a large capacity pack.

The minimum required capacity of a battery pack is dictated by the recommended charge rate of the battery cells and the expected peak charge current into the pack. The peak charge current is determined by the sum of the maximum current being delivered from the generator's rectifier and the maximum current being delivered from the solar charge controller. This peak charge current needs to be less than the recommended charge current of the battery pack. The recommended charge current of the battery pack scales up with the number of cells it has in parallel. Therefore, after determining the required number of cells in series to meet the desired pack voltage, the number of cells in parallel is determined so that this recommended charge current isn't exceeded.

The maximum allowable capacity of a battery pack is dictated by the weight and volume limits of the system's trailer. The number of battery cells in parallel is increased until either the system weight is within 10% of the trailer's weight limit or the system volume is within 10% of the trailer's volume limit. Because the batteries are dense, the weight limit is reached before the volume limit.

Table 8 describes the battery packs used in the design phase analysis. The weight of the minimum capacity 25.6V battery pack to be used with the 8kW generator forces the system weight to exceed into the 10% weight limit buffer. Therefore, no maximum capacity 25.6V battery pack is included to be used with the 8kW generator. Similarly, the

weight of the minimum capacity 51.2V battery pack to be used with the 8kW generator forces the system weight to completely exceed the weight limit. Again, no maximum capacity pack is included for this case.

Table 8: Battery Pack Options Considered for Design Phase

Battery Pack	Generator Power (kW)	Pack Voltage	Capacity (Ah)	Number of Cells in Series / Parallel	Weight (lbs)
A_min	3.8	25.6	437.4	8 / 324	278
A_max	3.8	25.6	1421.6	8 / 1053	904
B_min	3.8	51.2	298.4	16 / 221	380
B_max	3.8	51.2	714.2	16 / 529	909
C_min	3.8	307.2	43.2	96 / 32	330
C_max	3.8	307.2	125.6	96 / 93	959
D_min	5	25.6	518.4	8 / 384	330
D_max	5	25.6	1212.3	8 / 898	771
E_min	5	51.2	340.2	16 / 252	433
E_max	5	51.2	610.2	16 / 452	776
F_min	5	307.2	51.3	96 / 38	392
F_max	5	307.2	109.4	96 / 81	835
G_min	8	25.6	739.8	8 / 548	471
H_min	8	51.2	449.6	16 / 333	572
I_min	8	307.2	69.9	96 / 51	526
I_max	8	307.2	71.6	96 / 53	546

Solar Panels Used in Design Phase

The same solar panels are used for all configurations evaluated in this design phase. These solar panels are composed from the same LG monocrystalline cells used in the LG MonoX Neon LG300N1C-G3 solar panels. These solar cells are chosen due to their high stated efficiency of 18.3% and their availability through solar power distributors. These solar cells are arranged into custom solar panels that are designed to meet the maximum input power requirements of the smallest power solar charge controller used in this design phase. Therefore, the maximum output power of these solar panels cannot exceed the maximum power requirements of the smallest solar charge controller. The solar panel's maximum power is determined using Standard Test Conditions (STC) of 1000 W/m^2 irradiance at 25°C. The smallest power solar charge controller is the 24V, 80A Outback FLEXmax Extreme used with the 3.8kW, 25.6V system configuration (these system configurations will be summarized at the end of this

section). Because these solar panels are arranged to not exceed the maximum power requirements of the smallest solar charge controller, the panels should universally work with all of the configurations evaluated in this design phase. For the 307.2V battery packs, the same solar panels are just reconfigured for a higher voltage, but this reconfiguration should not affect the results of this simulation. Table 9 summarizes the characteristics of the solar panels used in the design phase.

Table 9: Design Phase Solar Panel Characteristics

Parameter	Value
Cell Type	Monocrystalline [84]
Cell Efficiency	18.3% [84]
Number of Cells Used	420
Panel Peak Power (at STC)	2100 W
Panel Peak Power (with VT Airport Average Irradiance)	897 W
Panel Weight	259 lbs
Panel Volume	20,866 in^3
Panel Area	15,120 in^2
Nominal Operating Cell Temperature (NOCT)	45°C [84]
Temperature Coefficient of Efficiency, β_t	0.42 %/°C [84]
Open-Circuit Voltage for Low Voltage/High Voltage Systems	79V / 324V

While the solar panels are sized using STC of 1000 W/m^2 irradiance, the simulation uses average irradiance data from the Virginia Tech Airport, which is significantly less than the STC irradiance. Therefore, the solar panels' output will be less in the simulation than their designed maximum output.

Conversion Equipment Used in Design Phase

More power conversion options could have been considered, but would not yield much more valuable information, since only the efficiency and weight of the power conversion equipment is used in the simulation. It seems straightforward that lighter, more efficient power conversion components are desired in a hybrid power system. However, the effects of a larger battery pack or higher power generator are not as straightforward to recognize without more detailed analysis. Therefore, the work done in the design phase is more focused on generator and battery pack selection.

The power conversion components are selected to meet the power and voltage requirements of the generator, battery pack, solar panels, and load. The components that are selected are the most efficient components that the author could find that fit the power and voltage requirements. It is possible that there are better options on the market, but these components should be adequate.

Two different solar charge controllers are used. One is used for 25.6V and 51.2V battery packs and the other is used for 307.2V battery packs. The high voltage solar charge controller is actually a DC/DC converter that can be programmed with the appropriate solar charge controller functionality. This converter is not environmentally rated or enclosed, so the weight and volumes given in its specifications are doubled in the simulation to include the enclosure that would be needed to house these converters. Two different rectifiers (battery chargers) are used: one for the lower voltage battery packs and another for the 307.2V battery packs. These rectifiers are paralleled to allow for higher generator power levels. Three different inverters are also used, one for each battery pack voltage. The inverter used for the 307.2V battery packs is actually a three phase inverter with 208VAC between lines. However, from each line to neutral the voltage is 120VAC. Therefore, it can be used for single phase power if taking each line separately. Two different DC-DC converters are used: one for the lower voltage battery packs and one for the 307.2V battery packs. The inverters and DC-DC converters are paralleled, if necessary, to meet the maximum expected load. Table 10 summarizes the characteristics of these power conversion components. The number of power conversion components put in parallel is recorded in Table 11.

Table 10: Power Conversion Components used in Design Phase

	Component	Input Voltage Characteristics	Output Voltage Characteristics	Efficiency (%)	Power Factor	Max Power / Current	Weight (lbs)	Volume (in^3)
Solar Charge Controllers	OutBack FLEXmax Extreme	0 to 150VDC [78]	0 to 73VDC [78]	96 [78]	N/A	80A [78]	22.6 [78]	980 [78]
	Flexiva DC/DC Converter Module	100 to 395VDC [85]	0 to 350.4VDC [85]	90 [85]	N/A	10A [85]	12	256
Rectifiers / Chargers	Delta-Q IC650	100 to 240VAC, 50 to 60 Hz, 1φ [86]	0 to 72VDC [86]	93.5 [86]	0.99 for 120VAC, 0.98 for 240VAC [86]	650W [86]	6.5 [86]	224 [86]
	BRUSA NLG513 (water-cooled)	100 to 240VAC, 48 to 62 Hz, 1φ [87]	200 to 520VDC [87]	93 [87]	0.99 [87]	3.68kW [87]	13.7 [87]	375 [87]
Inverters	OutBack GTFX2524	21 to 34VDC [88]	108 to 132VAC, 59.3 to 60.5 Hz, 1φ [88]	92 [88]	N/A	2500W [88]	62 [88]	1743 [88]
	OutBack GTFX3048	42 to 68VDC [88]	108 to 132VAC, 59.3 to 60.5 Hz, 1φ [88]	93 [88]	N/A	3000W [88]	62 [88]	1743 [88]
	Solar Edge SE9KUS	0 to 500VDC [89]	108 to 132VAC, 59.3 to 60.5 Hz, 3φ [89]	97.1 [89]	N/A	9000W [89]	79.7 [89]	4003 [89]
DC-DC Converters	SynQor NiQor NQ60x60HGx40	9 to 60VDC [49]	0 to 60VDC [49]	95 [49]	N/A	40A [49]	0.3 [49]	3 [49]
	BRUSA BSC614-24V	220 to 450VDC [90]	16 to 32VDC [90]	96 [90]	N/A	100A [90]	10.6 [90]	226 [90]

Summary of Configurations Used in Design Phase

The sixteen configurations analyzed in the design phase are summarized in Table 11.

Table 11: Summary of Design Phase Configurations

Generator Power	Pack Voltage	Pack Capacity	Generator	Battery Pack	Solar Charge Controller	Rectifier (Qty)	Inverter (Qty)	DC-DC Converter (Qty)
3.8kW	25.6V	Minimum	Move 4000	A_min	FLEXmax	IC650 (6)	GTFX2524 (2)	SynQor (5)
		Maximum	Move 4000	A_max	FLEXmax	IC650 (6)	GTFX2524 (2)	SynQor (5)
	51.2V	Minimum	Move 4000	B_min	FLEXmax	IC650 (6)	GTFX3048 (2)	SynQor (5)
		Maximum	Move 4000	B_max	FLEXmax	IC650 (6)	GTFX3048 (2)	SynQor (5)
	307.2V	Minimum	Move 4000	C_min	Flexiva DC/DC	NLG513 (2)	SE9KUS (1)	BSC614 (2)
		Maximum	Move 4000	C_max	Flexiva DC/DC	NLG513 (2)	SE9KUS (1)	BSC614 (2)
5kW	25.6V	Minimum	NL673L4	D_min	FLEXmax	IC650 (8)	GTFX2524 (2)	SynQor (5)
		Maximum	NL673L4	D_max	FLEXmax	IC650 (8)	GTFX2524 (2)	SynQor (5)
	51.2V	Minimum	NL673L4	E_min	FLEXmax	IC650 (8)	GTFX3048 (2)	SynQor (5)
		Maximum	NL673L4	E_max	FLEXmax	IC650 (8)	GTFX3048 (2)	SynQor (5)
	307.2V	Minimum	NL673L4	F_min	Flexiva DC/DC	NLG513 (2)	SE9KUS	BSC614 (2)
		Maximum	NL673L4	F_max	Flexiva DC/DC	NLG513 (2)	SE9KUS	BSC614 (2)
8kW	25.6V	Minimum	Isuzu	G_min	FLEXmax	IC650 (13)	GTFX2524 (2)	SynQor (5)
		Maximum	Isuzu	H_min	FLEXmax	IC650 (13)	GTFX2524 (2)	SynQor (5)
	51.2V	Minimum	Isuzu	I_min	FLEXmax	IC650 (13)	GTFX3048 (2)	SynQor (5)
		Maximum	Isuzu	I_max	FLEXmax	IC650 (13)	GTFX3048 (2)	SynQor (5)
	307.2V	Minimum	Isuzu	A_min	Flexiva DC/DC	NLG513 (3)	SE9KUS (1)	BSC614 (2)
		Maximum	Isuzu	A_max	Flexiva DC/DC	NLG513 (3)	SE9KUS (1)	BSC614 (2)

5 Simulation Results and Analysis

The simulation described in *3 Description of Model* is first validated using test data from the HEIT prototype system. Part of this validation is analyzing how a couple simulation parameters impact the accuracy of the simulation results. These simulation parameters include the complexity of the battery model and the efficiency of power conversion equipment. After validation, the design phase is carried out to determine the most fuel efficient hybrid system design. During this process, sixteen configurations are run through the simulation and their fuel consumption results are compared. Finally, a few of the design parameters are explored in more detail to analyze their impact on fuel consumption.

5.1 Validation of Model

For model validation, the simulation is run three times using the load profile seen in Figure 14 and the solar profile seen in Figure 22 for a length of 26.5 hours. These three simulation cases are explained in *5.1.1 The Three Simulation Cases used for Validation*. The fuel consumption and battery performance results of these simulations are compared to test data from the HEIT prototype system. The efficiency losses are then analyzed to see how different system components contribute to system inefficiency. Finally, the weight based fuel penalty is calculated for the prototype system.

5.1.1 The Three Simulation Cases used for Validation

One of the objectives during the validation stage of this thesis is to explore how increased complexity in the system model impacts simulation accuracy. The two parts of the model explored are the battery model and the conversion efficiency model. The three cases used during validation incorporate battery and converter efficiency models of varying complexity.

Simulation Case 1

The first simulation case uses the simple battery model described in *3.3.2 Simple Model with Constant VOC and Rint* and a simple converter efficiency model. This simple converter efficiency model uses a static conversion efficiency number for each converter. This static conversion efficiency is found from each converter's specification sheet. These efficiencies can be seen in Table 5. For the power supply used to rectify the generator's AC output, the efficiency number given in the table is multiplied by the power supply's power factor to be used in the simulation.

Simulation Case 2

The second simulation case uses the same simple battery model used in Case 1, but uses an efficiency derived empirically for the power supply instead of the efficiency number given in the power supply's specifications. This efficiency number is derived from the HEIT prototype system's test data. During the 26.5 hour test, the power supply's input and output power are measured. The power supply's output power is divided by its input power to give its efficiency at each one second interval of the test. The power supply's efficiency is then averaged over the entire duration of the test. This empirical efficiency is found to be 71.4% and is significantly higher than the efficiency derived from the power supply specifications of 60.2%.

Since conversion efficiency is often dependent on the converter's load and temperature, this empirically found efficiency is more accurate for the conditions seen in the prototype test. The reason for running a simulation with this more accurate empirical efficiency is to analyze whether a more complex converter efficiency model is required for future modelling. A more advanced converter efficiency model would compensate for the load and temperature experienced by the converter during the test and may yield significantly more accurate results than using a static efficiency found from a specification sheet.

Empirical efficiency numbers could have also been found for the solar charge controller and DC/DC converters with much more deliberation. However, using the

empirical efficiency for just the power supply yields significantly improved results, since the power supply is the least efficient converter in the system and handles most of the power conversion. The other converters are much closer to being 100% efficient and operate at lower power levels (only 400W for the solar charge controller and only 1300W for the DC/DC converters compared to 4500W for the power supply). Using empirical efficiencies for the other converters would probably not improve the simulation accuracy enough to necessitate the added work to find these values.

Simulation Case 3

The third simulation case uses the more complex battery model described in *3.3.3 Simple Model with SOC-dependent VOC and Rint* and the same empirical converter efficiency used in Case 2.

5.1.2 Validation Fuel Consumption Results

The fuel consumption for the three simulation cases are recorded over the simulation time and compared to the fuel consumption results gathered during the prototype test. These fuel consumption results can be seen in Figure 31. During the test, the fuel consumption was measured by weight. The fuel tank was placed on a scale with 0.1 lb resolution. The fuel weight was measured once per hour during the test to find the weight of fuel being consumed. This weight of fuel was then converted to volume of fuel using the measured density of the diesel of 6.8 lb/gal. In Figure 31 the fuel consumption data measured during the test are marked by black crosses at each data collection point. The Simulation Case 1 fuel consumption is shown in blue, the Simulation Case 2 fuel consumption is shown in green, and the Simulation Case 3 fuel consumption is shown in red.

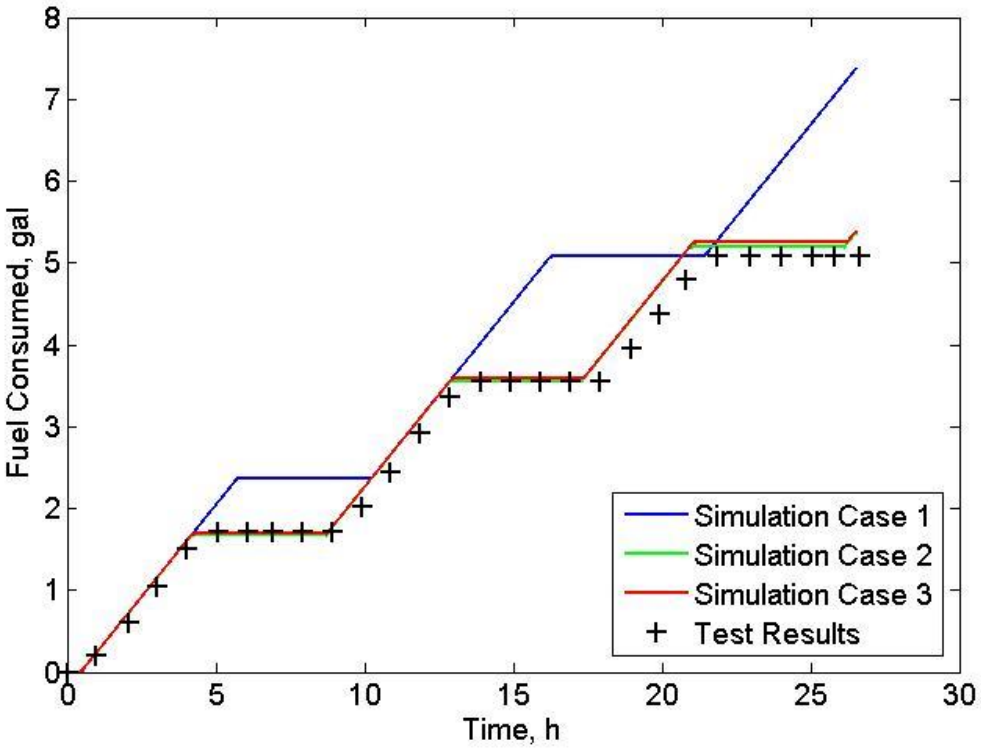

Figure 31: Validation Fuel Consumption

As can be seen in Figure 31, Simulation Case 1 does a poor job of tracking the actual fuel consumption of the system. The other two simulation cases track the actual fuel consumption much closer. Table 12 shows the fuel consumption results for the prototype test and three simulation cases. Simulation Case 1's final fuel consumption value is 45% greater than the fuel consumption recorded in the test results. This higher fuel consumption is expected since the efficiency value used for the power supply is more than 10% less than its measured efficiency over the test. This result shows that relying on a static efficiency value extracted from a specification sheet may introduce sizable error into simulation results. Since the efficiency of a converter will change with temperature and load applied, for the most accurate results the converter efficiency model should incorporate these parameters.

Using the average empirical efficiency value of 71.4% for the power supply leads to more accurate results; Simulation Case 2's fuel consumption is only 5.7% greater than the measured fuel consumption. Although this empirical efficiency value is still being

used as a static efficiency number for the simulation, it helps show how much the efficiency of a converter can change depending on load and environmental conditions. The load applied to the power supply was not quite the power supply's full rated load (4.5kW applied during test versus 5kW rated in specifications). The ambient temperature experienced by the system during the test also ranged from 38°F to 70°F, which probably isn't the temperature range used by the manufacturer to determine the efficiency of its power supply. Using this empirical efficiency in simulation shows how this change in efficiency can make a large impact on the fuel efficiency of the hybrid electric system.

Adding in a more complicated battery model does not improve fuel consumption accuracy by any significant amount. In fact, Simulation Case 3 has more fuel consumption error than Simulation Case 2 has, though by only a small amount. This increased fuel consumption results from increased battery energy losses using this more complicated model; Case 3 models 607Wh of total battery energy loss for the entire simulation cycle while Case 2 models only 320Wh of total battery energy loss. More information on system efficiency and energy losses will be provided in *5.1.4 Analysis of Efficiency Losses*.

Specific fuel consumption is found for the prototype test and for the three simulation cycles by dividing the total volume of fuel consumed by the energy supplied to the load over the entire test or simulation cycle. The specific fuel consumption of the system modeled using Simulation Case 1 is 46% greater than the specific fuel consumption measured during the test. This error is expected since Case 1 has 45% greater total fuel consumption. Likewise, the error in the specific fuel consumption found for Case 2 and Case 3 is similar in magnitude to the error in the cases' total fuel consumption.

Table 12: Fuel Consumption Results for Validation

	Total Fuel Consumed (gallons)	Error (% of Test Value)	Specific Fuel Consumption (gal/kWh)	Error (% of Test Value)
Prototype Test	5.08	N/A	0.149	N/A
Simulation Case 1	7.38	45.3	0.218	46.3
Simulation Case 2	5.37	5.7	0.159	6.7
Simulation Case 3	5.39	6.1	0.159	6.7

5.1.3 Validation Battery Performance Results

While fuel consumption is the most important parameter monitored during simulation and testing, the performance of the battery pack also needs to be monitored to explore the simulation's accuracy. The battery parameters monitored and analyzed in this thesis are the battery pack SOC and voltage.

Figure 32 shows the SOC of the prototype's individual battery modules throughout the test cycle. These SOCs are estimated by the battery pack's battery management system (BMS). The method the BMS uses to estimate SOC is proprietary, but some general information on SOC estimation can be found in *Battery Management*. As can be seen in the figure the SOC difference between modules increased to as much as 22.1% between the highest and lowest modules. This disparity between modules means that either the modules are not balancing as designed or the SOC estimation is losing accuracy for one or multiple modules. It is also possible that the disparity is resulting from both of these phenomena. Nonetheless, exploring the cause of this SOC disparity is not the focus of this thesis. These individual SOCs are averaged over the test to determine the entire battery pack's SOC. This battery pack SOC is shown in black in Figure 33. It should be noted that there is a period of 1.7 hours between 24.2 hours and 25.9 hours into test where the system computer loses communication with the BMS and stops updating battery parameters. The system was restarted to regain communication. This period of

dropout can be seen in Figure 32, Figure 33, Figure 34, and Figure 35.

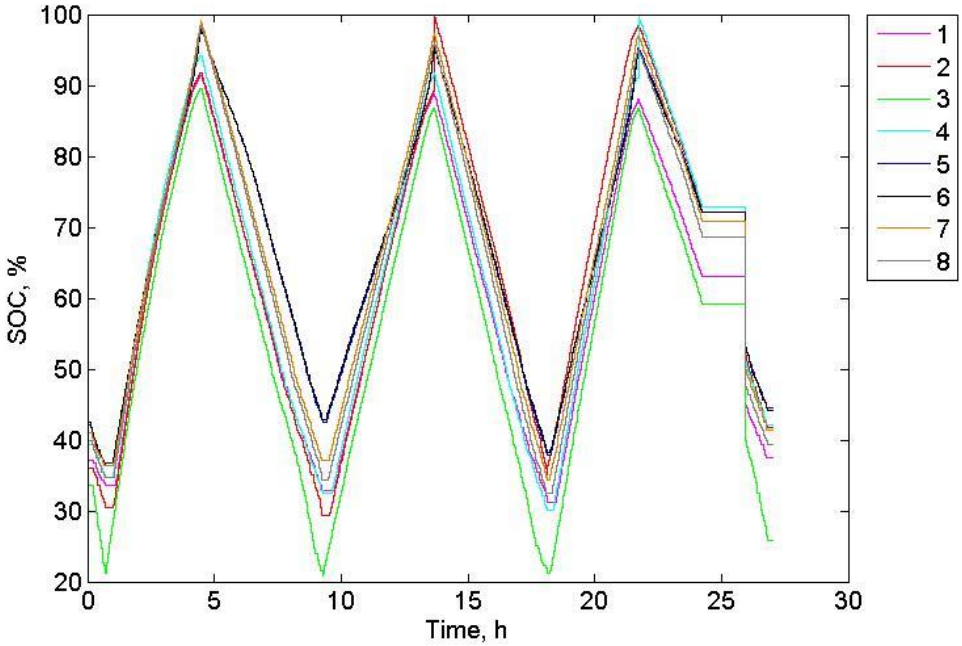

Figure 32: State of Charge of Individual Modules during Prototype Test

The prototype's measured battery pack SOC is compared to the battery pack SOC found through the three simulation cases. These results are shown in Figure 33, where Case 1's SOC is shown in blue, Case 2's SOC is in green, Case 3's SOC is in red, and the measured and averaged prototype SOC is in black. As was the case with the fuel consumption, Simulation Case 1 does a poor job of tracking the actual battery pack SOC. This poor performance is expected since the lowered power supply efficiency means the simulated charge current into the battery pack is less than the actual charge current. This effect can be seen in how the SOC rises slower for Simulation Case 1 than in the test data, even though the discharge rate is similar. Cases 2 and 3 track the actual battery SOC better. However, the charge and discharge slopes for these simulation cases are slightly steeper than what is seen in the actual SOC measurements.

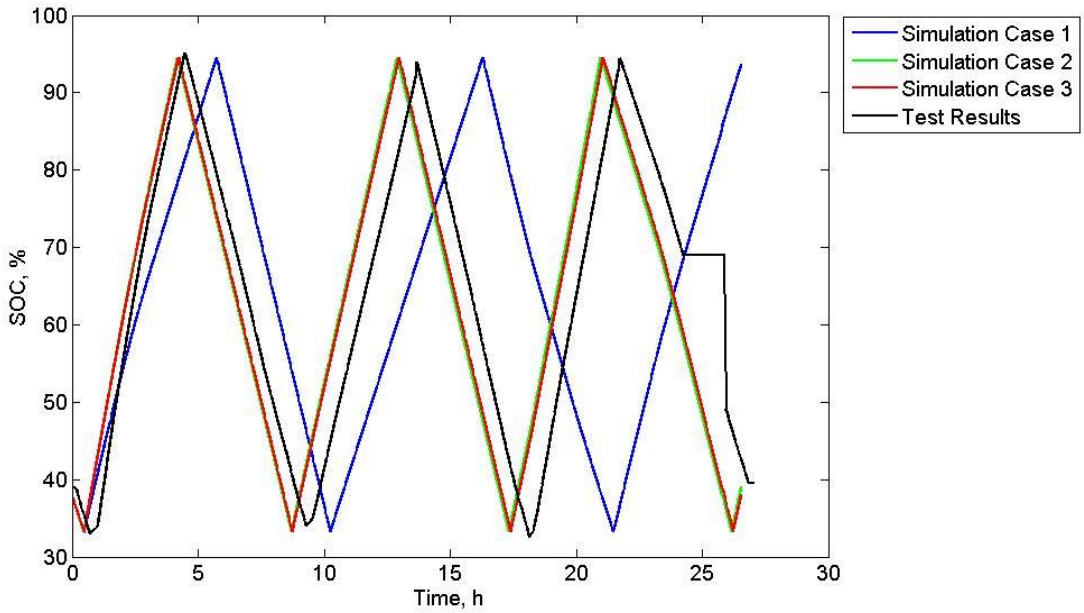

Figure 33: Validation Battery Pack State of Charge

Figure 34 shows the voltage of each individual battery module over the test cycle. Despite the large SOC differences seen between modules during the test, the voltages are relatively similar over the test. While the battery pack is charging, the voltages of the battery modules increase drastically at lower SOC and then increase at a slower rate until the modules are closer to fully charged. When the battery modules get close to being fully charged, their battery voltages again increase quickly. While the battery pack starts discharging, the voltages of the battery modules decrease quickly and then decrease at a slower constant rate until the low battery SOC set point is reached.

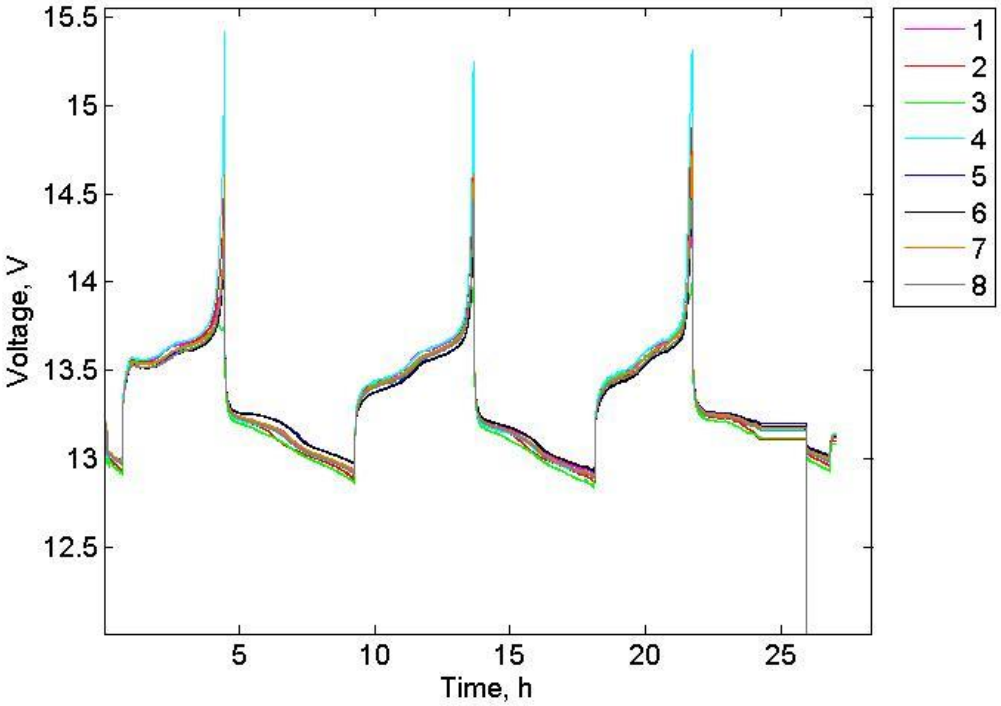

Figure 34: Voltage of Individual Battery Modules during Prototype Test

These individual battery module voltages are averaged and multiplied by two to calculate the prototype's battery pack voltage during the test. The battery voltage results of the three simulation cases (in blue, green, and red, respectively) are then compared to the calculated prototype battery pack voltage (in black), as seen in Figure 35. The battery pack voltages for the first two cases are not similar to the actual battery pack voltage. The battery pack voltages for these two cases are square waves where the voltage is one value while discharging and another value while charging. This result is expected as the open circuit voltage and internal resistance are constant values for these two cases. Evaluating Equation 2 in *3.3.2 Simple Model with Constant VOC and Rint* with these constant parameters leads to a simulated battery pack voltage as seen in Figure 35. In reality, these parameters change with SOC and temperature. Simulation Case 3 takes into account the SOC of the batteries when determining which open circuit voltage and internal resistance to use in the battery model at each time step. Although the battery cycles of Simulation Case 3 are out of phase with the battery cycles of the real battery pack, the voltage profile of each simulation battery cycle takes on a similar shape to the real battery pack's voltage

profile. The most visible difference is that the modeled battery pack voltage for Simulation Case 3 does not reach the same voltage level as the real battery pack at the end of a charge cycle.

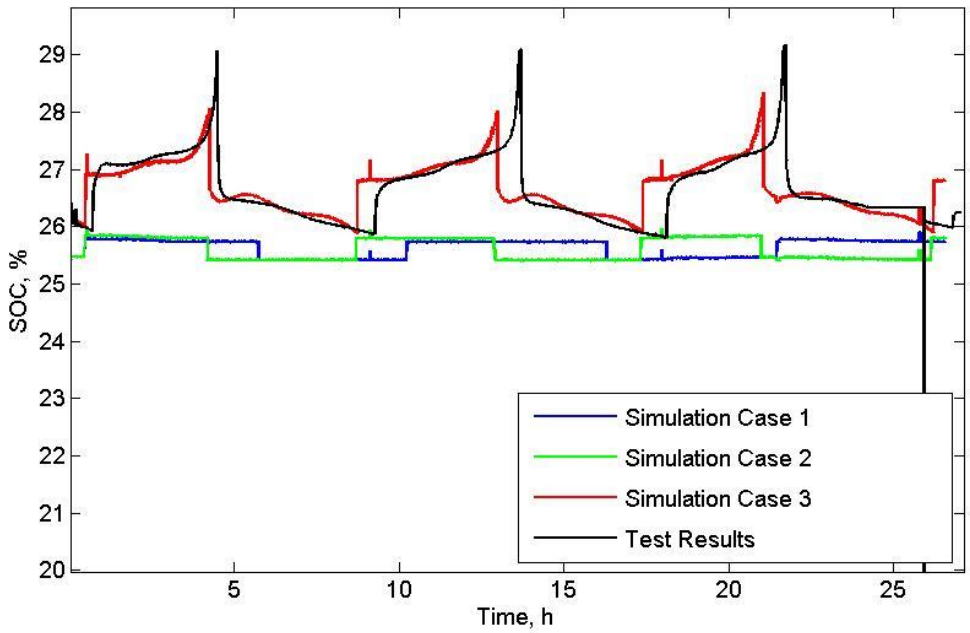

Figure 35: Validation Battery Pack Voltage

The battery performance results show that a more complex battery model can help track the battery pack voltage profile better than a simple model. However, the SOC of the battery pack over the simulation cycle does not change much with the complexity of the battery model.

5.1.4 Analysis of Efficiency Losses

Table 13 summarizes the energy results for the three simulation cases. The total load energy E_{load} and total PV energy E_{PV} are the same for all three cases, since these come from the actual load and PV power measurements during prototype testing. The total generator energy E_{gen} is the electrical energy the generator outputs over the entire simulation cycle. The total supplied energy E_{supply} is the sum of the total PV energy and total generator energy. The system's electrical efficiency is calculated using Equation 35, where $\Delta E_{batt,capacity}$ is the difference between the battery pack's capacity at the

beginning and end of the simulation. This battery capacity term is positive when the battery pack has higher capacity at the end of the simulation than at the beginning. This battery capacity term is factored into the system electrical efficiency calculation in an attempt to compensate for extra energy stored or released from the battery pack. When the simulation is used to find a more fuel efficient system design, this battery capacity term will be close to zero due to the SOC correction that is implemented.

Equation 35: Electrical Efficiency of System

$$\eta_{sys} = \frac{E_{load}}{E_{supply} - \Delta E_{batt,capacity}}$$

Table 13: Simulated Energy Results during Validation

	Case 1	Case 2	Case 3
Total Load Energy, $E_{load,tot}$ (kWh)	33.9		
Total PV Energy, E_{PV} (kWh)	2.1		
Total Generator Energy, E_{gen} (kWh)	73.8	53.7	53.9
Total Supplied Energy, E_{supply} (kWh)	75.9	55.8	56.1
System Electrical Efficiency, η_{sys} (%)	48.6	60.8	60.4
Total Energy Loss, $E_{loss,tot}$ (kWh)	35.8	21.9	22.2
Battery Losses, $E_{loss,batt}$ (kWh)	0.2	0.3	0.6
Battery Loss Fraction, LF_{batt} (%)	0.6	1.5	2.7
Cabling Losses, $E_{loss,cabling}$ (kWh)	0.4	0.3	0.3
Cabling Loss Fraction, $LF_{cabling}$ (%)	1.0	1.6	1.5
Accessory Losses, $E_{loss,acc}$ (kWh)	4.0	4.0	4.0
Accessory Loss Fraction, LF_{acc} (%)	11.1	18.2	17.9
Conversion Losses, $E_{loss,conv}$ (kWh)	31.2	17.2	17.3
Conversion Loss Fraction, LF_{conv} (%)	87.3	78.7	77.9

In Table 13 the battery, cabling, accessory, and conversion losses are tabulated. These energy losses are then summed to determine the total energy loss $E_{loss,tot}$. To show how much each factor contributes to the system's energy loss, a loss fraction is calculated for the battery, cabling, accessories, and converters. This loss fraction is calculated by dividing each factor's losses by the total losses. The contribution of energy losses are also depicted in Figure 36. As can be seen in the table and figure, the majority of energy losses are from conversion losses. The second most significant source of energy loss is the system's accessories. The accessory load is estimated based on the power

consumption of the computer, cooling fans, coolant pump, and diodes. The accessory load used for all simulations performed in this thesis is constant 150W. The cabling and battery are the smallest contributors to the system's energy loss. The simpler battery model in Cases 1 and 2 yields battery losses of around 0.2 to 0.3 kW, or less than 2% of the entire energy losses. The SOC-dependent battery model used in Case 3 yields higher battery losses of 0.6kW, but these losses are still less than 3% of the entire energy losses in the system. For all three cases, the cabling losses were 0.3 to 0.4 kW, or less than 2% of the entire energy losses.

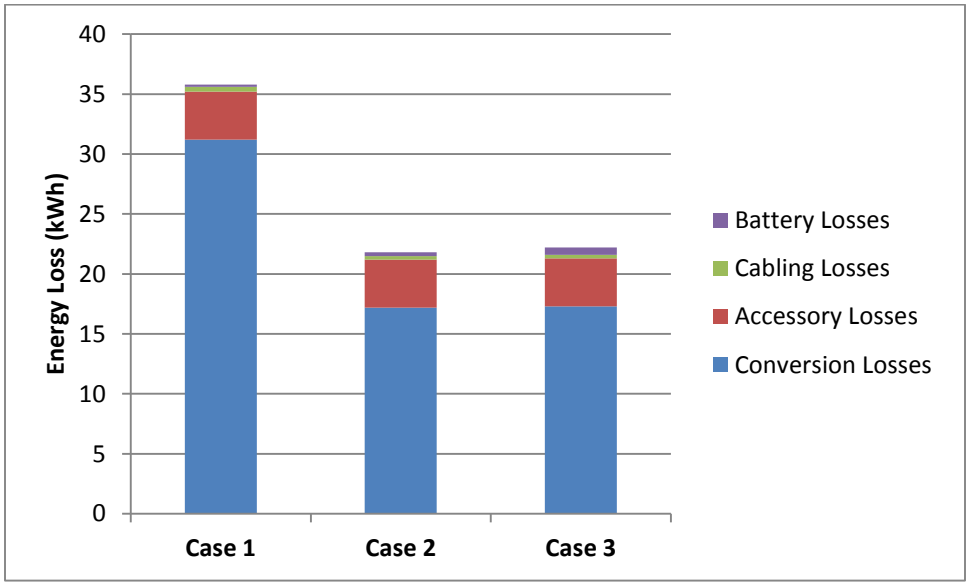

Figure 36: Energy Loss Contributions

These results show that the best way to focus engineering resources is on increasing converter efficiencies. A small increase in converter efficiency can increase system performance much more than a small increase in battery or cabling efficiency. Another valuable way to focus engineering resources is to minimize accessory loads by using more efficient computers, sensors, diodes, or cooling equipment. Designing a system that can be cooled through natural convection would ultimately eliminate the need for electrical power to cool the conversion equipment. However, these designs may increase system costs and complexity. Increasing the efficiency of converters would also help decrease required cooling power, since conversion energy loss is released as heat; the more this energy loss is minimized, less cooling power is needed to remove heat.

These results also show that in future simulation endeavors, the focus should be on increasing the accuracy and complexity of converter efficiency models, and not so much on increasing the accuracy and complexity of battery or cabling loss models. Conversion efficiency dominates electrical losses.

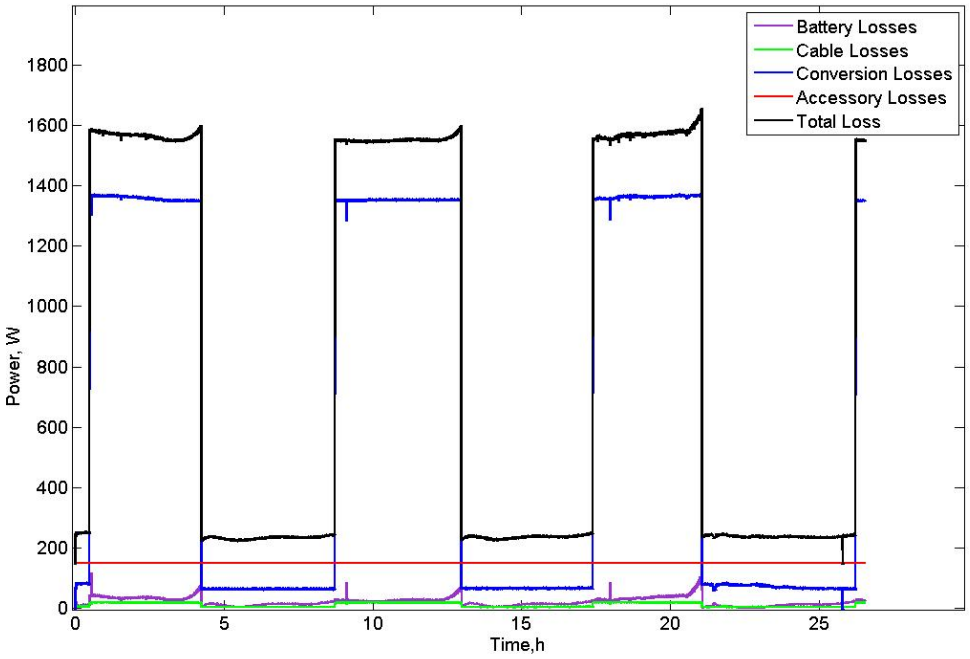

Figure 37: Validation Power Losses (Simulation Case 3)

Figure 37 shows the power losses over the course of the simulation for Case 3 (Cases 1 and 2 show similar profiles). The conversion losses (in blue) increase dramatically whenever the generator is charging the battery pack. This increase is due to the inefficient power supply being used to convert the generator's AC power. The battery and cabling losses (purple and green) are very small in comparison to these conversion and accessory losses (red).

5.1.5 Weight-Based Fuel Penalty for Prototype HEIT System

The weight-based fuel penalty is calculated for the prototype HEIT system using the weight of the components given in *4.1 Design of Existing System* and the relocation parameters given in *1.4 Design Parameters*, where the system is expected to move once a

week a distance of 40 miles. This penalty is calculated to be 0.425 gallons of diesel per day to transport the system. This fuel penalty is used in Equation 34 to find the overall fuel consumption of the system FC_{tot} for all three simulation cases and for the tested prototype system. These values are shown in Table 14. The addition of the weight-based fuel penalty increases the system's fuel consumption by approximately 9%.

Table 14: Weight-Based Fuel Penalty for Prototype System

	Case 1	Case 2	Case 3	Test Results
Weight-Based Fuel Penalty, FP_w (gal/day)	0.426	0.426	0.426	0.426
Operational Specific Fuel Consumption, FC_o (gal/kWh)	0.218	0.159	0.159	0.149
Overall Specific Fuel Consumption, FC_{tot} (gal/kWh)	0.232	0.173	0.173	0.163
Percent Increase (%)	6.4	8.8	8.7	9.3

5.2 Optimal Design Selection

The simulation is run multiple times using the sixteen configurations summarized in Table 11 of *4.2 Component Options for Design Phase*. The configuration with the lowest overall fuel consumption (including the weight-based fuel penalty) given no available solar power is chosen as the optimal design. Even though all sixteen configurations include solar panels, the amount of solar power available should not drive the final design decision. Due to the intermittent nature of solar power, the system that can provide the best fuel efficiency under conditions of no present renewable energy should be used. After this system is determined, the simulations are run again with the average VT airport solar irradiation data to determine the impact that solar power has on the systems' fuel consumption. Then, the losses and weight-based fuel penalty are analyzed for all sixteen configurations.

The simulation is also run using just a stand-alone generator on the same ammunition trailer for comparison purposes. The stand-alone generator used is a 5kW Northern Lights NL673L4 diesel generator, chosen because it meets the peak load demands of the Company COC load profile. During the simulation, the stand-alone generator's fuel consumption is derived by interpolating between specific fuel

consumption points shown in Figure 18 of *3.2 Generator Model* for each time step, given the system load. This stand-alone generator is directly connected to the 120VAC loads and is connected to the 28VDC loads through eight Delta-Q IC650 battery chargers (rectifiers). The stand-alone generator simulation includes a constant 50W accessory load.

Table 15 shows the simulation results for all sixteen configurations. The most fuel efficient system is marked in yellow. This system is the one with the 3.8kW generator and 307.2V maximum capacity battery pack. This system consumes approximately 22.7% less fuel than the stand-alone generator does. When including the weight-based fuel penalty of transporting the system, the selected hybrid system consumes about 21.2% less fuel than a stand-alone generator would. The least fuel efficient hybrid system is the one with the 8kW generator and 25.6V minimum capacity battery pack. This system consumes only 7.6% less fuel than a stand-alone generator would, and only 6.8% less when taking into account the weight-based fuel penalty of transporting the system.

Table 15: Design Results with No Solar Input – Fuel Consumption

Generator Power	Pack Voltage	Pack Capacity	FC_o (gal/kWh)	Improvement Over Stand-Alone Generator (% less fuel consumed)	FC_{tot} (gal/kWh)	Improvement Over Stand-Alone Generator (% less fuel consumed)
3.8kW	25.6V	Minimum	0.1164	18.7	0.1241	17.7
		Maximum	0.1156	19.3	0.1238	17.9
	51.2V	Minimum	0.1144	20.1	0.1222	18.9
		Maximum	0.1138	20.5	0.122	19.0
	307.2V	Minimum	0.1113	22.3	0.1191	21.0
		Maximum	0.1107	22.7	0.1188	21.2
5kW	25.6V	Minimum	0.1255	12.4	0.1333	11.5
		Maximum	0.1243	13.2	0.1324	12.1
	51.2V	Minimum	0.1232	14.0	0.1312	12.9
		Maximum	0.1224	14.5	0.1305	13.4
	307.2V	Minimum	0.1187	17.1	0.1265	16.1
		Maximum	0.1176	17.9	0.1257	16.6
8kW	25.6V	Minimum	0.1323	7.6	0.1404	6.8
		Maximum	N/A	N/A	N/A	N/A
	51.2V	Minimum	0.1298	9.4	0.138	8.4
		Maximum	N/A	N/A	N/A	N/A
	307.2V	Minimum	0.1254	12.4	0.1335	11.4
		Maximum	0.1251	12.6	0.1332	11.6
Stand-Alone Generator			0.1432	---	0.1507	---

Three major results can be observed from Table 15. The first result is that using a higher voltage battery pack decreases fuel consumption regardless of the generator size used in the system. This decrease in fuel consumption may be attributed to the smaller system currents and consequently lower cabling losses.

The second result is that larger capacity battery packs decrease fuel consumption by almost an insignificant amount (less than 1% when including the weight-based fuel penalty). This decrease in fuel consumption may be due to a decrease in battery losses. A larger capacity battery pack will have a lower internal resistance.

The third result is that using a smaller generator also yields lower fuel consumption. One thing to note is that the 3.8kW generator has better specific fuel

consumption at its full rated power than the other two generators have at their full rated power (0.0925 gal/kWh for the 3.8kW generator versus 0.098 gal/kWh for the 5kW generator and 0.1025 gal/kWh for the 8kW generator). However, this result still holds when running the 8kW, 307.2V, maximum capacity system with the same specific fuel consumption for its 8kW generator as the specific fuel consumption of the 3.8kW generator. When the 8kW, 307.2V, maximum capacity system is run with a generator specific fuel consumption of 0.0925 gal/kWh, the resulting simulation fuel consumption is still 2% greater than the 3.8kW, 307.2V, maximum capacity system's fuel consumption. This difference in fuel consumption cannot be due to any differences in power conversion efficiency since both systems use the same power conversion components. The difference is due to the additional space for extra battery capacity that is available in the system with the smaller generator. Since the generator is smaller, more battery capacity can be added. This added battery capacity decreases the internal resistance of the battery pack and also decreases the battery losses. While a smaller generator may be beneficial for its added space for extra battery capacity, finding the generator with the lowest full rated power specific fuel consumption can significantly benefit the system's overall fuel savings. Decreasing the generator's specific fuel consumption should be the design engineer's highest priority when selecting the generator.

Table 16 shows that adding solar power into the simulation does not change which system has the best operational fuel consumption. The 3.8kW, 307.2V, maximum capacity battery pack system still conserves the most fuel during operation, consuming 30% less fuel than the stand-alone generator. However, when including the weight-based fuel penalty, the 3.8kW, 307.2V, minimum battery pack system becomes the most fuel efficient, but only by a small amount (28.3% less fuel consumed versus 28.1% less fuel consumed).

Table 16 shows that the addition of the solar panels can decrease fuel consumption by another 8% over using just a stand-alone generator (from 22% to 30% less fuel consumption). Because the irradiation profile from the Virginia Tech Airport is smaller than in other places in the world, there is an opportunity for even more fuel

savings when in a location with more solar power. If wind power or scavenged power is added, the fuel consumption may dramatically decrease further.

Table 16: Design Results with Solar Input – Fuel Consumption

Generator Power	Pack Voltage	Pack Capacity	FC_o (gal/kWh)	Improvement Over Stand-Alone Generator (% less fuel consumed)	FC_{tot} (gal/kWh)	Improvement Over Stand-Alone Generator (% less fuel consumed)
3.8kW	25.6V	Minimum	0.1045	27.0	0.1123	25.5
		Maximum	0.1042	27.2	0.1123	25.5
	51.2V	Minimum	0.1023	28.6	0.1101	26.9
		Maximum	0.1023	28.6	0.1104	26.7
	307.2V	Minimum	0.1003	30.0	0.108	28.3
		Maximum	0.1002	30.0	0.1083	28.1
5kW	25.6V	Minimum	0.1124	21.5	0.1203	20.2
		Maximum	0.1113	22.3	0.1194	20.8
	51.2V	Minimum	0.1101	23.1	0.118	21.7
		Maximum	0.1093	23.7	0.1175	22.0
	307.2V	Minimum	0.1068	25.4	0.1147	23.9
		Maximum	0.1059	26.0	0.1141	24.3
8kW	25.6V	Minimum	0.1189	17.0	0.1271	15.7
		Maximum	N/A	N/A	N/A	N/A
	51.2V	Minimum	0.1162	18.9	0.1244	17.5
		Maximum	N/A	N/A	N/A	N/A
	307.2V	Minimum	0.1128	21.2	0.1209	19.8
		Maximum	0.1128	21.2	0.1209	19.8
Stand-Alone Generator			0.1432	---	0.1507	---

Figure 38 shows the fuel consumption over the simulation for the selected 3.8kW, 307.2V, maximum battery capacity hybrid system with and without solar input. The fuel consumption of the minimum battery capacity system is shown in dashed lines in the plot. The stand-alone generator's fuel consumption is also shown in the plot for comparison. As can be seen in the plot, the final fuel consumption of the minimum capacity system is close to the final fuel consumption of the maximum capacity system. This result shows how that increasing the battery capacity by a large amount only saves a small amount more fuel. The periods in the plot where the fuel consumption has zero slope is where the generator is off and the battery pack is meeting the load. The generator

is on for the majority of the cycle. The amount of time during the cycle the selected system is “quiet” (generator is off) ranges from about 6 hours without solar input to about 8 hours with the modest Virginia Tech Airport solar profile.

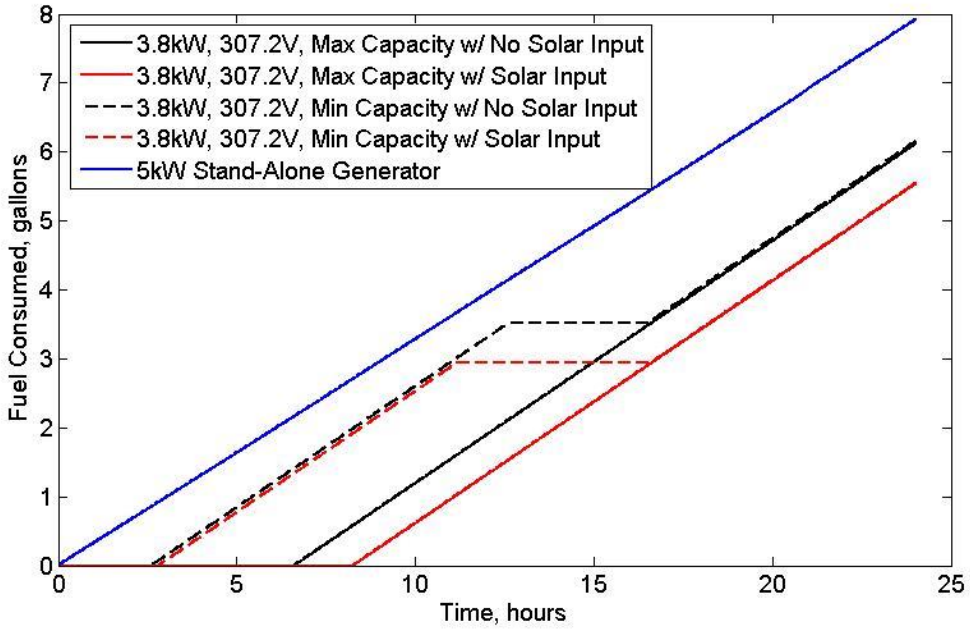

Figure 38: Fuel Consumption Plot for Selected System and Stand-Alone Generator

To better understand how energy is being lost in the system, the energy losses of the major components are tracked and recorded in Table 17. For the sixteen configurations evaluated, the power conversion losses account for 58% to 69% of the overall energy loss. This contribution is expected, as power conversion losses accounted for 78% of overall energy losses during validation. The next biggest source of energy loss is the accessory system, accounting for 22% to 33% of the overall losses. Cabling only accounts for between 1% and 4% of the overall losses. The battery losses range from almost insignificant for the systems with smaller generators to about 11% of the overall energy loss for the systems with the 8kW generator.

There are a few major trends that can be observed in Table 17. The first major trend is that conversion and cabling losses decrease with increasing battery voltage, regardless of the generator size. The decrease in cabling losses at higher voltages can be explained by lower system currents at higher voltages. Since power loss is proportional to

the square of current through the cable, decreasing the current through the cable is the most effective way to decrease these cabling losses. These smaller cabling losses also help decrease the conversion losses because the converters need to convert less power to counteract the cabling losses. The smaller power demand on the converters decreases their power losses. In this way, cabling losses can doubly impact the efficiency of the system. Not only would more energy be lost through the cables, but more energy is required to be converted meaning higher converter losses.

The second major trend is the decrease in battery losses when adding battery capacity. The maximum capacity battery packs will have less internal resistance as current is being shared among more battery cells. This lower internal resistance will lead to less energy lost through the battery. The battery losses can be decreased by more than 50% in some cases by maximizing the capacity of the battery pack. However, since battery losses account for only a small fraction of the overall losses, this improvement is still small.

The third major trend is the increase in battery losses for systems with larger generators. Since the generators are charging the battery pack at their full rated output, larger generators will be charging the battery pack with higher currents, so the battery losses will increase with the square of the charge current.

Finally, the overall system electrical efficiency is included in the table. For the evaluated hybrid systems, the electrical efficiency ranges from 78% to 84%. These system efficiencies are significant improvements over the prototype system's efficiency of 60%. The stand-alone generator is also included in this table. In terms of electrical efficiency, a stand-alone generator is more efficient than the hybrid systems (96% compared to 78% to 84%). However, higher electrical efficiencies are negated by the stand-alone generator's thermal inefficiency at low loads. At low loads, the generator's specific fuel consumption increases rapidly.

Table 17: Design Results with No Solar Input – Electrical Losses

Generator Power	Pack Voltage	Pack Capacity	Conversion		Cabling		Accessory		Battery		η_{sys} (%)
			E_{loss} (kWh)	LF (%)	E_{loss} (kWh)	LF (%)	E_{loss} (kWh)	LF (%)	E_{loss} (kWh)	LF (%)	
3.8kW	25.6V	Minimum	9.6	67.5	0.6	4.3	3.6	25.3	0.4	2.9	79.6
		Maximum	9.6	68.6	0.6	4.4	3.6	25.8	0.2	1.1	79.9
	51.2V	Minimum	8.8	66.9	0.4	2.9	3.6	27.5	0.4	2.7	80.9
		Maximum	8.7	67.8	0.4	2.9	3.6	28.0	0.2	1.2	81.2
	307.2V	Minimum	7.1	62.9	0.2	1.6	3.6	32.1	0.4	3.5	83.2
		Maximum	7.0	64.1	0.2	1.6	3.6	32.9	0.2	1.4	83.5
5kW	25.6V	Minimum	10.4	67.2	0.6	3.6	3.6	23.4	0.9	5.7	78.3
		Maximum	10.3	69.2	0.6	3.8	3.6	24.2	0.4	2.8	78.9
	51.2V	Minimum	9.5	66.9	0.3	2.3	3.6	25.4	0.8	5.4	79.6
		Maximum	9.4	68.5	0.3	2.4	3.6	26.1	0.4	3.0	80.1
	307.2V	Minimum	7.1	60.7	0.1	1.2	3.6	30.9	0.8	7.2	82.6
		Maximum	7.0	63.0	0.1	1.2	3.6	32.3	0.4	3.5	83.2
8kW	25.6V	Minimum	10.4	64.6	0.5	3.4	3.6	22.4	1.5	9.6	77.5
		Maximum	N/A	N/A	N/A	N/A	N/A	N/A	N/A	N/A	N/A
	51.2V	Minimum	9.5	64.4	0.3	2.2	3.6	24.4	1.3	9.0	78.9
		Maximum	N/A	N/A	N/A	N/A	N/A	N/A	N/A	N/A	N/A
	307.2V	Minimum	7.1	58.0	0.1	1.1	3.6	29.3	1.4	11.6	81.8
		Maximum	7.1	58.2	0.1	1.1	3.6	29.4	1.4	11.3	81.9
Stand-Alone Generator			1.0	44.9	0.04	1.8	1.2	53.3	N/A	N/A	96.1

The power losses for the selected 3.8kW, 307.2V, maximum battery capacity system are shown in Figure 39. The power losses increase when the generator is on. Total power loss remains below 600W for the entire simulation, with most of that 600W contributed to conversion losses. The cabling power losses are close to 0W during the simulation. The battery power losses are also very small, but increase when the battery is discharging at depleted capacity. The constant 150W accessory losses are also seen.

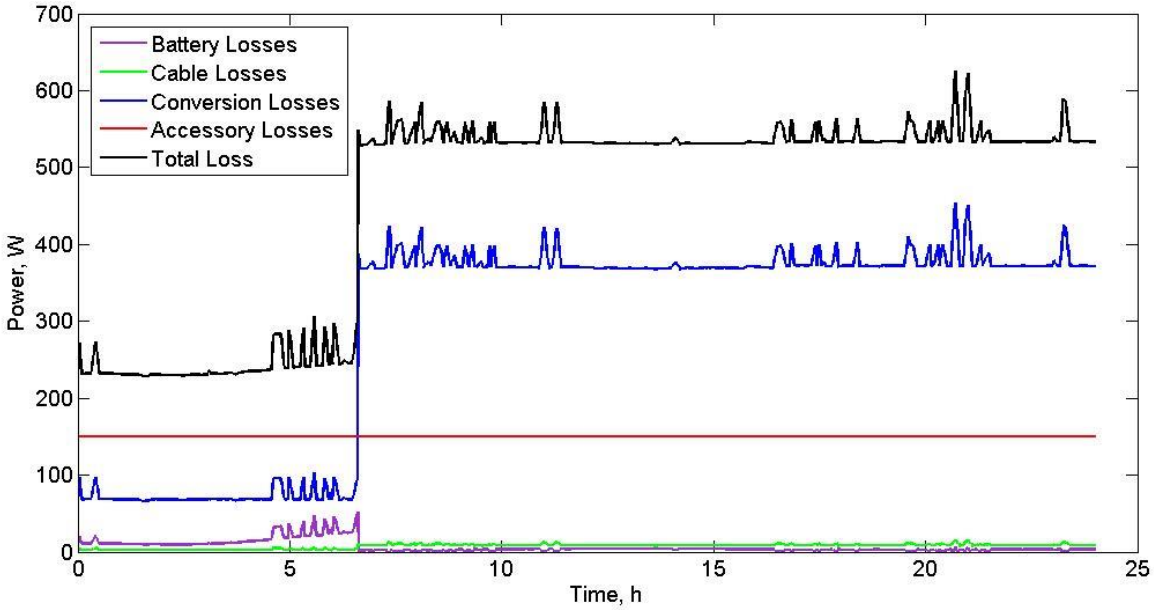

Figure 39: Power Losses for Selected System

The reason for developing a weight-based fuel penalty is to examine how the system weight and transportation increase the system's fuel consumption. A system that saves fuel during operation but requires much more fuel consumption during transport would not be worth the engineering resources to develop. Table 18 shows the impact of system transportation on overall fuel consumption. For the sixteen configurations under evaluation, the fuel consumption only increases about 6% to 7% when taking into account the fuel required to transport the system once a week a distance of 40 miles. Between the lightest and heaviest of the configurations, the amount of fuel required each day to transport the system only increases from 0.429 gal/day to 0.449 gal/day. This is only a 4.7% increase. The amount of fuel consumed to transport the stand-alone generator mounted on the ammunition trailer is 0.411 gal/day. Despite the stand-alone generator being almost 1200lbs lighter than the selected hybrid system, only 8.5% less fuel is consumed to move the stand-alone generator. This 8.5% difference is not enough to counteract the operational fuel saving benefits that the hybrid system provides.

Table 18: Design Results – Weight-Based Fuel Penalty

Generator Power	Pack Voltage	Pack Capacity	Weight (lbs)							FP_w (gal/ day)	Increase in Fuel Consumption (%)
			Gen	Conv	PV Array	Cables	Batt	Fuel Tank	Total		
3.8kW	25.6V	Minimum	271	187	259	14	278	75	1084	0.429	6.6
		Maximum	271	187	259	14	904	75	1710	0.449	7.1
	51.2V	Minimum	271	187	259	9	380	75	1180	0.432	6.8
		Maximum	271	187	259	9	909	75	1709	0.449	7.2
	307.2V	Minimum	271	140	259	5	330	75	1080	0.429	7.0
		Maximum	271	140	259	5	959	75	1708	0.449	7.3
5kW	25.6V	Minimum	390	200	259	14	330	75	1268	0.435	6.2
		Maximum	390	200	259	14	771	75	1710	0.449	6.5
	51.2V	Minimum	390	200	259	9	433	75	1366	0.438	6.5
		Maximum	390	200	259	9	776	75	1709	0.449	6.6
	307.2V	Minimum	390	140	259	4	392	75	1260	0.435	6.6
		Maximum	390	140	259	4	835	75	1703	0.449	6.9
8kW	25.6V	Minimum	665	233	259	17	471	75	1719	0.449	6.1
		Maximum	N/A	N/A	N/A	N/A	N/A	N/A	N/A	N/A	N/A
	51.2V	Minimum	665	233	259	10	572	75	1814	0.452	6.3
		Maximum	N/A	N/A	N/A	N/A	N/A	N/A	N/A	N/A	N/A
	307.2V	Minimum	665	154	259	5	526	75	1683	0.448	6.5
		Maximum	665	154	259	5	546	75	1704	0.449	6.5
Stand-Alone Generator			390	52	N/A	4	N/A	75	521	0.411	5.2

5.3 Exploration of Design Parameters

Some of the design parameters are explored to gain more insight into how they impact fuel consumption. The design parameters that are explored are the load profile, SOC dispatch strategy set points, and the weight-based fuel penalty. Simulations are run with these changed parameters using the system selected in *5.2 Optimal Design Selection*. This system has a 3.8kW generator and a 370.2V maximum capacity battery pack.

5.3.1 Exploration of Alternative Load Profiles

The first load profile parameter explored is the fraction of DC load and AC load in the Company COC profile. Six different DC fractions are analyzed: 0%, 20%, 40%, 60%, 80%, and 100%. After running the simulation with these different DC fractions, the

simulation is run again with two alternative load profiles. The first load profile is the aggressive load profile described in Figure 16 of *3.1 Load Profile Model*, with a 20% DC fraction. The second load profile is the residential load profile described in Figure 17 of *3.1 Load Profile Model*, with 0% DC fraction (a residence is expected to be powered from an AC power grid). Table 19 summarizes the results of these different simulation runs.

Table 19 shows that although the selected hybrid system is more efficient for load profiles with higher fraction of AC loads, the improvement over the stand-alone generator is not as great. For a load profile with 0% AC loads and 100% DC loads, the hybrid system consumes 23.2% less fuel than the stand-alone generator does. However, for a load profile with 100% AC load, the hybrid system only consumes 22.6% less fuel than the stand-alone generator does. The reason why the hybrid system is not as much of an improvement for higher AC loads is that a stand-alone generator outputs AC power and does not need any power conversion components, while the hybrid system requires two levels of power conversion between the generator and the AC load: the rectification of the generator output to charge the battery pack and the DC to AC conversion of the battery power to AC power for the AC loads.

Table 19 also shows that the selected hybrid system only improves fuel consumption by 7.4% over the stand-alone generator for the aggressive alternative load profile. This load profile has longer periods of high load where the stand-alone generator is close to its most fuel efficient output level. Meanwhile, the electrical losses of the hybrid system will only increase with these extended periods of high load. It is expected that as the average load of the load profile increases, the less the hybrid system will improve fuel consumption compared to a stand-alone generator.

The residential load profile gives the opposite effect, as the hybrid electric system becomes a much bigger improvement over a stand-alone generator (approximately 79% less fuel is consumed). Since this load profile has long durations of low load (below 1000W), the hybrid system is favored. The diesel engine in the stand-alone generator is extremely inefficient at loads below 1000W. It should be noted that the fuel consumption

of the stand-alone generator is skewed a high in the simulation of this load profile. Using linear interpolation to determine the generator's fuel consumption at low loads will exaggerate the fuel consumption because the generator's specific fuel consumption curve is closer to a power curve and would be less than the linear interpolated values. To gain more accuracy, more data points should be taken at low loads to build a more accurate specific fuel consumption curve at these low loads. Nonetheless, the hybrid system provides significant improvement over the stand-alone generator with this load profile. This result proves that this hybrid system could be successfully used to power rural households off-the-grid or households in disaster areas.

Table 19: Load Profile Exploration Results

Profile	% AC/% DC	Operational Specific Fuel Consumption (gal/kWh)		Hybrid Improvement (%)
		Stand-alone Generator	Selected Hybrid System	
Company COC Metered	0%/100%	0.1455	0.1117	23.2
	20%/80%	0.1450	0.1114	23.2
	40%/60%	0.1445	0.1111	23.1
	60%/40%	0.1439	0.1109	22.9
	80%/20%	0.1432	0.1107	22.7
	100%/0%	0.1425	0.1103	22.6
Aggressive	80%/20%	0.1177	0.1090	7.4
Home	100%/0%	0.5719	0.1208	78.9

5.3.2 Exploration of Alternative SOC Set Points

One of the bigger questions to answer when designing a hybrid system's dispatch strategy is how to determine the set points that yield the most fuel efficient results. Under the SOC Set Point dispatch strategy; these set points are the low and high battery SOCs used to determine when to turn on and off the generator, respectively. Table 20 displays the results of using four different pairs of set points with the selected hybrid system. For three of the set point ranges, the fuel consumption does not change. The fuel consumption does increase for the 50 to 60% set point range, but by only 0.2%. The problem with using a small set point range of 50 to 60% is that the generator is only off for only an

hour and a half between periods of charging the batteries. This excessive starting and stopping of the generator could wear the generator components faster.

This simulation does not include an accurate model for battery performance at SOC above 90%. Above 90%, the constant voltage charge stage takes over and this stage will most likely decrease the efficiency of the system as the generator must run at low power output for longer periods of time to charge the battery in this trickle charge range. A model that includes an accurate constant voltage charge stage would gain better results for fuel consumption up to 100% battery pack SOC.

Table 20: SOC Set Point Exploration Results

SOC Low Set Point (%)	SOC High Set Point (%)	Operational Specific Fuel Consumption (gal/kWh)
20	90	0.1107
30	80	0.1107
40	70	0.1107
50	60	0.1109

5.3.3 Exploration of Weight-Based Fuel Penalty

A deeper analysis of the weight-based fuel penalty is done to determine the point where the transportation fuel costs outweigh the fuel saving benefits of the hybrid electric system. The operational fuel consumption of the selected system under the Company COC load profile and no solar input is used for this analysis. However, the weight of the system is set to 0lbs, 1191lbs or 2470lbs. A 0lb system would be the ideal case where the hybrid system does not weigh anything. However, it still needs to be transported. The 1191lbs case is for the standalone generator system. The 2470lbs case is the maximum weight capacity of the trailer. The relocation frequency and distance are also adjusted for several cases. The relocation ranges from 40 miles per month to 200 miles per week. The results of this analysis are shown in Table 21 and are visualized in Figure 40.

Table 21: Exploration of Weight-Based Fuel Penalty Results

Trailer Weight (lbs)	Relocation Frequency	Relocation Distance (miles)	FP_w (gal/day)	FC_o (gal/kWh)	FC_{tot} (gal/kWh)	Increase in Fuel Consumption (%)
0	Once/Month	40	0.087	0.1107	0.1122	1.4
2470	Once/Month	40	0.106	0.1107	0.1126	1.7
0	Once/Week	40	0.374	0.1107	0.1174	6.1
2470	Once/Week	40	0.452	0.1107	0.1188	7.3
0	Once/Week	100	0.934	0.1107	0.1276	15.3
2470	Once/Week	100	1.13	0.1107	0.1311	18.4
0	Once/Week	200	1.87	0.1107	0.1445	30.5
2470	Once/Week	200	2.26	0.1107	0.1516	36.9
1191	Once/Week	200	2.05	0.1432	0.1804	26.0

The results show there is a base level of required fuel consumption that does not relate to the trailer's weight. For example, if a weightless trailer is transported 100 miles once per week, the transportation costs 0.93 gallons of fuel each day. If the trailer is fully loaded to 2470 pounds the transportation fuel consumption rises only 21% to 1.13 gallons of fuel each day. Therefore, if the goal is to reduce transportation fuel costs, the focus should be more on decreasing the distance and frequency the system has to move, not as much on the weight of the system. Focusing on reducing transportation distance would yield better results. This focus on reducing transportation distance is a logistics problem, and not an engineering design problem.

If the system is not transported often or very far, the increase in fuel consumption (from the operational fuel consumption to the overall fuel consumption) can be held to less than 10%. However, as transportation distance increases to 100 miles per week the fuel consumption increases up to 18%. When the transportation distance increases to 200 miles per week the fuel consumption increases up to 37%.

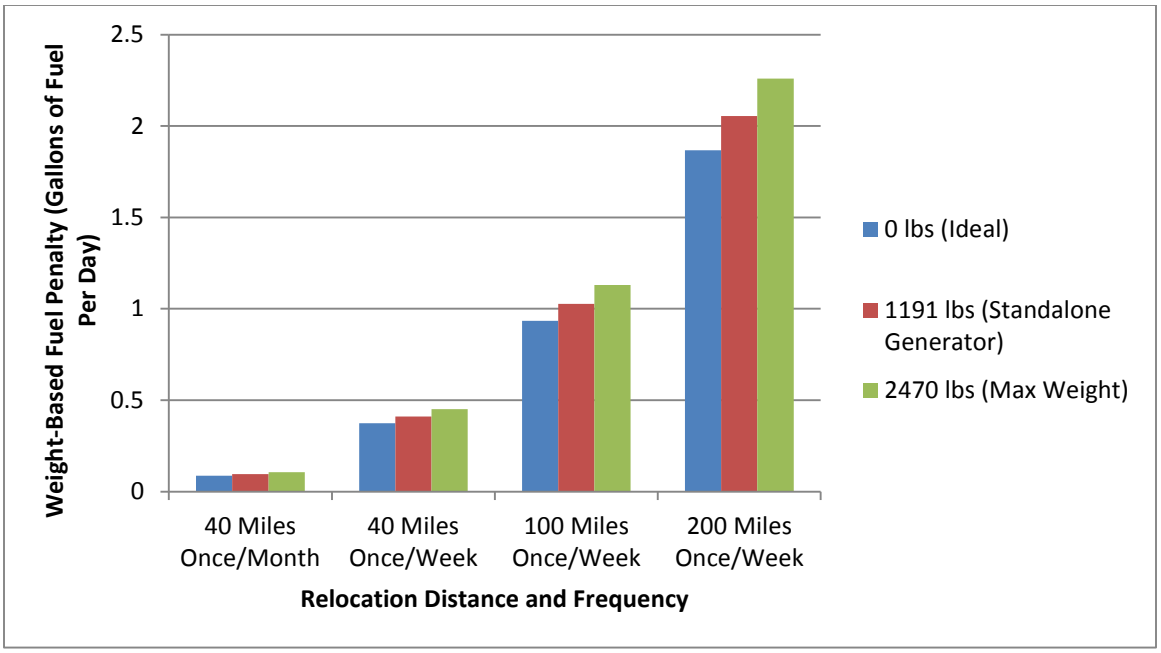

Figure 40: Effects of Weight and Transportation Schedule on Weight-Based Fuel Penalty

The point where the transportation fuel costs outweigh the fuel saving benefits of the hybrid electric system is found by determining the distance and frequency where the overall fuel consumption of the hybrid electric system begins to exceed the overall fuel consumption of the stand-alone generator. Because the stand-alone generator will weigh less than the hybrid power system, this cross-over point theoretically exists. However, even if the hybrid system is transported 1000 miles per week, its overall fuel consumption will still be less than the overall fuel consumption of a stand-alone generator transported 1000 miles per week (0.315 gal/kWh consumed for the hybrid system is still less than the 0.329 gal/kWh consumed by the stand-alone generator). Moving the system 1000 miles per week is not realistic, as the majority of the hybrid system's lifetime will be spent being transported and not actually powering anything. Therefore, realistically this cross-over point where the hybrid system's weight negates its fuel savings benefits does not exist. Given a load profile similar to the Company COC load profile, a properly designed hybrid system will most always be more fuel efficient than a stand-alone generator.

6 Conclusions

Many results and conclusions have been drawn from the work done in this thesis. The most important result is the proof that a properly designed mobile hybrid electric system can significantly conserve fuel compared to a competing stand-alone generator. This section explains the conclusions drawn from the validation, design, and exploration results, as well as the expected return on investment of the selected hybrid system. It then covers the future work that can be done to improve the simulation model and to improve system design.

6.1 Summary of Results

In this work, a model of a hybrid energy system is presented and validated using test data for a prototype system. This model is then used to determine a most fuel efficient system design given multiple configurations and components. Some of the design parameters are explored further to determine their impact on fuel consumption. Additionally, the return on investment is calculated for the selected hybrid system.

Conclusions Drawn from Validation Results

The major result drawn from the validation results is that the model presented in this thesis can accurately predict the fuel consumption of a hybrid system design to under 7% of the system's fuel consumption, given that the model uses the Company COC load profile and an accurate estimation of the converter efficiencies.

Much of the inaccuracy of the model can be attributed to inaccurate converter models or converter models that are too simplistic. The run of the model using the listed efficiency for the generator's rectifier increased the error up to 45% of the measured fuel consumption. Therefore, a converter model that calculates the converter efficiency as a function of the converter's load and temperature could increase the accuracy of the model.

The model works on many assumptions that may have also contributed to the inaccuracy of the model: the lengths of cabling between components, the magnitude of the accessory load, and the simplified battery model that ignores transient effects. Building a more complex model that does not use these assumptions may also increase the accuracy of the model.

It should also be noted that the measurements during the prototype test carried some resolution error and measurement noise. The simulation results may fall within tolerance of the measurement results if these measurement errors are including. Also the prototype test was imperfect. For example, the ambient temperature changed throughout the test and may have impacted generator, battery, and converter performance. The prototype system also had to be restarted due to a communication loss between the computer and battery management system. Measuring the fuel consumed by weight also added several facets of measurement error. Finally, the system parameters and load were measured using two separate data collection systems with different sampling rates. These different sampling rates needed to be reconciled to use the test data for validation purposes.

Conclusions Drawn from the Design of Most Fuel Efficient System

The most fuel efficient system is the system that uses the 3.8kW diesel engine generator and a 307.2V maximum capacity battery pack. Three important design tenets, described below, arise from the results of this work. Designing to these three major guidelines will help produce the most efficient towable hybrid system.

1. Maximize the system's electrical efficiency
2. Maximize the battery pack's voltage and capacity
3. Maximize the fuel efficiency of the generator's internal combustion engine at its full rated power

The first design guideline is straightforward; electrical losses directly impact a system's fuel efficiency. However, the most powerful way to increase the system's electrical efficiency is by selecting power conversion components with the highest

conversion efficiency and power factor possible. Conversion is the largest contributor to a system's electrical losses. A minor improvement in a converter's efficiency can make a significant improvement to the system's fuel efficiency. The second largest contributor to a system's electrical losses is the energy that is needed to run accessory systems. Focus on increasing the efficiency of the system computer, microcontrollers, and protective diodes can also make an impact on a system's fuel efficiency. Selecting power conversion components that can be cooled passively (natural convection) instead of actively (water or forced air convection) can also decrease the amount of energy being routed to accessories. Active cooling requires pumps and fans that can have sizeable power draw (the prototype system's water pump and fans drew about 60W to cool the rectifier). Finally, less focus should be put on decreasing cabling losses since these only comprise a small amount of the overall electrical loss.

The second design guideline is twofold: increase the battery pack's voltage and increase the battery pack's capacity. Increasing the battery pack's voltage can reduce the system's fuel efficiency by decreasing the current required in the system. As the current decreases, cabling and conversion losses become smaller. By reducing the battery pack's voltage, the first guideline is also being met. Increasing the battery pack's capacity can reduce the system's fuel efficiency a small amount by decreasing battery losses. Larger capacity battery packs have smaller internal resistance, and therefore, smaller battery losses. A more important reason for using a larger capacity battery pack is the added storage capability for renewable energy. Less fuel is necessary if energy is being supplied from renewable sources and scavenged power.

The third design guideline shows that when selecting a generator, the most important deciding factor is the internal combustion engine's fuel efficiency at its rated operating point. Selecting a generator with a high fuel efficiency at its rated operating point is more important than its rated power output, weight, or size. In general smaller generators can yield better system fuel efficiency results than larger generators, but only by a small amount. The only way a generator's power output matters is in that the generator should be sized to meet the average expected load on the system..

Conclusions Drawn from the Exploration of Design Parameters

The exploration of the load profiles, SOC set points, and weight-based fuel penalty yields a few significant results. It is shown that the load profile can dramatically change the fuel consumption of a hybrid energy system. A load profile with a high average load will make a hybrid system less effective at saving fuel. Conversely, a load profile with low average load greatly favors a hybrid system over a stand-alone generator due to the stand-alone generators poor fuel efficiency at low load. The fraction of AC power versus DC power in the load profile also impacts the effectiveness of the hybrid system in a small way.

The exploration of the SOC set points does not show any appreciable difference in the fuel consumption of the system when using a smaller range of SOC set points. However, if the difference between the high and low SOC set points is too small, the generator will be cycled with more frequency and can increase the rate of wear on the generator.

The exploration of the weight-based fuel penalty shows that the hybrid system will always be more fuel efficient than a stand-alone generator, even at great transportation distances. Also, it is shown that decreasing the fuel consumed during transportation is best done by limiting the distance and frequency that the system needs to travel. Reducing the weight only makes a modest improvement on the transportation fuel consumption.

Return on Investment

A hybrid electric alternative system's potential can be evaluated using return on investment (ROI) analysis. This analysis focuses on the amount of time it would take for the selected hybrid electric alternative to become more economic than the standalone generator system. Because the hybrid electric system is a more complex system that includes additional components like a battery pack, solar panels, and extra conversion equipment; its initial investment cost will be much higher than the initial investment cost of just a standalone generator. However, because the hybrid electric alternative does not

use as much fuel as the standalone generator system, eventually it will be the more economic option. To determine the length of time before a hybrid electric alternative begins saving money over the standalone generator, ROI analysis is carried out.

A standalone generator system would have initial cost determined by the cost of its generator, rectifier, and associated power distribution components (cabling, fuses, etc.). A hybrid electric system would have initial cost that includes the cost of its battery pack, solar panels, solar charge controller, rectifier, inverter, DC/DC converters, computer, switches, cooling equipment, and power distribution components. For the ROI analysis, the cost of the computer, switches, power distribution equipment, and hardware is ignored, as these components do not generally carry high costs. However, the sum of the costs of the major components is multiplied by 10% and added to the total to account for the costs attached to these minor components. Also, both the hybrid alternative and the standalone generator systems are assumed to use the ammunition trailer as their platform. The cost of this ammunition trailer is also ignored. The initial cost of each system is found using the present-day market cost of all the components. A breakdown of each component's cost can be found in *Appendix C: Return on Investment Analysis*. It is estimated that the standalone generator system carries initial investment cost of $13,090.00. The hybrid electric alternative is estimated to have an initial cost of $85,908.38, which is more than six times more expensive than the standalone generator system.

Over time, the cost of fuel consumption will eventually offset the hybrid alternative's large initial cost. For this ROI analysis, the $17.44/gal transportation cost estimate for the US military in Iraq in 2011 is used. This is the most recent cost estimate the author could find. Using this cost estimate and the fuel consumption results from *5.2 Optimal Design Selection*, it is determined that the hybrid electric alternative (with solar input) will become more economic than the standalone generator after approximately 4.9 years. This result means that the hybrid alternative would need to be used for at least five years before returning economic benefits.

It should be mentioned that this ROI analysis does not include maintenance or replacement costs for the generator and battery pack. The hybrid system's battery pack would degrade over many cycles and would eventually need to be replaced. The selected hybrid system's battery pack is estimated to cost $46,247.04. While the battery replacement cost does not favor a hybrid electric system, generator maintenance costs may be smaller for a hybrid electric system than for a standalone generator system. In the hybrid electric system, the generator is being run at its optimal load where it is less likely to become damaged. For a standalone generator, the generator could be run for long periods of time at low loads where it is more likely to wear and become damaged. Additionally, the generator is run for shorter duration in the hybrid system than in the standalone generator system. Fewer generator hours will help decrease the frequency that generator maintenance needs to occur. Further analysis should be carried out to determine how these maintenance and replacement costs affect the return on investment.

6.2 Future Work

There is much work that can be done in the future to improve the accuracy and utility of the simulation model.

The accuracy can be improved through a more complex converter model, inclusion of a battery degradation model, and more accurate specific fuel consumption plots for the internal combustion generators. Since converter efficiency is dependent on the load on the converter and its temperature, a more accurate model would include these parameters. Because conversion losses are the most significant energy losses in the hybrid electric system, improved accuracy in the converter model will go a long way in improving the accuracy of the overall system model. The inclusion of a battery degradation model can help make the model more accurate for describing system performance over long periods of time. For the batteries used in this simulation, the battery's depth of discharge can decrease to 80% of its original capacity after 2500 cycles [27]. Such an effect could have a large impact on overall system performance as the lifetime of the system increases. Finally, more accurate specific fuel consumption plots used in the generator model can help increase the accuracy in the fuel consumption

estimation. In the current model, the fuel consumption of the generator at low loads becomes more inaccurate than at high loads.

The utility of the simulation model can expand by including ways to optimize for other design goals, inclusion of wind turbine and scavenged power models, inclusion of fuel cells or microturbines, inclusion of more dispatch strategies, the inclusion of more system architectures, and the expansion of the model to hardware-in-the-loop capability.

Many design goals exist for hybrid power systems. Designing for increasing the fuel consumption of a system is just one of these design goals. These other design goals (reducing carbon footprint, increasing reliability, increasing battery lifetime, minimizing economic cost, and maximizing quality of power delivery) would require more variables to be included into the simulation. However, there may be an application where one of these design goals is desired.

The inclusion of wind turbine and scavenged power models can be beneficial in designing systems for applications where the main source of renewable energy is wind or scavenged power. Inclusion of microturbine and fuel cell models can also be beneficial when evaluating these budding power technologies and their utility in hybrid power systems.

While the SOC Set Point strategy is a commonly used strategy in hybrid energy systems, other dispatch strategies exist that may prove to be better at reducing fuel consumption. The load following strategy is a prevalent dispatch strategy which wasn't simulated with this model. Using a different system architecture may yield better results, as well. For example, an AC-coupled architecture may be better for load profiles that have primarily AC loads.

Finally, this simulation can be extended to a hardware-in-the-loop model to determine more efficient control strategies and to update component parameters. Hardware-in-the-loop simulations are used extensively to evaluate and design control strategies for hybrid vehicles in real-time [91]. This hardware-in-the-loop testing uses real-time controllers to run the vehicles' powertrains, drivelines, and driver models [91].

Hardware-in-the-loop simulations have also been used in hybrid power systems to optimize a battery's working conditions in order to extend its life [92]. This hardware-in-the-loop strategy can also be used to adjust the control strategy and set points of the hybrid power system over the system's operation to decrease its fuel consumption. This may be necessary if any parameter changes like the system's load profile. It may also be useful if a component becomes damaged and a new strategy is needed to change the system power flow to avoid this damaged component.

Bibliography

[1] P. &. P. Assistant Secretary of Defense for Operational Energy, "Energy for the Warfighter: Operational Energy Strategy," United States Department of Defense, Washington, DC, 2011.

[2] Army Environmental Policy Institute, "Sustain the Mission Project: Casualty Factors for Fuel and Water Resupply Convoys," Army Environmental Policy Institute, Arlington, VA, 2009.

[3] R. Rapier, "The U.S. Navy and Biofuels - Part III," EnergyTrends Insider, 30 October 2010. [Online]. Available: http://www.energytrendsinsider.com/2010/10/30/the-u-s-navy-and-biofuels-%E2%80%93-part-iii/. [Accessed 10 March 2015].

[4] S. Eaton, "Rep. Marcy Kaptur says gasoline for troops in Afghanistan costs $400 a gallon," Politifact, 23 May 2011. [Online]. Available: http://www.politifact.com/ohio/statements/2011/may/23/marcy-kaptur/rep-marcy-kaptur-says-gasoline-troops-afghanistan-/. [Accessed 9 March 2015].

[5] R. Tiron, "$400 per gallon gas to drive debate over cost of war in Afghanistan," The Hill, 16 October 2009. [Online]. Available: http://thehill.com/homenews/administration/63407-400gallon-gas-another-cost-of-war-in-afghanistan-. [Accessed 9 March 2015].

[6] S. Rolland and G. Glania, "Hybrid Mini-Grids for Rural Electrification: Lessons Learned," Alliance for Rural Electrification, Brussels, Belgium, 2011.

[7] A. Newman, "Hurricane Sandy vs. Hurricane Katrina," 27 November 2012. [Online]. Available: http://cityroom.blogs.nytimes.com/2012/11/27/hurricane-sandy-vs-hurricane-katrina/?_r=0. [Accessed 10 May 2015].

[8] Alliance for Rural Electrification, *Hybrid power systems based on renewable energies: a suitable and cost-competitive solution for rural electrification*, Alliance for Rural Electrification.

[9] M. Eroglu, E. Dursun, S. Sevencan, J. Song, S. Yazici and O. Kilic, "A Mobile Renewable House using PV/Wind/Fuel Cell Hybrid Power System," *International Journal of Hydrogen Energy*, vol. 36, pp. 7985-7992, 2011.

[10] M. S. Yazici, H. A. Yavasoglu and M. Eroglu, "A mobile off-grid platform powered with photovoltaic/wind/battery/fuel cell hybrid power systems," *International Journal of Hydrogen Energy*, vol. 38, pp. 11639-11645, 2013.

[11] Victron Energy, *MultiPower: Environment friendly all-in-one hybrid energy,* Victron Energy.

[12] D. McLean, *The NextEnergy Advanced Mobile Power & Energy Program,* US Army CERDEC, 2008.

[13] United States Marine Corps (USMC) Expeditionary Energy Office (E2O), "Brief to Industry: Mobile Electric Hybrid Power Sources (MEHPS)," 13 January 2013. [Online]. Available: http://www.hqmc.marines.mil/Portals/160/FINAL%20MEHPS%20Brief%20to%20Industry_0201.pdf. [Accessed 20 April 2015].

[14] General Dynamics Ordnance and Tactical Systems, *EFSS: Expeditionary Fire Support System,* St. Petersburg, Florida: General Dynamics Ordnance and Tactical Systems, 2008.

[15] Victron Energy, "Marine Generator Test," Victron Energy, 2007.

[16] E. C. Bobric, G. Cartina and G. Grigoras, "Clustering Techniques in Load Profile Analysis for Distribution Stations," *Andvances in Electrical and Computer Engineering*, vol. 9, no. 1, pp. 63-66, 2009.

[17] Z. Ning and D. S. Kirschen, "Preliminary Analysis of High Resolution Domestic Load Data," The University of Manchester, Manchester, UK, 2010.

[18] B. Root, "Doing a Load Analysis: The First Step in System Design," *Home Power*, pp. 38-44, May 1997.

[19] G. Lena, "Rural Electrification with PV Hybrid Systems," International Energy Agency, 2013.

[20] A. Fetters, "Discussion of Low Load "Diesel" Options," in *Alaska Wind-Diesel Workshop*, Seward, AK, 2013.

[21] M. H. Nehrir, C. Wang, K. Strunz, H. Aki, R. Ramakumar, J. Bing, Z. Miao and Z. Salameh, "A Review of Hybrid Renewable/Alternative Energy Systems for Electric Power Generation: Configurations, Control, and Applications," *IEEE Transactions on Sustainable Energy*, vol. 2, no. 4, pp. 392-403, 2011.

[22] P. F. Ribeiro, B. K. Johnson, M. L. Crow, A. Arsoy and Y. Liu, "Energy Storage Systems for Advanced Power Applications," *Proceedings of the IEEE,* vol. 89, no. 12, pp. 1744-1756, 2001.

[23] Battery University, "What's the Best Battery," Battery University, 2015. [Online]. Available: http://batteryuniversity.com/learn/article/whats_the_best_battery. [Accessed 10 May 2015].

[24] B. Deveney, "When to choose lithium-iron phosphate batteries," Electronic Products, 1 August 2010. [Online]. Available: http://www.electronicproducts.com/Power_Products/Batteries_and_Fuel_Cells/When_to_choose_lithium-iron_phosphate_batteries.aspx. [Accessed 10 May 2015].

[25] Battery University, "BU-403: Charging Lead Acid," Battery University, 11 May 2015. [Online]. Available: http://batteryuniversity.com/learn/article/charging_the_lead_acid_battery. [Accessed 12 May 2015].

[26] PowerStream Technology, "How to charge Lithium Iron Phosphate Rechargeable Lithium Ion Batteries," PowerStream Technology, 6 April 2015. [Online]. Available: http://www.powerstream.com/LLLF.htm. [Accessed 12 May 2015].

[27] Valence Technology, Inc., *U-Charge XP Battery Modules,* Austin, Texas: Valence Technology, Inc., 2014.

[28] F. Trinh, *A Method for Evaluating Battery State of Charge Estimation Accuracy,* Gothenburg, Sweden: Chalmers University of Technology, 2012.

[29] S. Wen, "Cell balancing buys extra run time and battery life," *Texas Instruments Incorporated Analog Applications Journal ,* pp. 14-18, 2009.

[30] M. Ehsani, Y. Gao and A. Emadi, "Chapter 3: Internal Combustion Engines," in *Modern Electric, Hybrid Electric, and Fuel Cell Vehicles: Fundamentals, Theory, and Design - 2nd Edition,* Boca Raton, Florida, CRC Press, 2010, pp. 67-104.

[31] A. Stiel and M. Skyllas-Kazacos, "Feasibility Study of Energy Storage Systems in Wind/Diesel Applications Using the HOMER Model," *Applied Sciences,* vol. 2, no. 4, pp. 726-737, 2012.

[32] C. Rayment and S. Sherwin, *Introduction to Fuel Cell Technology,* Notre Dame, Indiana: University of Notre Dame, 2003.

[33] G. Pearson, M. Leary, A. Subic and J. Wellnitz, "Performance Comparison of Hydrogen Fuel Cell and Hydrogen Internal Combustion Racing Cars," in *Sustainable Automotive Technologies, 3rd International Conference,* 2011.

[34] Afcon Holdings Shlomo Group, *Micro Gas Turbine Engine,* Afcon Holdings Shlomo Group.

[35] C. D. Barley and C. B. Winn, "Optimal Dispatch Strategy in Remote Hybrid Power Systems," *Solar Energy,* vol. 58, no. 4, pp. 165-179, 1996.

[36] M. Vandenbergh, C. Garza and A. Notholt-Vergara, "Overview of Supervisory Control Strategies including a MATLAB Simulink Simulation Tool," International Energy Agency (IEA) Photovoltaic Power Systems Programme (PVPS), Kassel, Germany, 2012.

[37] M. A. Vazquez, *Optimizing the Spinning Reserve Requirements,* Manchester, United Kingdom: University of Manchester, 2006.

[38] Energy Storage Association, "Spinning Reserve," Energy Storage Association, 2015. [Online]. Available: http://energystorage.org/energy-storage/technology-applications/spinning-reserve. [Accessed 18 March 2015].

[39] T. Hove and H. Tazvinga, "A Techno-Economic Model for Optimizing Component Sizing and Energy Dispatch Strategy for PV-Diesel-Battery Hybrid Power Systems," *Journal of Energy in South Africa,* vol. 23, no. 4, pp. 18-28, 2012.

[40] J. M. Lujano-Rojas, C. Monteiro, R. Dufo-Lopez and J. L. Bernal-Agustin, "Optimum Load Management Strategy for Wind/Diesel/Battery Hybrid Power Systems," *Renewable Energy,* vol. 44, pp. 288-295, 2012.

[41] S. Yamamoto, J. Park, M. Takata and T. Hashimoto, "Basic Study on the Prediction of Solar Irradiation and its Application to Photovoltaic-Diesel Hybrid Generator System," *Solar Energy Materials and Solar Cells,* vol. 75, no. 3-4, pp. 577-584, 2004.

[42] P. P. Groumpos, R. C. Cull and A. F. Ratajczak, "An Overview of Control Aspects of a Village Stand-Alone Photovoltaic Power System," *IEEE Transaction on Power Apparatus and Systems,* vol. 103, no. 10, pp. 2845-2853, 1984.

[43] P. Groumpos and G. Papegeorgiou, "An Optimum Load Management Strategy for Stand-Alone Photovoltaic Power Systems," *Solar Energy,* vol. 46, no. 2, pp. 121-128, 1991.

[44] K. Khouzam and L. Khouzam, "Load Prioritization and Shedding in Photovoltaic Power Systems," *Solar Cells,* vol. 31, no. 6, pp. 505-511, 1991.

[45] A. Moreno, J. Julve, S. Silvestre and L. Castaner, "A Fuzzy Logic Controller for Stand Alone PV Systems," in *IEEE Photovoltaic Specialists Conference,* 2000.

[46] D. Lowe, "How Power Supplies Turn AC into DC in Electronic Circuits," Electronics , [Online]. Available: http://www.dummies.com/how-to/content/how-power-supplies-turn-ac-into-dc-in-electronic-c.html. [Accessed 12 May 2015].

[47] M. Wens and M. Steyaert, "Chapter 2: Basic DC-DC Converter Theory," in *Design and Implementation of Fully-Integrated Inductive DC-DC Converters in Standard CMOS,* Springer Netherlands, 2011, pp. 27-63.

[48] C. Reitsma, *An Introduction to Inverters and Applications,* Calvin College.

[49] SynQor, Inc., *Technical Specification: NQ60W60HGx40,* Boxborough, Massachusetts: SynQor, Inc., 2013.

[50] General Cable, "NEMA Receptacle and Plug Chart," [Online]. Available: http://www.generalcable.com/NR/rdonlyres/75CFEE81-ACDA-4F60-9E22-4CC19C14F343/0/Pg9698_NEMA_Chart.pdf. [Accessed 21 April 2015].

[51] Gateway Cable Company, "Connectors, Receptacles, and Adapters," Gateway Cable Company, 2013. [Online]. Available: http://www.tgccompany.com/connectors-receptacles-assemblies.html#11674728. [Accessed 21 April 2015].

[52] K.-c. Bae, S.-c. Choi, J.-h. Kim, C.-y. Won and Y.-c. Jung, "LiFePO4 Dynamic Battery Modeling for Battery Simulator," in *IEEE International Conference on Industrial Technology (ICIT),* Busan, Korea, 2014.

[53] J. Lo, *Effect of Temperature on Lithium-Iron Phosphate Battery Performance and Plug-in Hybrid Electric Vehicle Range,* Ontario, Canada: University of Waterloo, 2013.

[54] Valence Technology, Inc., *IFR18650e Cell Datasheet,* Austin, Texas: Valence Technology, Inc., 2008.

[55] United States Department of Energy Energy Efficiency & Renewable Energy Vehicle Technologies Program, "2011 Nissan Leaf - VIN 0356: Advanced Vehicle Testing - Beginning-of-Test Battery Testing Results," United States Department of Energy, Idaho National Lab, Idaho, 2011.

[56] M. J. Meyer, *Understanding the Challenges in HEV 5-Cycle Fuel Economy Calculations Based on Dynamometer Test Data,* Blacksburg, Virginia: Virginia

Polytechnic Institute and State University, 2011.

[57] K. Morita, K. Shimamura, N. Iwai and K.-i. Shimizu, "Fuel Economy and Exhaust Emissions Test Procedure for Hybrid Electric Vehicles - Comparison of Continuous Repeating Mode, Linear Approximation and SAE J1711," in *Electric Vehicle Symposium 18*, Berlin, Germany, 2001.

[58] J. Renze and W. E. W, "Law of Large Nuimbers," MathWorld - A Wolfram Web Resource, [Online]. Available: http://mathworld.wolfram.com/LawofLargeNumbers.html. [Accessed 10 April 2015].

[59] R. M. Moore, S. Ramaswamy, J. M. Cunningham and K. H. Hauer, "A Dynamic Simulation Tool for the Battery-Hybrid Hydrogen Fuel Cell Vehicle," *Fuel Cells*, vol. 6, no. 5, pp. 387-402, 2006.

[60] K. Wipke, M. Cuddy, D. Bharathan, S. Burch, V. Johnson, T. Markel and S. Sprik, "ADVISOR 2.0: A Second-Generation Advanced Vehicle Simulator for Systems Analysis," in *North American EV & Infrastructure Conference and Exposition (NAEVI 98)*, Phoenix, Arizona, 1998.

[61] National Renewable Energy Laboratory, "National Solar Radiation Database 1991-2005 Update: User Manual," National Renewable Energy Laboratory, Golden, Colorado, 2007.

[62] A. Rouhani, H. Kord and M. Mehrabi, "A Comprehensive Method for Optimum Sizing of Hybrid Energy Systems using Intelligence Evolutionary Algorithms," *Indian Journal of Science and Technology*, vol. 6, no. 6, pp. 4702-4713, 2013.

[63] Safeco Electric Supply, "NEC 2008: Table 310.16," 2008. [Online]. Available: http://www.safecoelectric.com/images/resources_pdf/NEC2008%20Table%20310.16.pdf. [Accessed 6 April 2015].

[64] United States Department of Defense, *MIL-STD-810G Test Method Standard: Environmental Engineering Considerations and Laboratory Tests*, Washington, DC: United States Department of Defense, 2008.

[65] Tyco Electronics, "Wire Calculation and Instructions," [Online]. Available: http://www.te.com/catalog/Overview/WireCalculations.pdf. [Accessed 7 April 2015].

[66] PowerStream, "Wire Gauge and Current Limits Including Skin Depth and Strength," PowerStream, 6 April 2015. [Online]. Available: http://www.powerstream.com/Wire_Size.htm. [Accessed 7 April 2015].

[67] RapidTables, "Wire Gauge Size Chart," RapidTables Online Reference & Tools, [Online]. Available: http://www.rapidtables.com/calc/wire/wire-gauge-chart.htm. [Accessed 7 April 2015].

[68] Nondestructive Testing Resource Center, "The International Annelaed Copper Standard," Nondestructive Testing Resource Center, [Online]. Available: https://www.nde-ed.org/GeneralResources/IACS/IACS.htm. [Accessed 8 April 2015].

[69] M. Holt, "Don't Let Voltage Drop Get Your System Down," Electrical Construction & Maintenance, 1 June 2004. [Online]. Available: http://ecmweb.com/code-basics/dont-let-voltage-drop-get-your-system-down. [Accessed 8 April 2015].

[70] E. A. Frame, J. Redfield, G. Wendel, V. Iyengar, J. Harris and W. Olson, "M1078 Hybrid Hydraulic Vehicle Fuel Economy Evaluation," US Army TARDEC Fuels and Lubricants Research Facility, Southwest Research Institute (SwRI), San Antonio, Texas, 2012.

[71] M. D. Fingerholz, *A Hybrid Approach to Tactical Vehicles,* Monterey, California: Naval Postgraduate School, 2011.

[72] AM General, "M1097A2 HMMWV Specifications," [Online]. Available: http://www.amgeneral.com/files/specs-sheet-m1097a2.pdf. [Accessed 1 April 2015].

[73] B. Boundy, S. W. Diegel, L. Wright and S. C. Davis, "Appendix A: Lower and Higher Heating Values of Gas, Liquid and Solid Fuels," in *Biomass Energy Data Book: Edition 4*, Oak Ridge, Tennessee, Oak Ridge National Laboratory, 2011, p.

201.

[74] "Air - Density and Specific Weight," The Engineering ToolBox, [Online]. Available: http://www.engineeringtoolbox.com/air-density-specific-weight-d_600.html. [Accessed 3 April 2015].

[75] M. Ehsani, Y. Gao and A. Emadi, "Chapter 2: Fundamentals of Vehicle Propulsion and Brake," in *Modern Electric, Hybrid Electric, and Fuel Cell Vehicles: Fundamentals, Theory, and Design - 2nd Edition*, Boca Raton, Florida, CRC Press, 2010, pp. 19-65.

[76] G. Sovran and D. Blaser, "A Contribution to Understanding Automotive Fuel Economy and Its Limits," in *SAE International*, Washington, DC, 2003.

[77] Northern Lights, Inc., *NL673L4 Specifications and Dimensions,* Seattle, Washington: Northern Lights, Inc., 2013.

[78] OutBack Power, Inc., *FLEXmax Extreme Charge Controller,* Arlington, Washington: OutBack Power, Inc., 2014.

[79] OutBack Power, Inc., *FLEXmax Series Charge Controllers (FLEXmax 80, FLEXmax 60) Owner's Manual,* Arlington, Washington: OutBack Power, Inc., 2013.

[80] Magna-Power Electronics, Inc., *Magna-Power Electronics Programmable DC Power Supplies: Technology and Feature Overview,* Flemington, New Jersey: Magna-Power Electronics, Inc..

[81] New World Case, Inc., "3U Zarges Rackmount Case 45803," New World Case, Inc., [Online]. Available: http://www.customcases.com/ecom/product/275/699/3U_Zarges_Rackmount_Case_45803.html. [Accessed 13 April 2015].

[82] Volpi Tecno Energia, "Diesel Marine Generator Totally Water-Cooled - MOVE 4000 - 3.5 kW - 3000 RPM," Volpi Tecno Energia, [Online]. Available: http://www.volpitecno.com/dettagli_prodotti.aspx?language=en&id=96&cat=26. [Accessed 1 May 2015].

[83] Central Maine Diesel, "Isuzu 8,000 Watt Diesel Generator," Central Maine Diesel, 2015. [Online]. Available: http://www.centralmainediesel.com/order/800TS.asp?page=800TS. [Accessed 1 May 2015].

[84] LG North America Solar Business Team, *MonoX Neon LG300N1C-G3,* Englewood Cliffs, New Jersey: LG Electronics U.S.A. Inc., 2013.

[85] Flexiva, *DC/DC Converter Module 0...350V DC,* Amtsberg, Germany: Flexiva.

[86] Delta-Q Technologies Corporation, *Delta-Q IC650 650W Industrial Battery Charger,* Burnaby, Canada: Delta-Q Technologies Corporation, 2014.

[87] BRUSA Elektronik AG, *NLG513 - On - Board - Charger,* Sennwald, Germany: BRUSA Elektronik AG, 2015.

[88] OutBack Power, Inc., *GTFX & GVFX Series Grid-Interactive True Sinewave Inverter/Charger,* Arlington, Washington: OutBack Power, Inc..

[89] SolarEdge Technologies, Inc., *SolarEdge Three Phase Inverters for North America,* Israel: SolarEdge Technologies, Inc., 2014.

[90] BRUSA Elektronik AG, *BSC6 - Bidirectional Auxiliary Supply Converter,* Sennwald, Germany: BRUSA Elektronik AG, 2015.

[91] S. Jiang, D. Medonza and J. Kitchen, "A Flexible Hardware-in-the-Loop Testing System for Hybrid Powertrain," *SAE Technical Paper*, pp. 1-5, 2015.

[92] Y. Xiao-kun, H. Hong-wen, P. Lian-yun and Z. Xiaolin, "Hardware-in-the-loop simulation on a hybrid power system," in *4th International Conference on Power Electronics Systems and Applications (PESA),* Hong Kong, 2011.

[93] Kijiji, "Northern Lights 6kW diesel generator," eBay International AG, 9 June 2015. [Online]. Available: http://www.kijiji.ca/v-tool-other/calgary/northern-lights-6kw-diesel-generator/1078775953?enableSearchNavigationFlag=true.

[Accessed 10 June 2015].

[94] Manelservice Gruppi Elettrogeni, "VTE MOVE 4000 Veicolare-Terrestre," Manelservice Gruppi Elettrogeni, 2012. [Online]. Available: http://lnx.manelservice.com/ecommerce/vendita-ge_marini-VTE+MOVE+4000+VEICOLARE%2BTERRESTRE-101.html. [Accessed 10 June 2015].

[95] EV Drives, "Delta-Q IC650 On-Board 24V Battery Charger 940-0001," EV Drives, 2015. [Online]. Available: http://www.evdrives.com/product_p/cgr-940-0001.htm. [Accessed 10 June 2015].

[96] AA Portable Power Corp, "LiFePO4 18650 Rechargeable Cell: 3.2V 1200 mAh 18A Rate, 3.84Wh - UN38.3 Passed -," Batteryspace.com, 2015. [Online]. Available: http://www.batteryspace.com/lifepo4-18650-rechargeable-cell-3-2v-1200-mah-18a-rate-3-84wh-ul-listed-un38-3-passed-ndgr.aspx. [Accessed 10 June 2015].

[97] Metric Mind Corporation, "Price List," Metric Mind Corporation, 9 June 2015. [Online]. Available: http://www.metricmind.com/price-list/. [Accessed 10 June 2015].

[98] Wholesale Solar, "SE9000A-US Three-phase SolarEdge Grid-tie Inverter," Wholesale Solar, 2015. [Online]. Available: http://www.wholesalesolar.com/products.folder/inverter-folder/SE9000.html. [Accessed 10 June 2015].

[99] Wholesale Solar, "LG Mono X NeoN LG300N1C 300-watt Solar Panel," Wholesale Solar, 2015. [Online]. Available: http://www.wholesalesolar.com/products.folder/module-folder/LG/LG300N1C.html. [Accessed 10 June 2015].

[100] Wholesale Solar, "Outback Power Flexmax Extreme," Wholesale Solar, 2015. [Online]. Available: http://www.wholesalesolar.com/products.folder/controller-folder/Outback-power-flexmax-extreme.html. [Accessed 10 June 2015].

[101] Manelservice Gruppo Elettrogeni, "VTE MOVE 4000 Veicolare-Terrestre," Manelservice Gruppo Elettrogeni, 2012. [Online]. Available: http://lnx.manelservice.com/ecommerce/vendita-ge_marini-

VTE+MOVE+4000+VEICOLARE%2BTERRESTRE-101.html. [Accessed 10 June 2015].

Appendices

Appendix A: Test Procedure for Measuring Specific Fuel Consumption of Northern Lights 5kW Generator

The HEIT prototype system uses a 5kW Northern Lights NL673L4 generator. Because the specific fuel consumption of the generator varies with operating conditions, a test was conducted to build its specific fuel consumption curve for its operation in Blacksburg, VA, given an elevation of 2,080 feet and an ambient temperature of 23°C. The resulting specific fuel consumption curve is used in the thesis' model for system analysis. The test procedure is described in the following list.

1. One gallon of the generator's diesel fuel is weighed using a scale with resolution of 0.05 lbs. This weight is used to determine the diesel fuel's density
2. An 18 gallon fuel tank is filled with fuel and then weighed. This weight is the initial fuel weight for the test
3. The generator is run for one hour at full load to warm up its system.
4. A resistive load bank is connected to the generator that allows for load steps of 120W, 1490W, 2380W, 2950W, 3500W, 4000W, 4500W, and 4950W.
5. The generator is run with 120W load for one hour
6. At the end of the hour, the generator is shut off and the weight of the fuel tank is measured. The difference in the weight before and after running the generator for 1 hour at this load step is measured.
7. The volume of fuel consumed over this load step is calculated by dividing the weight difference by the density of the fuel.
8. The specific fuel consumption of the generator at this load step is calculated by dividing the volume of fuel used at this load step by the load step multiplied by one hour.
9. Steps 5 through 8 are repeated at the other load steps to complete the specific fuel consumption curve of the generator.

Appendix B: Example Calculations for Expected Cable Currents

Objective: Calculate the cabling loss from the system's DC bus to the inverter when the AC load is 1000W.

Given:

- AC load has voltage 120Vrms
- Inverter efficiency $\eta = 90\%$
- Cabling length $L = 5$ ft, each cabling run is $2L$
- The cabling between the inverter and AC load is 12AWG with resistance R_{cable2} of 1.588 mΩ/foot
- The cabling between the DC bus and inverter is 2AWG with resistance R_{cable1} of 0.1563 mΩ/foot
- DC Bus Voltage $V_{bus} = 307.2$ V
- AC Load $P_{Load} = 1000$ W

Diagram:

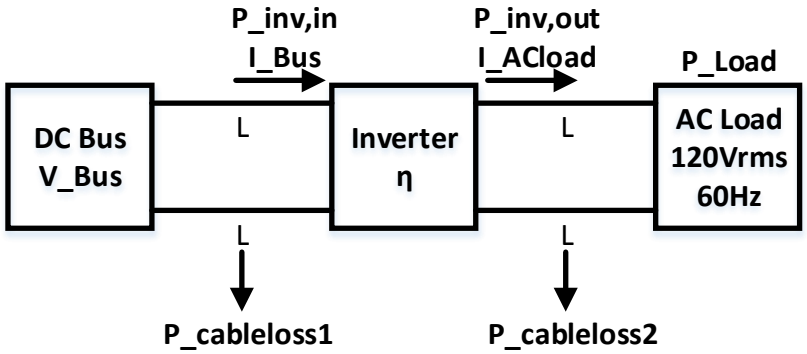

Solution:

Starting with the power output from the inverter:

$$P_{inv,out} = P_{Load} + P_{cableloss2}$$

The AC load is known to be 1000W. The cabling loss $P_{cableloss2}$ can be found using

$$P_{cableloss2} = {I_{ACload}}^2 R_{cable2}(2L)$$

where the cable current I_{ACload} is found using

$$I_{ACload} = \frac{P_{load}}{120\ \text{Vrms}}.$$

Using these equations, the power output from the inverter $P_{inv,out}$ is found to be 1001.1W.

Now, the power input to the inverter $P_{inv,in}$ needs to be found using

$$P_{inv,in} = \frac{P_{inv,out}}{\eta} = \frac{1001.1\ \text{W}}{0.9} = 1112.3\ \text{W}.$$

The cabling loss between the DC bus and inverter $P_{cableloss1}$ can now be found using

$$P_{cableloss1} = {I_{Bus}}^2 R_{cable1}(2L)$$

where the cable current I_{Bus} is found using

$$I_{Bus} = \frac{P_{inv,in}}{V_{Bus}}.$$

Finally, the cabling loss between the DC bus and inverter $P_{cableloss1}$ is found to be 0.02W.

Appendix C: Return on Investment Analysis

Two systems are analyzed during the return on investment (ROI) analysis. The first is the standalone generator system and the second is the selected hybrid electric alternative system found in this thesis. The initial costs for the components in each system are recorded in the table below. The cost of each system's components are summed. This sum is multiplied by 10% and added back to the sum to determine the total initial cost of each system. This 10% additional cost is used to cover expenses for the system's computer, cooling system, switches, cabling, fuses, and hardware.

Standalone Generator				**Selected Hybrid System**			
Component	**Qty**	**Cost Per Unit ($)**	**Initial Cost ($)**	**Component**	**Qty**	**Cost Per Unit**	**Initial Cost ($)**
5kW Generator	1	8,500.00 [93]	8,500.00	3.8kW Generator	1	7,172.49 [94]	7,172.49
Rectifiers	8	425.00 [95]	3,400.00	Battery Cells in Battery Pack	8928	5.18† [96]	46,247.04
Total + 10% ($)			13,090.00	Rectifiers	2	2,849.00 [97]	5,698.00
				Inverters	1	2,235.00 [98]	2,235.00
				DC/DC Converters	2	6,118.00 [97]	12,236.00
				Solar Panels	7	480.00†† [99]	3,360.00
				Solar Charge Controller	1	1,150.00††† [100]	1,150.00
				Total + 10% ($)			85,908.38

† The battery cells used in the ROI analysis are not exactly the same as the cells used in the system analysis. The cells used in the earlier analysis presented in the thesis did not have an available price. However the cells used for ROI analysis are of the same chemistry and similar size.

†† The solar panels used in the system analysis are constructed of individual cells. The price of these individual cells could not be found. However, solar panels that are constructed from these cells were found. Since these solar panels have 300W

output, and the analysis solar array has 2100W output, the price of these solar panels is multiplied by seven to approximate the cost of the analyzed solar panels.

††† The price of the solar charge controller used in the system analysis could not be found. However, the price of a similar solar charge controller is used.

After determining the initial cost of each system, the cost of the fuel used each day is determined for each system. The overall specific fuel consumption of the standalone generator and selected hybrid system (with solar) are used here. These values are determined using the analysis in the main work of this thesis. The overall specific fuel consumption of the standalone generator system is 0.1507 gal/kWh, while the overall specific fuel consumption of the selected hybrid system (with solar) is 0.1083 gal/kWh. These overall specific fuel consumption values are multiplied by the average cost of transporting fuel to a combat zone $17.44/gal. This multiplication will give the cost of fuel used per kWh.

$$\text{Standalone Generator Cost of Fuel per kWh} = (\$17.44/\text{gal})\left(0.1507\,\frac{\text{gal}}{\text{kWh}}\right)$$
$$= \$2.63/\text{kWh}$$

$$\text{Selected Hybrid System Cost of Fuel per kWh} = (\$17.44/\text{gal})\left(0.1083\,\frac{\text{gal}}{\text{kWh}}\right)$$
$$= \$1.89/\text{kWh}$$

The cost of fuel per kWh is then multiplied by the daily load energy (55.3kWh/day) to determine the cost of fuel used each day.

$$\text{Standalone Generator Cost of Fuel per Day} = (\$2.63/\text{kWh})\left(55.3\,\frac{\text{kWh}}{\text{day}}\right)$$
$$= \$145.44/\text{day}$$

$$\text{Selected Hybrid System Cost of Fuel per Day} = (\$1.89/\text{kWh})\left(55.3\,\frac{\text{kWh}}{\text{day}}\right)$$
$$= \$104.52/\text{day}$$

Now, the cost of each system as a relation to time can be determined. These next two equations can then be plotted against time to find the crossover point where the

selected hybrid system begins to cost less than the standalone generator system. The plot below shows this crossover point. The selected hybrid system becomes the more economic option after about 1782 days or 4.9 years.

$$\text{Standalone Generator Cost} = \$13{,}090.00 + (\$145.44/\text{day}) \times \text{time}$$

$$\text{Selected Hybrid System Cost} = \$85{,}908.38 + (\$104.52/\text{day}) \times \text{time}$$

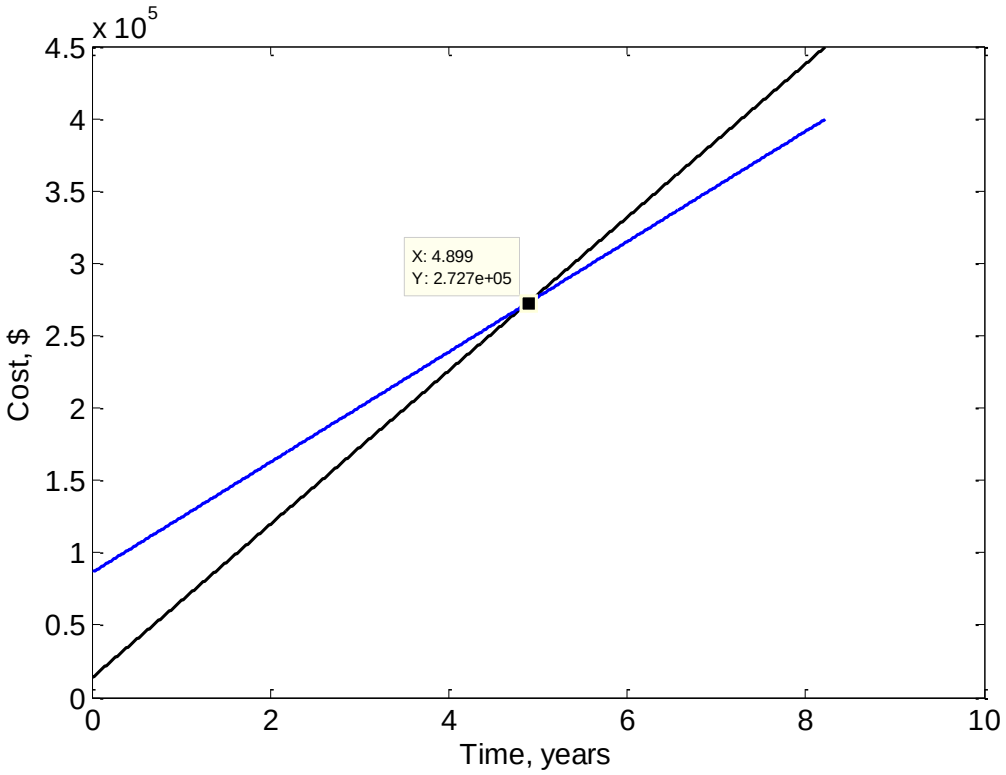

Appendix D: Simulation Code

The model presented in this thesis is simulated using MATLAB. Due to the length of the code used in this thesis, it is not printed in this document. However, this code can be acquired by contacting the author at chris.delbarga@gmail.com.